

Experimental and Computational Assessment of Locomotor Coordination and
Complexity Following Incomplete Spinal Cord Injury in the Rat

by

Brian Hillen

A Dissertation Presented in Partial Fulfillment
of the Requirements for the Degree
Doctor of Philosophy

Approved July 2012 by the
Graduate Supervisory Committee:

Ranu Jung, Chair
Jitendran Muthuswamy
Devin Jindrich
Gary Yamaguchi
James Abbas

ARIZONA STATE UNIVERSITY

August 2012



This work is licensed under the Creative Commons Attribution-NonCommercial-ShareAlike 3.0 Unported License. To view a copy of this license, visit <http://creativecommons.org/licenses/by-nc-sa/3.0/> or send a letter to Creative Commons, 444 Castro Street, Suite 900, Mountain View, California, 94041, USA.

ABSTRACT

Spinal cord injury (SCI) disrupts the communication between supraspinal circuits and spinal circuits distal to the injury. This disruption causes changes in the motor abilities of the affected individual, but it can also be used as an opportunity to study motor control in the absence or limited presence of control from the brain. In the case of incomplete paraplegia, locomotion is impaired and often results in increased incidence of foot drag and decreased postural stability after injury. The overall goal of this work is to understand how changes in kinematics of movement and neural control of muscles effect locomotor coordination following SCI. Toward this end, we examined musculoskeletal parameters and kinematics of gait in rats with and without incomplete SCI (iSCI) and used an empirically developed computational model to test related hypotheses. The first study tested the hypothesis that iSCI causes a decrease in locomotor and joint angle movement complexity. A rat model was used to measure musculoskeletal properties and gait kinematics following mild iSCI. The data indicated joint-specific changes in kinematics in the absence of measurable muscle atrophy, particularly at the ankle as a result of the injury. Kinematic changes manifested as a decrease in complexity of ankle motion as indicated by measures of permutation entropy. In the second study, a new 2-dimensional computational model of the rat ankle combining forward and inverse dynamics was developed using the previously collected data. This model was used to test the hypothesis that altered coordination of flexor and extensor muscles (specifically alteration in burst shape and timing) acting at the ankle joint could be

responsible for increases in incidence of foot drag following injury. Simulation results suggest a time course for changes in neural control following injury that begins with foot drag and decreased delay between antagonistic muscle activations. Following this, beneficial adaptations in muscle activation profile and ankle kinematics counteract the decreased delay to allow foot swing. In both studies, small changes in neural control caused large changes in behavior, particularly at the ankle. Future work will further examine the role of neural control of hindlimb in rat locomotion following iSCI.

ACKNOWLEDGMENTS

My advisor, Ranu Jung has contributed significantly to the work presented here. I thoroughly enjoyed our talks about science, those relating to the work here as well as others.

James Abbas showed me who we do this work for. Gary Yamaguchi introduced me to the world of musculoskeletal modeling and helped me with the data collection methods. Devin Jindrach demonstrated to me to be critical of everything I read.

My wife, Stefany Coxe was here with me on this project before we were married and saw it through to the end with significant help on the statistics involved as well as helping me to understand and explain my data.

My parents and brother made sure I had fun and kept me grounded while I was buried in science.

Mallika Fairchild experienced the lab with me (and everything that entailed), helping each other out where we could. Tsukasa Kanchiku trained me in the surgical techniques used in this study, something which enriched my life. James Lynskey always kept true to the science. Daniele Protas and Peter Bremer were extremely helpful in electrode design and construction as well as data collection. This work was supported by NIH R01-NS054282

TABLE OF CONTENTS

	Page
LIST OF TABLES.....	viii
LIST OF FIGURES.....	ix
CHAPTER	
1 INTRODUCTION.....	1
Motor Control	1
Central pattern generators: the rhythmic core	2
Voluntary control of locomotion	3
Peripheral reflexive control of locomotion	3
CPGs and Coordination.....	5
Rhythm generation in CPGs	6
Left-right and flexor-extensor coordination	6
Spinal Cord Injury	7
Rat Model of Incomplete Spinal Cord Injury	9
Neuromusculoskeletal Modeling.....	10
Skeletal models.....	11
Muscle models.....	12
Modeling dynamics	13
Objectives.....	14
Rationale	15
Significance.....	17
Organization of the Dissertation.....	17

CHAPTER	Page
2 JOINT-SPECIFIC CHANGES IN LOCOMOTOR COMPLEXITY IN THE ABSENCE OF MUSCLE ATROPHY FOLLOWING INCOMPLETE SPINAL CORD INJURY IN THE RAT	19
Introduction.....	19
Methods.....	23
Spinal cord injury surgery.....	23
Hindlimb treadmill kinematics	24
Coordination.....	26
Complexity measures.....	28
Musculoskeletal properties	30
Statistical analysis	31
Results.....	31
Open field locomotion indicates mild injury.....	31
Passive muscle parameters indicate a lack of muscle atrophy.....	31
3D locomotor kinematics indicate decrease in complexity.....	32
Discussion.....	36
Lack of change in musculoskeletal parameters.....	36
Changes in locomotor coordination in absence of atrophy.....	38
Joint-specific changes in locomotor complexity.....	41

CHAPTER	Page
Conclusions.....	44
3 EFFECTS OF SPINAL CORD INJURY INDUCED CHANGES IN MUSCLE ACTIVATIONS ON FOOT DRAG IN A COMPUTATIONAL RAT ANKLE MODEL.....	59
Introduction.....	59
Methods.....	63
Study groups.....	63
Surgical procedures.....	64
Ankle treadmill kinematics.....	65
Musculoskeletal properties.....	66
Musculoskeletal model.....	69
Simulation protocol.....	72
Results.....	74
Locomotion measures indicate mild-moderate injury.....	74
Musculoskeletal parameters show no difference between sham injured and iSCI rodents.....	75
Computational model.....	75
Decreased activation delay decreases likelihood of foot swing.....	77
Trapezoidal activation profile increases chance of foot swing.....	77
Muscle atrophy increases chance of foot swing.....	78

CHAPTER	Page
Injured kinematic profiles increase chance of foot swing...	78
Summary of all factors	79
Discussion	79
Conclusions	84
4 CONCLUSIONS	99
Summary	99
Locomotor Control	100
Significance.....	101
Future Work	102
Changes in muscle activations following iSCI.....	102
Higher degree-of-freedom model	105
Experimentally measured muscle forces	106
REFERENCES	108

LIST OF TABLES

Table		Page
2-1.	Hindlimb muscle properties in sham and iSCI rats.	55
2-2.	PE analysis of joint angles	56
2-3.	PCA analysis of hindlimb joint angles	57
2-4.	Phase delays for inter- and intralimb coordination	58
3-1.	Simulation parameters	96
3-2.	Musculoskeletal geometry.....	97
3-3.	Ankle musculoskeletal properties	98

LIST OF FIGURES

Figure		Page
2-1.	Permutation entropy method.	46
2-2.	Basso-Beattie-Bresnahan (BBB) locomotor scores for 4 weeks post injury.	47
2-3.	Locomotor kinematics during treadmill walking in a contused rat.	48
2-4.	Limb joint angles averaged across all cycles per animal.	49
2-5.	Interlimb coordination during locomotion.	50
2-6.	Intralimb coordination during locomotion.	51
2-7.	Joint angle measures based on the whole gait cycle	52
2-8.	Joint angle measures based on gait subcycles.	53
2-9.	Joint angle values at liftoff and touchdown.	54
3-1.	Procedures for determining musculoskeletal geometry.	86
3-2.	Musculoskeletal model organization.	87
3-3.	Musculoskeletal model components	88
3-4.	Modified Hill-type muscle model	89
3-5.	Basso-Beattie-Bresnahan (BBB) locomotor scores for 4 weeks post injury.	90
3-6.	Treadmill ankle joint kinematics	91
3-7.	Ankle moment at stance-to-swing transition: sham and iSCI kinematics	92
3-8.	Ankle moment at stance-to-swing transition: drag kinematics	93
3-9.	Ankle moment for all combinations of model factors.	94

Figure	Page
3-10. Main effect of each model factor	95

Chapter 1

INTRODUCTION

Spinal cord injury (SCI) is an example of a large perturbation of motor control. The typical pathway of brain to spinal cord to muscle is disrupted. This disruption causes large changes in the motor abilities of the affected individual, but it can also be used as an opportunity to study motor control in the absence or limited presence of control from the brain. Many people think of the brain as the seat of all nervous control of our body, but, as many experiments show, there is much going on past the brainstem. These impairments can cause significant changes in locomotion which often results in increased incidence of foot drag and decreased stability after injury. In this dissertation, motor control following spinal cord injury (SCI) is assessed using computational and kinematic techniques. Prior to discussing the particular studies, I will address relevant background. This includes a review of motor control and coordination in the locomotor system, the properties of spinal cord injury, and the computational modeling methods.

Motor Control

The motor systems of the human body are able to produce *voluntary*, *rhythmic*, and *reflexive* movements [1]. Just as each of these types of movement is distinct, they are significantly intertwined with one another. This is particularly true in the case of locomotion. Typically, initiation of locomotion is a *voluntary* event. Other voluntary movements include many feed forward adaptations to the gait pattern in the presence of perturbations. The central pattern generators for

locomotion are *rhythmic* in nature, providing the basic pattern of muscle activations necessary for movement. Finally, the length, force, and cutaneous receptors supply *reflexes* which provide feedback adaptations to the locomotor pattern. These three categories of movement are roughly mirrored in the structures of neural control: a basic pattern of rhythmic activity produced in the spinal cord (*rhythmic*) is regulated by descending input from the brain (*voluntary*) as well as peripheral pathways (*reflexes*) [2].

Central pattern generators: the rhythmic core

Neural circuits within the spinal cord are organized to produce rhythmic motor output. This rhythmic core can function like a central pattern generator (CPG) for control for locomotion. In the absence of supraspinal or sensory input, the CPG can provide the basic locomotor rhythm [2-4]. The CPG is not a single structure responsible for all locomotion, but a distributed, hierarchal system [5-8]. The simplest CPGs can control flexion-extension and left-right alternation [4]. These simple CPGs are conceptually organized as half-center models, first proposed by Brown [9]. The half-center model provides a simple alternation, with one output more active while the other is less active. Central to this design is reciprocal inhibition. In reciprocal inhibition, activation of one side inhibits the activation of the other side [10]. When left-right and flexor-extensor pattern generators are coupled, the basic locomotor pattern emerges. The CPG alone can provide this basic rhythm in the absence of supraspinal input [11], local sensory input [12], or both [13] in quadrupeds, provided the right tonic excitatory stimulus. However, this is not the case in humans where bilateral complete lesions of the corticospinal

tract (a lateral pathway) cause near complete loss of the ability to walk [14].

Coordination of neural components within the CPG is discussed in more detail below.

Voluntary control of locomotion

While not strictly required for ongoing control of locomotion, inputs from the brain play a large role in gait. The medial system is responsible for adjustments in posture, diffusely targeting the proximal and axial muscles [15, 16]. The lateral system contributes to fine control and voluntary modifications of gait [17, 18].

When comparing human locomotion with that of other mammals, the basic properties remain [19, 20] though there are some differences. As mentioned above, the corticospinal tract plays a significant role in human locomotion. The rubrospinal tract (also a medial pathway) plays a much larger role in cat and monkeys than in humans [21]. In monkeys, the rubrospinal tract can compensate for damage to the corticospinal tract [22]. Finally, the brain is responsible for voluntary initiation of locomotion [23].

Peripheral reflexive control of locomotion

As mentioned above, the CPG can function without input from peripheral sensory afferents. However, these inputs function to adapt the CPG to the real world [3].

These inputs generally come from three sources: stretch receptors, providing muscle length and velocity; Golgi tendon organs, providing muscle force; and cutaneous receptors, providing touch [1].

Stretch receptors and Golgi tendon organs are grouped together to describe proprioception, the sense of body position. Proprioception has a number of very specific roles in locomotion. Stimulating the stretch receptors in the extensors of the hip can initiate stepping in spinalized cats [24]. Unloading of the Golgi tendon organ of the ankle extensors is essential to initiation of swing [25]. Proprioception also plays a large role in regulation of walking speed. For instance, locomotor rhythm can be controlled by rhythmic movements of the hip [26]. Finally, proprioception modifies the level of muscle activity through a number of reflexes. The simplest is the stretch reflex. This reflex functions to prevent change in length of a muscle. When the muscle (agonist) is lengthened, the stretch reflex activates the agonist along with any synergists while inhibiting any antagonists [1]. During locomotion, the Golgi tendon reflex also functions in the same way; increases in muscle load are met with increased excitation of the muscle [27]. Together, these reflexes work as a positive force feedback system, increasing activation of the muscle under increased loads during stance. Decreases in loads, such as seen during the use of a body weight support harness, significantly decrease the outputs of antigravity muscles [28]. The functions of these reflexes can also be phase dependent; responses to stretch are twice as large during stance when compared to swing [29].

Cutaneous inputs also serve an important role during locomotion. Denervation of cutaneous receptors causes temporary loss of precision walking, though treadmill walking is retained [30]. Stimulation of the dorsal surface of the foot causes a reflex to increase clearance of the foot. Such stimulation causes immediate knee

flexion followed by flexion of the hip and ankle in order to step over an obstacle [31]. Plantar stimulation leads to phase dependent responses. During swing, plantar stimulation causes excitation of the flexors, while during stance, it causes excitation of the flexors [32]. Thus the plantar cutaneous receptors help provide stability during stance and obstacle clearance during swing. These results are also different at the ends of the subphases of gait. Plantar cutaneous stimulation at the stance-to-swing transition causes ankle flexion (to allow foot swing), while during late swing it provides ankle extension (to reach the ground) [32].

CPGs and Coordination

The model of the central pattern generator presented above is a simple representation of some of its components. Current research points to the CPG being made of two separate functional layers [7]: the first layer is the rhythm generating layer described above, responsible for determining cycle speed and phase durations, and the second layer is the pattern shaper, responsible for coordination of multijoint and multilimb movements. This two-layer model had been used in neural network control of functional electrical stimulation devices [33]. In addition to this functional distribution in the CPG, there is also an anatomical one. The hindlimb CPG is distributed across the entire lumbar enlargement [34]. Moreover, this distributed CPG has a rostral-caudal gradient in rhythmogenic capability, such that rostral segments (those that control the hip) have a greater capacity to generate rhythms than caudal segments (those that control the knee and ankle) [4]. This leads the hip oscillator to entrain the caudal

oscillators during locomotion [35]. This may be one reason why hip motion so directly resets the locomotor cycle.

Rhythm generation in CPGs

Within the spinal cord, excitatory interneurons play a key role in rhythm generation [4]. However, the cord itself is also activated by reticulospinal neurons that receive inputs from the mesencephalic locomotor region (MLR) and lateral hypothalamus [23]. However, control of cycle period and subphase duration is highly task dependent. During walking, changes in speed are accomplished by changes in stance duration, while swing duration remains relatively constant [36]. This extensor (stance phase) dominated step cycle is due to intrinsic properties of the spinal cord in spontaneously generated fictive locomotion in spinal cats [37]. However when locomotion is initiated in the brain (MLR), fictive locomotion is flexor (swing phase) dominated. This may indicate that swing phase is more dominated by supraspinal inputs than stance phase.

Left-right and flexor-extensor coordination

Left-right coordination is required for correct alternation of opposite limbs. Commissural interneurons (CINs, neurons with axons that cross the midline of the spinal cord) are likely responsible for this left-right coordination [38]. This network of neurons is distributed across the hindlimb section of the spinal cord [39]. CINs have two categories: intrasegmental and intersegmental. Intrasegmental CINs organize left-right coordination by synapsing with spinal interneurons in the same segment on the contralateral side of the cord, including

those involved in the stretch reflex [40]. They may also directly target motoneurons with excitatory and inhibitory signals [41]. Intersegmental CINs have axons that project through at least 2 segments [42, 43]. Descending CINs have excitatory and inhibitory versions which help coordinate flexor and extensor alternation across segments and sides of the animal [44, 45]. Thus, left-right coordination is maintained by a specific set of neurons in the spinal cord.

Flexor-extensor alternation requires inhibitory networks. When inhibition is blocked, flexors and extensors activate at the same time [46]. Appropriate coordination of multiple muscles across the joint and the limb requires complex circuitry. Some of this coordination comes from circuits involved in left-right coordination (as mentioned above), but flexor-extensor coordination is retained following spinal cord hemisection [47]. Therefore, ipsilateral networks could coordinate flexors and extensors. Stretch reflexes have rhythmic activity during locomotion and are a likely source of this coordination [48, 49].

Spinal Cord Injury

Spinal cord injury (SCI) affects many people and can cause significant deficits in activities of daily living, many specifically relating to motor control. In addition to a decrease in neural connectivity across the local injury site, there are a number of adaptations following injury that are similar to deficits due to disuse [50]. These include atrophy and increase in fatigability to muscles, hyper-excitability of motoneurons distal to the injury, and changes in the local spinal circuitry [51].

Combined, these alterations produce the symptoms seen following injury in locomotion and other physiological processes [52, 53].

Current annual incidence of SCI in the US is about 40 cases per million population [54]. Most injuries occur to males and those between the ages of 16 and 30. While most patients survive initial hospitalization, SCI decreases lifespan by about 7% per year following the injury [55]. While people with little spinal tissue damage tend to regain function [56], those with severe injuries rarely regain independence [57]. Clinical assessment takes a number of forms, but the American Spinal Injury Association (ASIA) impairment scale is one of the most commonly used. This scale assesses sparing of sensory function and muscle strength in the upper and lower limbs in order to determine both the location and severity of the injury [58]. An ASIA score of “A” represents a functionally complete injury (cSCI), where no sensory or motor function remains below the level of the injury. “B,” “C,” and “D” are incomplete injuries (iSCI) where some function is retained. An ASIA score of “E” represents normal motor and sensory function.

As spinal cord injury disrupts motor and sensory control distal to the injury, bowel, bladder, and sexual dysfunction may occur [59]. Complications include pain [60], decreased fertility [61], and autonomic dysreflexia [62]. Pressure ulcers also play a significant role in life following SCI [63]. Acute care following SCI involves monitoring the vital signs of the patient [64] and removing bone fragments [65]. The only other standard in acute care is the administration of

methylprednisolone [66, 67]. While this has been shown to improve long term recovery in some studies, the therapeutic benefits are disputed [68, 69] and is only still used in some locations.

Musculoskeletal changes following spinal cord injury are similar to those seen in most disuse paradigms [51]. Complete unloading of the limbs, as seen in individuals primarily using a wheelchair, can lead to bone losses at 3-4% per month [70, 71]. In cases where unloading is less drastic, losses should be correspondingly lower. Muscle undergoes significant atrophy following injury [72], accompanied by a shift in muscle fiber type toward fast, fatigable units [73].

Rat model of incomplete spinal cord injury

While animal models differ from humans in numerous ways as already mentioned, such as stepping for complete transection injury, they still fill a valuable role in investigation of SCI. A great deal of our understanding of motor control has come from studies of quadrupedal animal models, specifically the cat and the rat. While the bipedal locomotion of humans is different from quadrupedal locomotion, both are based on the same general model of neural control of locomotion [74, 75]. Quadrupeds have differences in supraspinal control, and importantly for studies of SCI, they can provide rhythmic CPG outputs in the absence of supraspinal or sensory inputs.

In spite of these shortcomings, the rat model is currently one of the most studied and best understood models of SCI because it reflects many of the pathophysiological consequences observed after spinal injury in humans. In

particular, the rat contusion injury model closely mimics the incomplete injury typically seen in humans [76, 77]. In incomplete SCI (iSCI), some motor or sensory function is preserved distal to the injury site. Deficits following injury include decreased walking speed, altered weight bearing, poor balance, reduced propulsion, and foot drag [78]. The rat model has even been used in bipedal walking mode studies to allow comparisons of gait between humans and rats [79, 80]. However, rat recovery from iSCI occurs on a much shorter time scale than humans; rats typically reach a plateau in recovery of locomotor function within 4 weeks of injury, regardless of the injury severity [81].

A great deal of information is available on a number of functional impairments due to SCI in the rat, including the effects of injury on physiology [82] and behavior [83]. The general time course of rat hindlimb locomotor recovery following SCI has been characterized using the Basso, Beattie, Bresnahan locomotor recovery score [84]. This type of behavioral testing is similar to clinical scales such as the ASIA impairment scale mentioned previously. Full kinematic, kinetic and electrophysiological analysis has also been completed in the rat model [85-88]. Locomotor deficits following injury include changes in forelimb-hindlimb coordination, loss of body weight support, decrease in stability, and foot drag [84].

Neuromusculoskeletal Modeling

Neuromusculoskeletal modeling refers to computer models of motion produced by the muscular and skeletal system, driven by the nervous system [89]. Each of

these systems has a distinct history and relevance to the final output.

Neuromusculoskeletal models have been used to adapt rehabilitation protocols following neurological injury [90, 91], to analyze athletic performance [92], and to modify functional electrical stimulation controllers [33, 93].

Skeletal models

Currently, musculoskeletal modeling programs are used to determine the equations of motion for a particular model as well as to calculate moment arms and musculotendon lengths. Often these are split up into two parts, where the graphical representation of the skeletal system is defined in one program (SIMM, Motion Analysis Corporation; AnyBody, AnyBody Technology; etc.) and the dynamics are calculated in another (SDFast, PTC; Autolev, Online Dynamics Inc.; MATLAB, Mathworks Inc.; etc) [94]. As with all models, some assumptions and simplifications must be made. With skeletal models, the first question is one of dimensionality: the number of degrees of freedom and muscles. If the number of muscles in the proposed model is greater than the number needed to control all degrees of freedom, then the model will be redundant for some tasks and specialized approaches are needed to address this redundancy [94]. In the case of locomotion, dimensionality is often reduced to a single plane [95] as most of the action takes place in that plane. For simplicity and to reduce muscle redundancy, the number of muscles in the model is often reduced to the minimum number needed to control the kinematic degrees of freedom [96]. Bone segments are often modeled as rigid bodies with one to three rotational degrees of freedom connecting them. This simplification may fail to capture the complexity

of motion at a joint [97]. As with all assumptions, they must be appropriate to the task being studied and simplifications should fit the goal of the model.

The last aspect of the skeletal model is the muscle attachments. Muscles are usually modeled as connecting to the skeleton at a discrete point or multiple discrete points, determining the direction of force produced by the muscle on the skeleton. The locations of muscle attachments also determine the muscle moment arms and lengths/velocities of the muscle when muscle models are added to the skeletal model [98]. Wrapping points may be added when necessary to account for wrapping of muscles and tendons around joints [99].

Muscle models

Muscle models generally fall in to two categories: Huxley-type models [100] that estimate the forces involved in microscopic cross-bridge formation in the muscle fibers, and Hill-type models [101] that characterize whole muscle force levels based on a number of physiological properties. Huxley-type models are not typically used in multiple muscles systems as they are very complex and are governed by multiple differential equations which are computationally intensive to compute numerically [89]. Hill-type muscles contain elastic elements in series (tendon and aponeurosis) and parallel (passive muscle stiffness) with a contractile element (representing the force generation in the muscle). The contractile element is determined based on the basic properties of muscle contraction as detailed in the basic equation:

$$F_m(t) = f(v) \cdot f(l) \cdot a(t) \cdot F_m^{max}$$

Where $F_m(t)$ is the force of the muscle at time t , $f(v)$ is the normalized velocity dependent force, $f(l)$ is the normalized length dependent force, $a(t)$ is the time varying muscle activation level (0-1), and F_m^{max} is the maximum isometric muscle force. The force-length relationship is roughly inverted U-shaped with maximal force at the middle of the range of the muscle. The force-velocity relationship is a roughly negative sigmoid curve, with highest forces during eccentric contractions and lowest forces at highest concentric speeds [102]. Activation is determined by neural control of the muscle, often estimated from electromyogram (EMG) signals. These EMG signals can then be translated into population-based motor unit recruitment [103, 104].

Modeling dynamics

Musculoskeletal models are typically solved in one of two ways: forward dynamics and inverse dynamics. Forward dynamics models work in the order of natural events. Neural signals activate muscle models which generate forces and movements. These models are well suited for the study of pathological motion [105] because the developer of the model can individually set each parameter. Forward dynamics models have a number of associated problems. First, muscle activation is often estimated from EMG values which are highly variable, especially in dynamic conditions. Second, it is difficult to accurately determine skeletal geometry and muscle attachment points. Finally, small errors in estimates of joint torques result in large errors in position [89].

In an inverse dynamics model, motion is input and muscle force and neural control are then inferred or predicted from the motion. Inverse dynamic simulations also have their share of problems. First, moment of inertial and mass must be accurately calculated for each segment. This is particularly difficult in animals with poorly-defined segmental boundaries such as rats. Also, predicting muscle forces from joint torques is difficult when multiple muscles span the joint.

Both forward dynamics models and inverse dynamics models use the same biomechanical system and physics [106, 107]. Some research has been done with hybrid forward-inverse models that utilize aspects of both types of simulations [89, 108, 109].

Objectives

The long term goal of this work is to determine the mechanisms by which spinal cord injury affects rodent locomotion and use these findings to help develop therapies for improving function following SCI. The goal of this dissertation is to determine the effects of iSCI on rodent neural control of hindlimb locomotion. There were two specific aims toward this goal.

Specific Aim 1: To test the hypothesis that locomotor kinematic complexity decreases following iSCI in the rat.

Passive hindlimb musculoskeletal data and behavioral locomotor data during treadmill walking were collected from rats with sham and mild thoracic contusion

injuries to investigate changes in gait complexity and coordination following injury.

Specific Aim 2: To test the hypothesis that altered coordination of flexor and extensor muscles (specifically burst shape and timing) acting at the ankle joint could be responsible for increases in incidence of foot drag following injury.

A 2D model of the rat ankle was developed to test effects of neural control on the likelihood of foot drag in the rat. Data was collected on lower hindlimb geometry including joint position and muscle attachment point locations. The model incorporated the foot and lower leg segments, the ankle joint, and flexor and extensor muscles. Muscle activation (burst shape and inter-muscle activation delay), muscle atrophy, and ankle kinematic profile were varied according to measured and reported values.

Rationale

As mentioned previously, following spinal cord injury, many physiological changes take place, most notably to the motor and sensory nervous system caudal to the site of injury. As a result of the neural impairments, further adaptations are seen in the musculature, specifically atrophy and a shift in muscle fibers toward faster types. Many injuries occur at the thoracic level, causing loss of leg control as well as bladder, bowel and sexual function impairments. The loss of leg control leads to changes in functional motor behavior, reflected in gait performance.

In order to understand how neural and muscle changes affect recovery following iSCI as measured in locomotion, we need to assess relevant indices for motor impairment and recovery. For the musculoskeletal system, we collected relevant geometry of the rigid body system, including muscle attachment points and joint centers of rotation. We have also collected locomotor kinematics to identify changes in gait following injury.

By using a computer model, we can test a variety of permutations that are either difficult or impossible to test experimentally. Specifically, this allows us to test out how changes in neural control can affect locomotion in the absence of muscular changes, and vice versa. We can also see the interaction effects between the two, i.e. changes in activation profile might only have an effect in the atrophy, not the non-atrophy case. Our approach utilizes a rigid body approach for the biomechanical system which is valid due to the low bone strains seen in rat locomotion. Hill-type models are used for the muscles as they accurately represent the muscle level forces based on experimental data [110]. Our system uses a combination of SimMechanics [111] and Virtual Muscle [103] to represent the musculoskeletal system while neural drive is modeled as a simple function. These two software packages have been used for these types of biomechanical systems in simple models successfully.

The rat model is currently one of the most studied and best understood models of SCI being used. Rats have been used to study the effects of iSCI at both the cellular (*in vivo* and *in vitro*) and behavioral level due to the similarity of several

secondary injury characteristics to those that occur in humans after SCI [76, 77]. While rats are not bipedal, their locomotor characteristics have analogues in human movement. The Basso, Beattie, Bresnahan locomotor recovery score outlines the general time course of rat hindlimb locomotor recovery following SCI similar to clinical measures of human locomotion following injury [84].

Significance

SCI affects 250,000 Americans at around 10,000 a year [54]. The largest proportion of injuries is due to risk seeking behaviors, usually in young males. As it tends to afflict younger people, it is with them for many years and can have significant impact on their quality of life. Additionally, living with SCI often has a high financial burden [112]. As there is currently no cure, any intervention or rehabilitation therapy that alleviates the consequences of loss of function and activities of daily living or removes or mitigates any of the deleterious effects of spinal cord injury on physiological function would be greatly beneficial to the person injured. Scientifically, SCI is of interest as it acts like a major perturbation to the normally functioning nervous system and offers an opportunity to understand neural plasticity and response to perturbation.

Organization of the dissertation

This chapter has introduced the concepts and rationale for the studies presented in this dissertation. Following this, each chapter (2-3) addresses one of the specific aims above, in order. Each of these chapters is self contained. Finally Chapter 4 summarizes the work, presents the overarching conclusions reached from the

work and proposes future work relevant to those conclusions. A combined set of references is included at the end.

Chapter 2

JOINT-SPECIFIC CHANGES IN LOCOMOTOR COMPLEXITY IN THE ABSENCE OF MUSCLE ATROPHY FOLLOWING INCOMPLETE SPINAL CORD INJURY IN THE RAT

Introduction

As a result of spinal cord injury (SCI) the connections between the brain and the spinal circuitry below the injury are disrupted. This leads to adaptations in the neurons of the brain and spinal cord as well as changes to the sensory afferents and motoneurons [82, 113, 114]. Along with these neural changes, the muscles in the distal limb undergo changes similar to those seen in many disuse paradigms. For example, the muscles tend to atrophy and muscle fibers shift towards faster twitch, more fatigueable ones [51, 115-117]. These effects on muscle properties have been well studied in humans and other animals for a variety of disuse paradigms including weightlessness, bed rest, stroke, partial body support and constrained limbs [50, 118, 119]. As SCI related muscular and neural impairments affect the legs, locomotion is often used as a measure of impairment and recovery.

Both musculoskeletal and nervous system impairments may contribute to the behavioral impairments seen following iSCI. While one might expect aberrant neural control to dominate locomotor impairments following incomplete SCI (iSCI), data in humans has suggested that timing of voluntary initiation of ankle movement (control) is unaltered and loss of muscle strength (specifically dynamic

muscle strength) may be responsible for maladaptive changes in ankle gait patterns [120, 121]. However, dynamic muscle strength (for instance, time to maximal contraction) may rely on neural control, not solely muscle strength. Additionally, neural control of muscle in an isolated, voluntary, movement is significantly different than movement during gait [122]. Finally, the neuromuscular junction (NMJ) may be altered by SCI. In complete spinally transected animals, NMJ transmission failure increases somewhat following injury [123]. However, the effect is not large and should be significantly smaller in mild-moderate contusion animals.

Following stroke, the overarching control system for gait is simplified. Even in normal individuals, synergies in muscle activations during locomotion are common [124]. For instance, knee extensors and the hip abductors activate at the same time to provide body support during stance [125]. While these synergies exist in normal subjects, they are numerous and varied. Following stroke, these synergies collapse to just one pair: one for flexion and one for extension of the whole limb, indicating a decrease in motor control complexity [126]. This decrease in complexity may be due to unmasking of the primitive gait controller in the spinal cord when there is reduced input from supraspinal centers [127]. This idea is one of some debate however, with an alternative hypothesis that these synergies are purely due to constraints in the task being performed [128].

As iSCI also results in disruption of supraspinal motor control of the limbs a similar loss of complexity effect could be seen in iSCI. This could lead to

movements in the hindlimb being synchronized such that all joints are either extending or flexing in unison. There are a number of complexity measures that can be used to analyze time series data such as joint angle locomotor data. Synchronization of cyclic joint activation can be measured with principal components analysis and alterations in phase delay between the joint motions. Principal components analysis assesses how similar time series are to one another [129]. As the joints (hip, knee, and ankle) become synchronized, fewer and fewer components would be required to describe the motion of all three joints. Joint synchronization can also be measured by examining the phase delays between the activation of joints within a limb. As the phase delay becomes closer to 0 (exactly in phase), the joint motions become more synchronized. Joint kinematic complexity can be measured on a joint by joint basis by looking at permutation entropy of the joint angle time series. This measure assesses how likely it is for the joint angle to continue in the same direction from one time point to the next [119].

When adapting to incomplete SCI, gait characteristics of healthy subjects are often compared with those of injured subjects to determine recovery. However, injured subjects can often achieve gait which is stable and efficient that is not the same as normal; temporally normal control of gait related muscle activity is not required for recovery of gait following injury [130]. Identifying these new patterns and adapting rehabilitation patterns around them may improve functional recovery[131].

The rat model is currently one of the most studied and best understood models of SCI being used [76, 77]. Many researchers have studied the effects of SCI in the rat on a number of functional impairments and measured the effects of injury at multiple levels of physiology [82] and behavior[83]. The general time course of rat hindlimb locomotor recovery following SCI has been characterized using the Basso, Beattie, Bresnahan locomotor recovery score [84]. However, there has been relatively little research into specific hindlimb kinematics, with some notable exceptions [85, 88, 132, 133]. Also, little information has been collected on the muscles in the rat hindlimb, usually only a few muscles per study [115, 134, 135].

This study addresses the hypothesis that iSCI impairs gait coordination and decreases locomotor complexity. This is accomplished by assessing complexity of 3D joint kinematics during treadmill locomotion and measuring musculoskeletal parameters in rats four weeks following either a sham injury or a mild-moderate spinal cord contusion injury. No previous study has analyzed changes in kinematics complexity along with known levels of muscle atrophy. The analyzed data indicate that spinal contusion injury leads to impaired coordination and decreases in locomotor complexity, and that this loss can occur in the absence of muscle atrophy. Additionally, a novel set of musculoskeletal data were obtained that could be useful in the development of an empirically derived neuromusculoskeletal computational model for the rodent hindlimb.

Methods

Experimental data were collected from 12 female, adult, Long-Evans rats (270-300g). Six rats received sham injuries and six received a mild-moderate spinal cord contusion injury. All rats were kept on a 12 hour light/dark cycle with ad libitum food and water. The study was approved by the Institutional Animal Care and Use committee (IACUC) of Arizona State University and complies with the Guide for the Care and Use of Laboratory animals.

Spinal cord injury surgery

Rats were randomly selected to undergo T8 vertebral (T9 spinal) sham or mild-moderate incomplete contusion injury (iSCI). Surgery was performed under aseptic conditions similar to [136]. Rats were anesthetized under 1-2% isoflourane and given an injection of the analgesic buprenorphine (0.02-0.05 mg/kg). The vertebral process of T8 was removed and a U-shaped laminectomy was performed. For animals in the contusion (iSCI) group, T7 and T9 were clamped in place and a mild-moderate contusion (154 ± 3 kdynes) was performed with an IH Instruments force controlled impactor for a T9 spinal level contusion. Following contusion or laminectomy, the muscles were closed in layers using resorbable sutures and the skin closed with wound clips (which were removed 1-2 weeks following surgery). The animal was then given injections of 5 cc of sterile saline, and 33.3 mg/kg of Cefazolin antibiotic and allowed to wake slowly on a heated pad.

Animal care post surgery consisted of twice daily bladder expression until the animal was able to void on its own along with twice daily injections of saline, buprenorphine (as above) and antibiotic (as above) for the first 7 days following injury. Saline administration was continued if the animal remained dehydrated and antibiotic administration continued an additional week if the animals showed signs of urinary tract infection from a urinalysis test strip. Following surgery, animals were allowed to move freely in their cages for 4 weeks. Behavioral analysis consisting of the Basso, Beattie, and Bresnahan (BBB) 21 point locomotor score [84] was collected on the animals every day for the first week and each week thereafter in order to verify injury severity. Rats were observed for 4 min by two experimenters in order to score hindlimb function. The scale takes into account milestones representative of locomotor recovery including motion in the leg, paw position, coordination and weight support.

Hindlimb treadmill kinematics

Prior to the spinal cord surgery, animals were allowed to acclimatize to their new environment for one week and trained to walk on a treadmill (Columbus Instruments) for 2 days for 10 min each at a progression of speeds from 0-21 meters/min. 3D kinematic data was collected 4 weeks post injury on both sets of animals as described previously [88]. Briefly, animals were anesthetized under 1-2% isoflourane, shaved as necessary, and cone-shaped reflective markers were attached bilaterally to the bony prominences of the ankle (lateral malleolus), knee (femoral condoyle), hip (greater throchanter and iliac crest), shoulder (greater tubercle), elbow (lateral epicondyle), and wrist (ulnar head). In addition, a strip

of reflective tape was placed around the fifth metatarsal of the hindlimb, close to its attachment. The markers were not spherical, as is desirable for centroid calculations, but their small size (approximately 5 mm) minimized any error. Markers were placed while the animal lay on its side. Video was recorded from 4 infrared-sensitive cameras with co-localized infrared light sources (2 on each side of the animal). A 36 point static calibration object was first recorded. Following calibration, the animal was placed on the treadmill. Kinematic data was recorded at treadmill speeds starting at 11 m/min, increasing to 21 m/min in 2 m/min increments. The speed was increased each time the animals completed at least 5 continuous stable step cycles (in the middle of the treadmill at a constant speed). The entire process took approximately 5-10 min per animal. If an animal was unable to complete all speeds on the first day, the task was repeated the next day. No animal took more than 2 days to complete all speeds.

Video was imported into Vicon Peak-Motus® software for analysis. The calibration object was digitized for odd and even fields. A segment containing 5 stable step-cycles at 21 m/min was identified and imported into Peak-Motus. Video was manually synchronized using timestamps on the video. All reflective markers were digitized and the data was processed into joint angle versus time and marker 3D position data versus time. Gait cycles, swing, and stance phases were identified by marking lift off (the first frame where the toe was not contacting the treadmill) and touchdown (the first frame where the toe contacted the treadmill) events for each limb. Joint angles, hindlimb coordination, and joint

(specifically hip and toe) and segment positions were assessed for changes with time. Data was scaled to the hindlimb cycle and averaged across all cycles per animal. Specific joint angle values were also collected at swing and stance maxima and minima as well as phase transitions between swing and stance. Data from two of the animals (one sham and one iSCI) proved to be incompatible with the kinematic analysis software (most likely due to footfall event marking) and were excluded from most analyses. Unless specifically mentioned, n=5 animals per group were used.

Coordination

In addition to displaying each joint independently, angle-angle plots were created to display information about coordination. Intralimb coordination was displayed as hip vs. knee, hip vs. ankle, knee vs. ankle, and shoulder vs. elbow. Interlimb coordination was displayed as each joint, left vs. right. These plots can be used for qualitative assessment of a number of features of locomotion [88, 137]. When one joint moves while the other is held constant, a vertical or horizontal line is present in the plot. A continuously changing phase relationship between the two joints is indicated by diagonal segments, with negative slopes indicating an out-of-phase relationship and positive slopes indicating an in-phase relationship. Finally, in the interlimb coordination plots only, symmetry around the $y=x$ axis can be used to assess symmetry in the joint kinematics.

For quantitative analysis, phase delay was calculated for a number of intra- and interlimb combinations. Intralimb coordination was calculated for Hip-Knee and

Hip-Ankle. Interlimb coordination was calculated for forelimb-forelimb, hindlimb-hindlimb, and forelimb-hindlimb. Following methods used previously [88, 138], the relative phase of movement of one joint or limb was assessed with respect to its pair. For interlimb coordination, this involved comparing touchdown events between the respective limbs. For intralimb coordination, the point of maximum flexion for each joint during the swing phase was used. Each step cycle was normalized to % gait cycle. Each defining point (footfall or swing maximum) for the first half of the pair was denoted as τa_i , $i = 0, 1, 2, \dots N$ and the second of each pair as τb_i , $i = 0, 1, 2, \dots N$, where N is the number of points in the cycle. The phase of the second with respect to the first is then calculated using the following equation [139].

$$\phi(\tau a b_i) = \frac{(\tau a_i - \tau b_i)}{(\tau a_{i+1} - \tau a_i)}, \tau b_i < \tau a_i < \tau b_{i+1}$$

While left-right phase gives us some information about symmetry (the closer it is to 0.5 the more symmetric the gait is), a second symmetry measure was also used. In the following method, symmetry was assessed by using right side to predict the left side at each point in time. This measure used kinematics, which were normalized to the gait cycle. Assuming the joint angle movement is symmetric (as it should be in normal animals), the right side joint angles can be used to predict the left side joint angles with a phase lag of half of the cycle. The difference between the point and its prediction (the symmetry error) can be calculated with the following equation [138].

$$SYM_E = \sqrt{\frac{\sum_n \left(\frac{\theta R_i - \theta L_{i+hp}}{\sqrt{2}} \right)^2}{n}}$$

θR_i is the angle of the right side joint at point i , θL_{i+hp} is the angle of the left side joint at the point one half the cycle period ahead of the right side, and n is the number of point in the cycle.

Complexity measures

Permutation entropy (PE) [140] was calculated for both unaveraged (raw) hindlimb trajectories and cycle-averaged trajectories for each joint angle.

Permutation entropy quantifies the probability that a signal will remain similar from one segment to the next. Changes in the direction of the signal (positive to negative slope, for instance), indicate increases in complexity, while a steadily decreasing slope would indicate less complexity [141]. Thus a signal with multiple phases per cycle would have higher complexity than one with only one phase per cycle. Permutation entropy ranges from 0 to 1, with higher values having higher complexity. The method used here comes from Olofsen [142], based on the work of Cao [143]. First, angle trajectories were segmented into 3 point motifs. The motifs were then classified into one of 6 possible categories (Figure 2-1). The number of motif's belonging to each category was counted to obtain the probability (p_i) of each one occurring. PE was calculated using the standard Shannon uncertainty formula.

$$PE = - \frac{\sum p_i \times \ln(p_i)}{\ln(\text{number of motifs})}$$

As mentioned, PE was calculated for both averaged trajectories (a compilation trajectory of both left and right sides for each joint) and raw, unaveraged trajectories for each joint separately.

In the context of time series data, principal component analysis (PCA) is used to assess the similarity of waveforms with one another. It is used to reduce the dimensionality of data or to determine the highest sources of variation within the data [144]. PCA was used to determine the loss in complexity in overall hindlimb gait following injury. If more variance in the gait data is accounted for by lower order principal components, then this may indicate that gait complexity has reduced, and the joints are moving more in synchronization with one another. Thus, as the value for the first principal component (PC1, the percentage of variance account for by that component) increases, the complexity of the system decreases. In the case of hindlimb angle trajectories, as PC1 approaches 100%, the three joints of the hindlimb become in phase with one another such that all three joints are flexing and extending together. This would be a much simpler pattern than is seen in normal subjects. Analysis was performed using the PRINCOMP function in MATLAB on the set of three hindlimb angle trajectories for both hindlimbs for each animal then averaged across groups (sham and iSCI). When using the three hindlimb joint trajectories instead of multiple subjects, the maximum number of the principal components is 3, so data reduction is limited. Instead of counting the number of principal components required to reach a specified variance, amount of variance accounted for by the first principal component was assessed. The method used was similar to those performed on

single joint angle across subjects [144-146], but the three hindlimb joint angles were compared as opposed to multiple subjects. The different time points represent the different “variables” in a standard PCA analysis. PCA was performed on each hindlimb of each animal and the proportion of variance accounted for by the first and the sum of the first 2 principal components was obtained.

Musculoskeletal properties

Following 3D kinematics, rats were euthanized under heavy anesthesia (40 mg/kg sodium pentobarbital plus supplementary 1-5% isoflourane) and the hindlimb was separated from the remaining tissue. Hindlimb muscles were carefully dissected to lactated ringer’s solution. Muscles included gastrocnemius (medial and lateral heads), soleus, tibialis anterior, biceps femoris (knee and hip portions), semitendinosis, vastus (lateral and medial heads), and rectus femoris. All dissected muscles were weighed after light dabbing to remove surface liquid. Some muscles had their volume measured by displacement in a graduated cylinder; volume measurements were used only to calculate muscle density. Muscles were split along the belly and fiber pennation angle was measured using a goniometer and fiber length measured using a digital caliper. Individual fibers or fiber bundles were dissected from the belly of the muscle and placed on a glass slide with a small hole in the center. An 8 mW helium-neon (red) laser was beamed through the fiber and the first octave locations of the diffraction patterns were measured. Diffraction was converted to sarcomere length using the following equation. $d \sin \theta = n\lambda$ where d is the sarcomere length, theta is the

angle of diffraction, n is the diffraction order, and λ is the laser wavelength [147].

Statistical analysis

Differences in parameters between sham and iSCI groups were analyzed using standard t-tests with $p = 0.05$. In cases where both hindlimbs were measured independently, left and right limb values were considered repeated measures for data analysis. All statistical analyses were run in SAS 9.2 (SAS institute Inc, Cary, NC).

Results

Open field locomotion indicates mild injury

Sham injured animals showed normal locomotion on the BBB scale following injury. As seen in Figure 2-2, the initial deficits seen in the iSCI animals recovered to and plateaued at a BBB score of appropriately 15 (indicating hindlimb weight support with consistent forelimb-hindlimb coordination) by 2 weeks. Note the early recovery of hindlimb weight support (BBB 8-13).

Passive muscle parameters indicate a lack of muscle atrophy

Table 2-1 summarizes all measured individual muscle parameters. Muscle parameters showed no difference between sham and iSCI groups. As expected, pennation angle, fiber length and sarcomere length also showed no difference. Pennation angle tended to be greater in the distal muscles than in the proximal muscles, with non-pennate muscles seen in the knee flexors and hip extensor. Average muscle density was 0.97 ± 0.11 g/ml for sham and 1.00 ± 0.14 g/ml for

iSCI groups. Average animal masses were: 284 ± 10 g pre-injury sham, 283 ± 4 g pre-injury iSCI, 305 ± 15 g 4 weeks post-injury sham and 318 ± 24 g 4 weeks post-injury iSCI. This indicated that the iSCI animals may have gained more weight following surgery than the sham animals, possibly due to decrease in general activity following injury.

3D locomotor kinematics indicate decrease in complexity

Large differences in coordination were seen between sham and iSCI animals. Figure 2-3 shows joint angle kinematics and footfall measures during treadmill walking from one contusion animal, 4 weeks post injury. The black traces are for the left limb and the green traces are for the right limb. The solid vertical lines are touch-down and the dotted vertical lines are lift-off. For footfall, the black sections represent swing and the white sections stance. Joint angles for left and right limbs are shown with footfall patterns. As seen in Figure 2-4 (averaged across the groups), at each hindlimb joint, there is a noted change in the joint angles. The largest difference is seen in the ankle. During the ankle joint excursions, only one local maximum is seen as opposed to two pre-injury (one during stance and one during swing). In the hip trajectory, a lower range of motion was noted but the waveform was not qualitatively different. Table 2-2 summarizes the joint angle measures obtained at discrete time points during the gait cycle. At the ankle, each of the measured values was different between the sham and iSCI groups. In particular, ankle range of motion and lift off value for the joint angle are much higher in the iSCI group than the sham group. The knee has a lower range of motion following injury.

Permutation entropy of the unaveraged limb joint angle trajectories indicated a decrease in complexity of movement at the ankle with a corresponding increase in complexity at the knee (Table 2-3). The decrease in ankle movement complexity is likely due to the loss of the second local maximum in the trajectory (the ankle goes from biphasic to monophasic). The increase in knee movement complexity may mean the opposite. No other significant differences were found.

Permutation entropy of averaged joint angles continued to show the decrease in movement complexity at the ankle, but with no commensurate increase at the knee. This may indicate that the change to the complexity of movement at the knee may reflect step-to-step variations while the changes to the movement complexity at the ankle reflect within cycle changes. The movement complexity change at the ankle likely is due to the loss of the second local maxima in the ankle trajectory.

Interlimb coordination waveforms (L-R joint comparisons) emphasized the changes due to injury with significant differences seen in the knee and ankle coordination following injury (Figure 2-5). The hip joint showed a lower range of motion but the results were qualitatively similar to the pre-injury data. These observations of joint angle trajectory profiles obtained four weeks post injury were similar to those reported for animals with similar levels of contusion two weeks post injury but receiving neuromuscular electrical stimulation therapy [138].

As also seen in the interlimb coordination plots, symmetry was maintained about the diagonal following injury. Ankle-ankle plots were simplified due to lack of the second local maxima in the individual angle trajectories. Knee-knee plots showed a cruciform pattern, where one side is moving only when the contralateral side is not. Forelimb coordination was mostly unaffected by the injury. As is visually clear from the interlimb left-right coordination plots and symmetry error measurements confirm, there was no decrease in symmetry following iSCI for any of the hindlimb joints. In fact, there was more symmetry at the knee following injury (sham: $10.7^\circ \pm 1.1^\circ$, iSCI: $7.7^\circ \pm 0.3^\circ$, $p=0.03$), though the difference is small. This could be due to the decreases range of motion in the iSCI group, minimizing errors in the measure as both groups are still very symmetric in general, with results similar to normal and rats receiving electrical stimulation therapy in another study [138]. Table 2-5 shows the results of phase delay in intralimb and interlimb comparisons. Left-right hindlimb and left-right forelimb pairs showed no difference in phase delay between groups. This is somewhat expected as these animals were walking quite competently. Forelimb-hindlimb coordination was significantly altered, however. The phase delay was shifted approximately 50% (sham: 0.75 ± 0.22 , contusion: 0.55 ± 0.31 , $p<0.05$). This indicates that the gait shifted from a traditional walk pattern (each limb ~25% cycle delayed from the previous one) to something like a trot (where forelimb-contralateral hindlimb pair are alternating 50% out of phase with one another) [148].

Intralimb coordination plots were also simplified, particularly when looking at the Hip-Ankle. (Figure 2-6) Plots that lie close to the $y=x$ or $y=-x$ diagonal reflect joint motions that are occurring more in sync with one another, as opposed to the more temporally complex pattern of joint motion seen in normal gait. Hip-Ankle coordination simplified significantly, with the two joints extending and flexing in unison for much of the gait cycle. Ankle-Knee plots showed a loss of the second co-extension phase with the ankle pre-extended before the knee begins extension. Sham and iSCI animals showed significantly different Hip-Knee and Hip-Ankle phase delays as well ($p<0.005$), confirming the qualitative assessment in the hindlimb intralimb coordination figures (Table 2-5). Forelimb intralimb coordination was unaffected by the injury, as expected. This was confirmed by the Shoulder-Elbow phase delay which showed no significant difference between groups. These data are also similar to those reported in [138] for rats two weeks post injury that received 5 days of electrical stimulation therapy.

PCA analysis quantified the complexity of movement for the entire hindlimb by assessing the three hindlimb angle trajectories for each individual animal's kinematics. Analysis was performed on the unaveraged joint kinematics of each leg of each animal and averaged together for each group (sham and iSCI). Each component's contribution to the overall variance of the hindlimb kinematics was compared between groups in Table 2-4. The only effect seen is a trend toward a decrease in complexity in the iSCI group. The lack of significance might be due to the small sample size and minimal impact to gait by the 4th week following a mild-moderate injury. The first components of the PCA analysis most likely

account for the gait cycle and the coordination between the flexors within the limb (and likewise the extensors) while the second and third components represent the intricacies of the joint trajectories. As the first component accounts for more and more of the variance, the three joints of the limb become more in phase with one another such that they could be controlled by a single neural signal.

Discussion

In this study, data were collected from a set of mildly injured rats in the chronic phase of recovery (4 weeks post-injury) where muscle atrophy was negligible, but significant locomotor impairments were still seen during walking. These impairments resulted in changes in kinematic complexity due to changes in neural control. The ankle specifically was particularly sensitive to loss of supraspinal control. No study to date has shown a decrease in kinematic complexity following incomplete spinal cord injury in rat, particularly when overall gait recovery was as complete as shown here. We also showed that changes in kinematic complexity were joint specific, indicating that different joints are under differing control in locomotion. Finally I collected musculoskeletal parameters from iSCI rats.

Lack of change in musculoskeletal parameters

Musculoskeletal parameters were collected to determine presence or lack of atrophy for iSCI rats four weeks post injury. Gregory et. al [149] looked at muscle disuse following complete transection injury in order to assess interspecies

differences between rats and humans, but only assessed fiber type changes, not atrophy. Liu et. al [150] compared cross sectional area of hindlimb muscles for 18 weeks following a contusion injury (BBB: 11.1). They showed muscle atrophy in all muscles for the first 3 weeks following injury, with a gradual return to pre-injury values starting at week four, with all muscles recovering by 12 weeks. As their injury level was slightly higher than in this study and a different strain was used (Sprague-Dawley), the minor difference in results is consistent with our findings.

In a study of contusion injured rats, Hutchinson et. al. [115] measured changes in muscle masses following injury. They used a higher level of injury (approximately 4-5 points lower in the BBB) and observed atrophy (~19%) in the gastrocnemius even 10 weeks post injury. In the current study, higher BBB scores were observed, indicating a lower level of injury. This led to weight bearing occurring a few days earlier, thus ameliorating the effects of the injury on muscle atrophy [151]. Also of note, the rats in the current study gained weight following injury, while the rats in Hutchinson et al.'s study lost weight, possibly leading to an increase in atrophy rate. When compared to a weight-matched set of sham controls, the muscle masses for rats in the current study are approximately 1% (TA) to 23% (soleus) greater than those reported by Hutchinson. This could be due to differences in strain. As mentioned earlier, muscle fiber type representation can change following injury, with percentage of slower fibers decreasing and percentage of faster fibers increasing [51]. However, as rat fiber types are predominantly fast to begin with [152], this effect should be minimal.

Of the muscles measured, only the soleus (a fairly small muscle) has a large proportion of slow fibers.

Other studies have examined atrophy in different experimental paradigms. In a 2 week hindlimb unloading experiment, significant (41%) atrophy was seen in the soleus, a slow twitch muscle, while a smaller decrease (18%) was seen in the extensor digitorum longus [153]. While the course of this experiment was shorter, the unloading paradigm represents a more severe disuse paradigm than our contusion injury. Also, the effects were more prominent on the slow muscles, of which the soleus is the only member in the rat hindlimb [152].

Changes in locomotor coordination in absence of atrophy

Along with the lack of muscle atrophy, a loss of complexity in gait following injury was identified. PCA analysis indicated that iSCI animals had slightly more coordinated flexion and extension phases in the gait cycle, but this effect was small and was not statistically significant. PCA has not been applied in this fashion before, but the analysis technique could be an important tool to assess gait with higher levels of injury or larger sample sizes. However, the analysis could be complicated by the fact that the 3 joint trajectories are from a single animal and the results may appear different than those used in other types of PCA analysis of joint kinematics where each joint (hip, etc.) is assessed independent from one another [144].

In the intra-limb coordination plots (with the exception of the Knee-Hip plot), the waveforms appear to collapse to a diagonal in the injured animals, implying that

the joint motions for injured animals become coordinated around just two control signals (flexion and extension) as seen in stroke[126]. This is most noticeable in the Ankle-Hip plot. Lack of complexity in injured animals is also supported by the hindlimb phase delay data, which showed a decrease in phase delay in the Hip-Ankle in the iSCI animals; the peaks of the two angle trajectories came closer to one another in time. Ankle and knee joints, however, became more out of phase with one another following injury. This change may have counteracted the decrease in phase delay between the hip and ankle when using PCA. Thus the decrease in phase delay between the hip and ankle (which would indicate a decrease in complexity in the PCA) was counteracted by the increase in phase delay between the ankle and knee (which would indicate an increase in complexity in the PCA).

The overextension of the ankle observed in this study is likely directly due to the loss of supraspinal control following injury[87]. However, as the locomotor system attempts to maintain similar foot position when re-establishing gait[154], compensation must take place at the other joints. Knee-knee angle plots show a symmetric, consistent pattern following injury so it is likely that the knee compensates for ankle overextension. EMG data from normal rats indicate that a second burst in knee extensor muscles during the last part of stance may be, in part, responsible for development of propulsive force[88]. The absence of normal late-stance knee extension in injured animals could indicate that the injury caused loss of muscle strength or alternatively, the loss of a second peak in EMG activity of knee extensors. As iSCI animals in this study did lose the second peak but did

not have muscle atrophy, this loss of kinematic complexity is most likely due to loss of supraspinal control (the loss of the second EMG burst) and not loss of muscle strength. Finally, as indicated in Figure 2-4, the overextension in the ankle and lower range of motion in the knee tended to counteract each other, indicating that remaining impaired control signals to the hindlimb can be used to establish correct foot position.

The cruciform pattern seen in intralimb coordination (Figure 2-5) is not unique to this study. In Jung et. al. 2009, rats were given the same level of injury as reported in this study. One week following the injury they were given 5 days of patterned electrical stimulation to the hip muscles in order to produce a locomotor pattern at the hip. 3D kinematics were then collected 14 days post injury (dpi). In both the current study and Jung, BBB scores indicated that the animals were nearly recovered; however, the animals permanently altered their gait as indicated by kinematics. The post-therapy animals developed a cruciform pattern in the Knee-Knee angle plots [138](14 dpi, 7 days post therapy) similar to that observed in the iSCI animals in this study at 28 dpi, suggesting that the stimulation therapy accelerated recovery following injury. While this pattern was greatly different than that seen in normal animals, the animals were able to reach the targeted treadmill speeds with ease. Along with this similarity was one in forelimb-hindlimb coordination. In both Jung and the current study, forelimb-hindlimb coordination shifted from approximately 50% out-of-phase to 100% out-of-phase. As this gait is stable and effective, it is a successful endpoint for locomotor recovery despite not matching pre-injury patterns.

Changes in hip control have been used to allow foot position to remain the same following SCI [155]. Hip range of motion was smaller in our studies than in other studies performed in similar conditions [88, 138]. This is likely due to changes in the position of the animal while the hip markers were applied. When the animal is on its side (as was done in this study), the skin tends to be closer to the spine than when it is in a walking position (as was used in the studies mentioned above), causing the markers to be closer to the floor than desired.

The changes to forelimb-hindlimb symmetry were also of note. In normal rats, the two limbs are approximately 25% out of phase with one another. This leads to the standard rhythmic walking pattern normally observed in rats. Following injury, however, the two limbs become completely out of phase with one another. This may also indicate a decrease in complexity.

Joint-specific changes in locomotor complexity

While PCA analysis did not prove a decrease in complexity in the whole limb kinematics, PE analysis of individual joint kinematics showed joint-specific changes in complexity. PE also showed itself to be a sensitive measure of gait. A relatively small change in PE at the ankle led to very large changes in ankle angles. While analysis of control of locomotion tends to focus on the joints as similar structures (i.e., receiving similar input from sensors, supraspinal sources, and the CPG [156]), the results of this study emphasize the importance of also considering specific roles for individual joints [157-159]. In general, all joints do receive similar input from all sources of locomotor control. A tonic drive from

the brain initiates gait and provides feed-forward adaptations to perturbations [2, 160]. The CPG and pattern shapers produce the basic profile for gait [7].

Sensory information from muscles spindles, Golgi tendon organs, and cutaneous receptors modify the gait pattern [156, 161]. A number of specific aspects of gait are less general than this however, with each joint being affected differently by feed-forward supraspinal control or reflex sensory input during different phases of the gait cycle. Data from guinea fowl show a proximal to distal gradient in neuromechanical control; proximal muscles use more feed-forward control and the distal muscles less [158].

The stance-to-swing transition has been extensively studied and shown to be controlled by hip flexion [162] and ankle force [159]. The significant role of hip position in control of gait is possibly why there is very little change in the hip kinematics. It is mostly sinusoidal to begin with (quite simple) so any changes would have large effects on the rest of the limb. A biphasic hip cycle, for instance, could lead to premature swing initiation.

Ankle muscle amplitude is as much as 70% controlled by local sensors [163] which may be even greater when supraspinal control is decreased [164]. This may be due to a very high proprioceptive gain in the ankle muscles [165, 166]. Due to the high reliance of the ankle on sensory input for motor control, the lack of significant muscle forces or cutaneous input during swing may contribute to the ankle flexor muscles (Tibialis Anterior) continued activation until the end of stance. This would lead to the lack of the normal end swing ankle extension as

was seen in the iSCI animals in this study. Studies in humans indicate that the ankle has little to no feed-forward control following incomplete injury while the hip still maintains a large feed-forward component [157]. In the absence of planned foot placement, the ankle stays flexed for the duration of swing and loses its second minima/maxima. This hypothesis is further supported by the type of injury sustained. As described in the surgical methods for the experiment, the contusion injury applied to the animals strikes the dorsal surface of the cord. This leads to significant damage to the dorsal tracts [136]. In the rat, the primary dorsal tracts are the dorsal corticospinal tract, the fasciculus gracilis (trunk and hindlimbs) and the fasciculus cuneatus (forelimbs) [167, 168]. In rats, the corticospinal tract serves a very limited purpose, only directly controlling individual digit movements [169, 170]. However, it also serves to modulate lumbar stretch reflexes [169]. As the ankle is primarily controlled by local reflexes, damage to the dorsal corticospinal tract would lead to significant changes in ankle control.

As with the initiation of foot swing, the ankle tends to act as a controller for the hip, with ankle-foot loads modulating hip torques [157, 171]. In humans following iSCI, the ankle has little to no feed-forward control while the hip still has a significant amount (though both still have significant feedback control)[157]. The lack of feed-forward control at the ankle may serve a positive purpose. In guinea fowl, feed-forward planning for perturbations during overground locomotion has a more negative effect on gait than an unplanned perturbation [172].

The knee mostly functions to couple the hip to the ankle. It contains many multiarticular muscles, coupling it with the proximal and distal joints. Knee extensors are synergistic with ankle extensors and inhibit ankle flexors [173]. The knee-ankle synergy is further increased following stroke [174]. The knee contains functional neural connections to the hip as well. The extensors in the hip are coupled to the knee via the stretch reflex [175]. Changes in the knee joint angle excursions are then likely due to the changes in control of the other joints [176]. Brain-spinal interactions provide dynamic stability for motor control. Interruptions caused by the contusion are likely to also affect the regularity of the output from the intrinsic spinal CPGs that would affect kinematics at all joints [177]. Further investigations will thus be necessary to determine the actual control mechanism at play at each joint and the overall limb.

Conclusions

In this study, treadmill walking was used to assess locomotor capabilities. The data showed that changes in kinematic complexity were joint-specific, indicating that different joints are under differing control in locomotion. Specifically, the ankle showed a decrease in complexity of movement, likely due to its unique role in locomotion. The ankle showed only a modest decrease in complexity but this accompanied a large change in ankle angles showing the sensitivity of the PE measure for gait analysis. Animals in this study showed a complete lack of changes to measured musculoskeletal parameters. This may indicate that weight bearing within 6 days following injury is sufficient to ameliorate the disuse-induced changes in the muscles.

Despite the injury, the animals do achieve stable and efficient gait, able to reach the desired 21 m/min speed used for data collection. Following the injury, communication between the hindlimbs and the brain is reduced and locomotor impetus shifts toward the local circuitry of the spinal cord and sensors. As such, a more primitive gait is unmasked. Despite these changes the animals were able to achieve locomotion that would look normal to the naïve observer. While rats may regain effective locomotion following injury, communication is never fully restored and thus the animal must adapt to use the local hindlimb circuitry for locomotion resulting in proficient gait. This data suggests that evaluation of hindlimb EMG and the timing of these signals may further demonstrate the loss of complexity in movement seen following injury, specifically at the ankle.

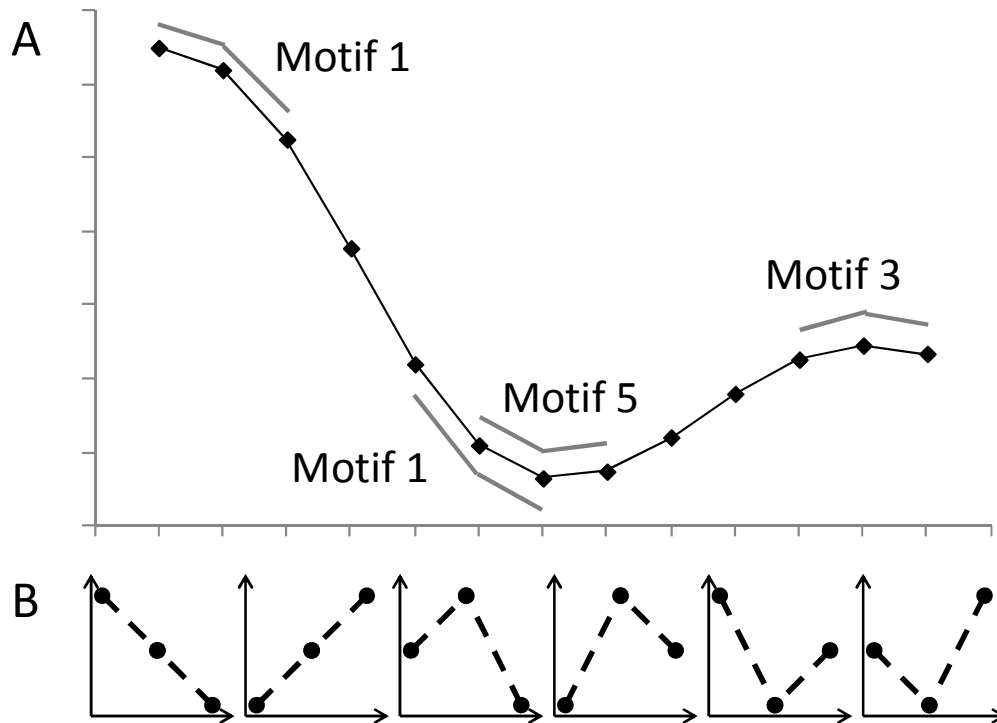


Figure 2-1 - Permutation entropy method.

Permutation entropy (PE) was calculated for both unaveraged hindlimb trajectories as well as cycle averaged trajectories for each joint angle. Permutation entropy quantifies the probability that a signal will remain similar from one segment to the next. Changes in the direction of the signal (positive to negative slope, for instance), indicate increases in complexity, while a steadily decreasing slope would indicate less complexity. A unitless number 0-1 describes the results, with higher values having higher complexity. The angle trajectories are segmented into 3 point motifs (A). The motifs are then classified in to one of 6 possible categories (B). PE is then calculated using the standard Shannon uncertainty formula.

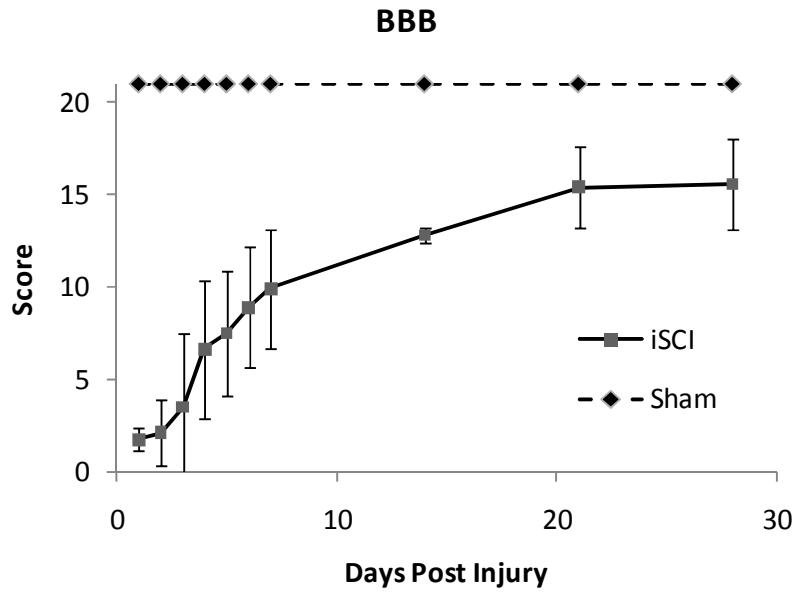


Figure 2-2 - Basso-Beattie-Bresnahan (BBB) locomotor scores for 4 weeks post injury.

Sham injured rodents had a score of 21 indicating no injury. The BBB score for the iSCI group increased from 2, at 1 day post injury and plateaued at approximately 15 indicating recovery of hindlimb weight support and forelimb-hindlimb coordination. Data are mean±SD.

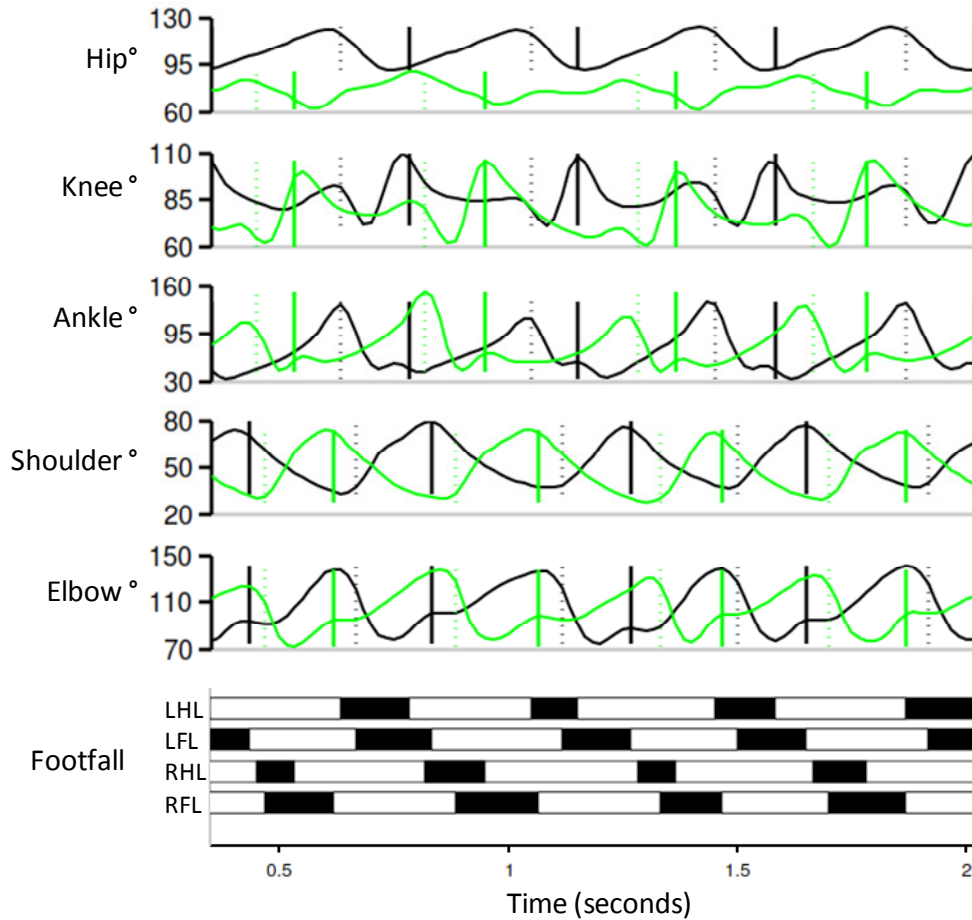


Figure 2-3 - Locomotor kinematics during treadmill walking in a contused rat.

Joint angle kinematics and footfall measures during treadmill walking from one contusion animal (T9 spinal level), 4 weeks post injury. The black traces are for the left limb and the green traces are for the right limb. The solid vertical lines are touch-down and the dotted vertical lines are lift-off. For footfall, the black sections represent swing and the white sections stance. LHL, left hindlimb; LFL, left forelimb; RHL, right hindlimb; and RFL, right forelimb. This animal is beginning to regain the second local maxima in ankle joint kinematics.

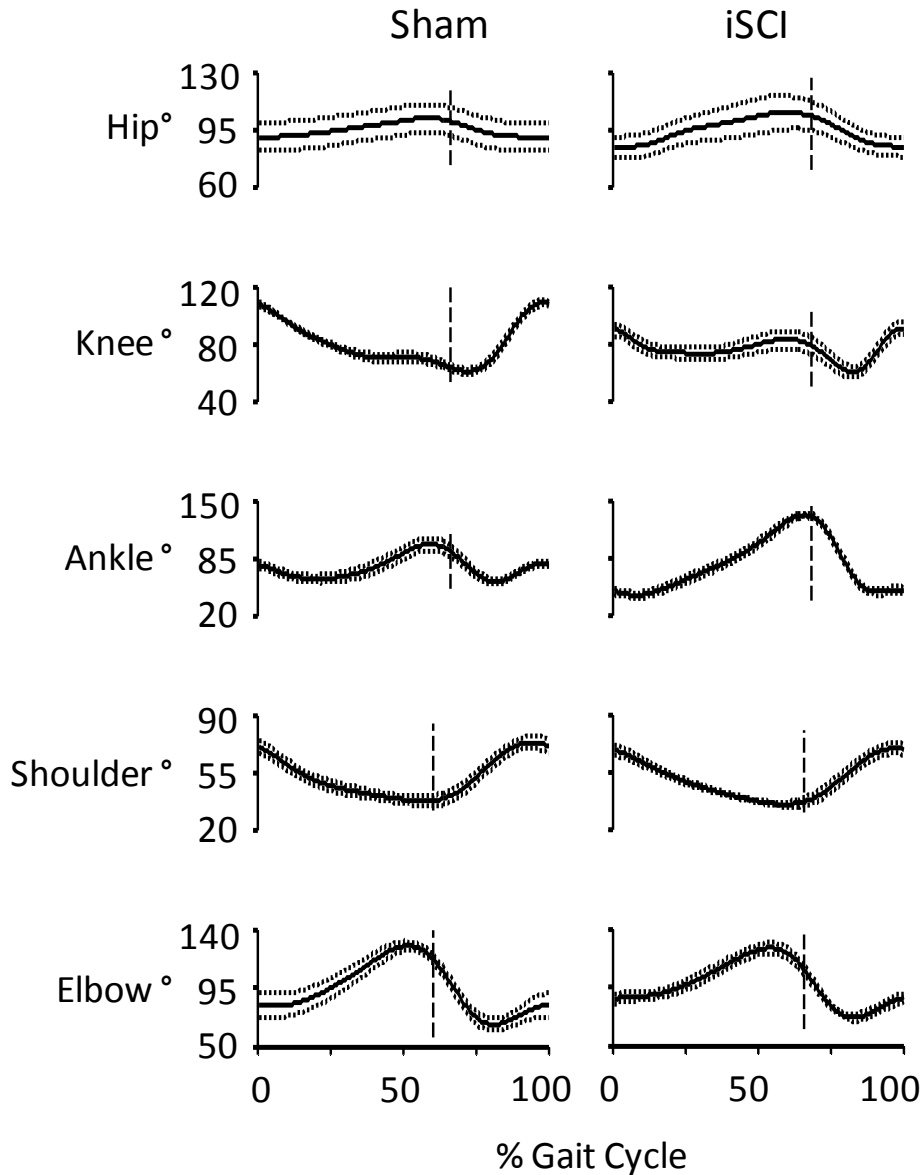


Figure 2-4 - Limb joint angles averaged across all cycles per animal.

Range of motion in the hip and ankle was greater in the iSCI group, particularly in the ankle due to overextension toward the end of the stance phase. Additionally, the angle trajectory of the iSCI animals shows one instead of two local maxima as seen in the sham group. The second local maximum is a result of pre-activation of the gastrocnemius in preparation for touchdown. As expected, forelimb trajectories are mostly unchanged following injury. Data are mean \pm SEM degrees, $n=5$ per group. Vertical line indicates lift off.

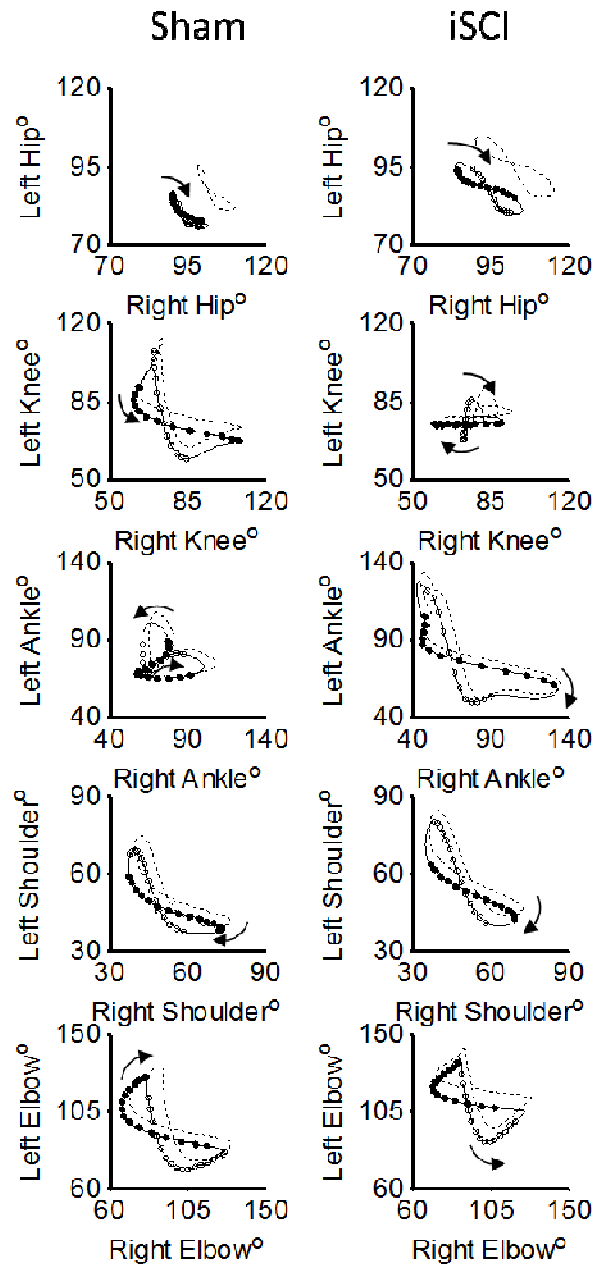


Figure 2-5 - Interlimb coordination during locomotion.

Left-right coordination plots for sham and incomplete spinal cord injury (iSCI) groups. Following injury, symmetry is maintained about the diagonal. Ankle-Ankle plots are simplified due to weakened control signals to the distal joint and the loss of the biphasic nature of the joint angle kinematics. Knee-Knee plots show a cruciform pattern where one side is moving only when the contralateral side is not. Forelimb coordination is mostly unaffected by the injury. Lines are mean (solid) plus SEM (dashed). Circles mark a time spacing of 8.33 ms with solid indicating stance and open indicating swing. $n = 5$ per group.

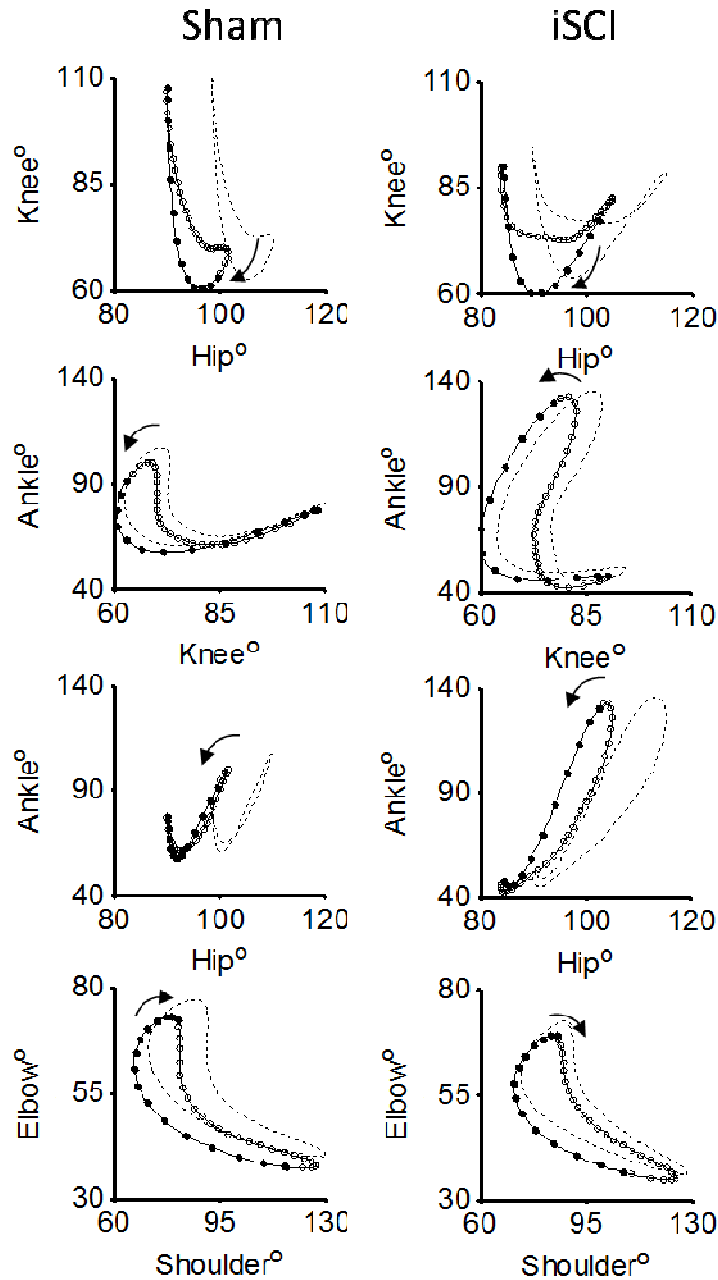


Figure 2-6 - Intralimb coordination during locomotion.

Intralimb joint-joint coordination plots for sham and incomplete spinal cord injury (iSCI) groups. Forelimb intralimb coordination is expectedly unaffected by the injury. Hip-Ankle coordination simplifies significantly with the two joints extending and flexing in unison. Ankle-Knee plots show a loss of the second co-extension phase with the ankle pre-extended before the knee begins extension. Lines are mean (solid) plus SEM (dashed). Circles mark a time spacing of 8.33 ms with solid indicating stance and open indicating swing. $n = 5$ per group.

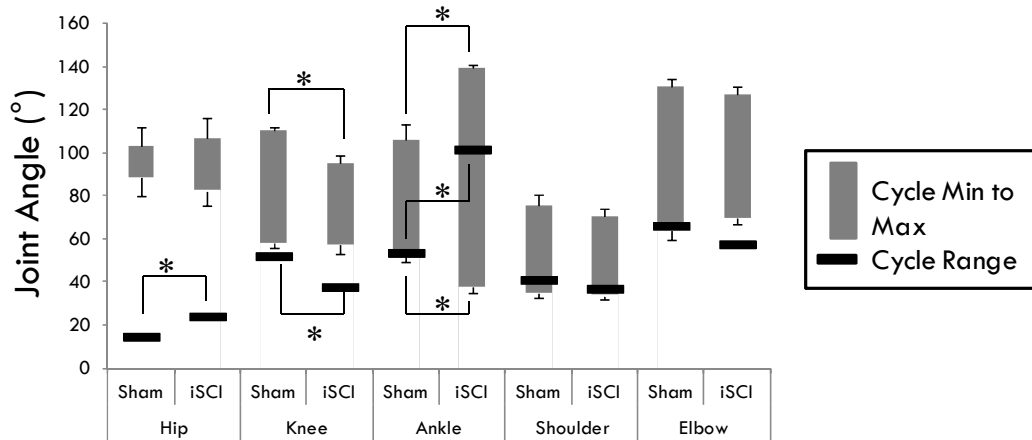


Figure 2-7 - Joint angle measures based on the whole gait cycle.

Joint angle values for cycle minimum, cycle maximum and cycle range for all measured joints for both sham injury and incomplete spinal cord injury (iSCI) groups. Large increases were noted in all measures at the ankle, particularly at cycle max (overextension) and in cycle range when comparing iSCI to sham animals. The range of motion and cycle max for the knee were decreased in iSCI animals when compared with sham. Hip range of motion also increased. Mean±SEM degrees for 5 rats per group. (*) indicates $p < 0.05$.

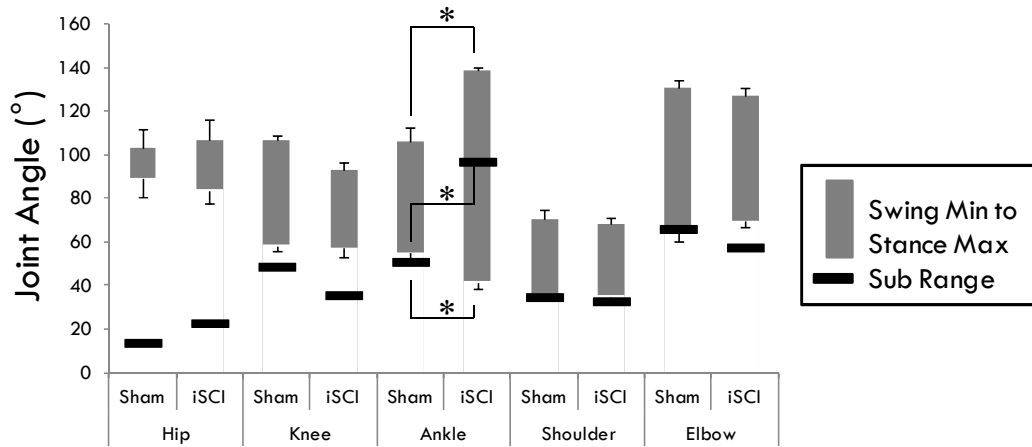


Figure 2-8 - Joint angle measures based on gait subcycles.

Joint angle values for swing phase minimum, stance phase maximum and subcycle range for all measured joints for both sham injury and incomplete spinal cord injury (iSCI) groups. Large changes were noted in all measures at the ankle, particularly in stance max (overextension) and subcycle range. No significant changes were noted at any other joint. Mean±SEM degrees for 5 rats per group. (*) indicates $p < 0.05$.

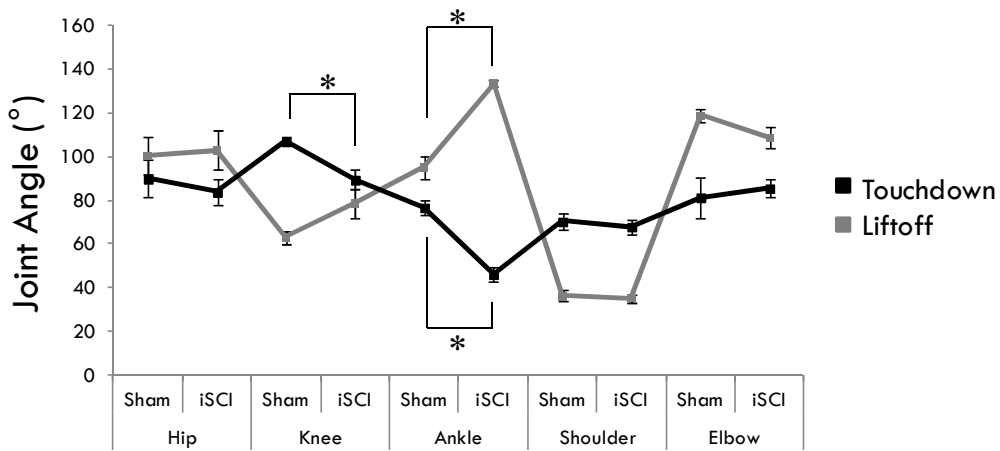


Figure 2-9 - Joint angle values at liftoff and touchdown.

Joint angle values for liftoff and touchdown for all measured joints for both sham injury and incomplete spinal cord injury (iSCI) groups. In the sham animals, knee angles values at liftoff and touchdown are very different from one another and ankle angle values are very similar to one another. For iSCI animals, the opposite is true. Knee values become similar to one another and ankle values become vastly different. Mean \pm SEM degrees for 5 rats per group. (*) indicates $p < 0.05$.

Table 2-1 - Hindlimb muscle properties in sham and iSCI rats.

	Muscle Weight (g)		Pennation Angle (deg)		Fiber Length (mm)		Sarcomere Length (mm)	
	Sham	Contusion	Sham	Contusion	Sham	Contusion	Sham	Contusion
GM	0.80 ± 0.10	0.82 ± 0.10	29.7 ± 9.0	23.3 ± 5.6	10.63 ± 4.53	7.77 ± 0.62	1.99 ± 0.15	2.12 ± 0.23
GL	1.24 ± 0.20	1.18 ± 0.11	31.0 ± 7.4	27.3 ± 7.6	10.92 ± 6.57	9.93 ± 2.36	2.03 ± 0.07	2.10 ± 0.19
SOL	0.18 ± 0.03	0.18 ± 0.02	24.3 ± 11.2	21.0 ± 1.4	9.81 ± 3.04	8.69 ± 3.70	2.23 ± 0.11	2.14 ± 0.23
TA	0.69 ± 0.06	0.66 ± 0.03	32.3 ± 11.6	26.3 ± 9.0	13.32 ± 3.16	11.72 ± 3.98	2.24 ± 0.32	2.07 ± 0.25
VL	1.13 ± 0.09	1.22 ± 0.13	28.9 ± 4.6	27.3 ± 6.6	12.78 ± 1.08	13.67 ± 2.21	2.09 ± 0.06	2.09 ± 0.39
VM	1.60 ± 0.08	1.51 ± 0.17	21.8 ± 17.9	22.5 ± 3.5	11.96 ± 4.21	14.76 ± 2.63	2.24 ± 0.40	2.18 ± 0.06
RF	0.88 ± 0.15	0.86 ± 0.07	27.3 ± 2.1	34.2 ± 4.3	8.25 ± 1.59	8.19 ± 1.87	2.02 ± 0.19	1.95 ± 0.15
ST	1.28 ± 0.23	1.22 ± 0.27	0.0 ± 0.0	0.0 ± 0.0	29.96 ± 3.49	26.18 ± 5.15	2.12 ± 0.18	2.05 ± 0.14
BFk	2.09 ± 0.33	2.12 ± 0.27	0.0 ± 0.0	0.0 ± 0.0	26.92 ± 1.70	22.45 ± 3.69	1.99 ± 0.17	2.03 ± 0.16
BFh	1.02 ± 0.24	0.90 ± 0.16	0.0 ± 0.0	0.0 ± 0.0	25.87 ± 9.85	22.70 ± 5.77	2.01 ± 0.09	1.94 ± 0.17

Muscle weight, pennation angle, fiber length and sarcomere length were obtained for Gastrocnemius Medialis (GM), Gastrocnemius Lateralis (GL), Soleus (SOL), Tibialis Anterior (TA), Biceps Femoris-hip extensor (BFh), Biceps Femoris-knee flexor (BFk), Semitendinosis (ST), Vastus Lateralis (VL), Vastus Medialis (VM), and Rectus Femoris (RF). Statistically significant differences were not observed for any measures between groups, suggesting absence of muscle atrophy. Standard deviation was also similar between groups for all measures. Data are Mean ± SD, n=5 per group.

Table 2-2 - PE analysis of joint angles

Unaveraged	Hip	Knee	Ankle	Shoulder	Elbow
sham	0.61 ± 0.07	0.58 ± 0.05	0.65 ± 0.01	0.55 ± 0.04	0.57 ± 0.04
contusion	0.57 ± 0.08	0.64 ± 0.02	0.57 ± 0.04	0.54 ± 0.02	0.56 ± 0.05
p-value	0.31	0.004 *	<.0001 *	0.63	0.91
Averaged					
sham	0.39 ± 0.01	0.38 ± 0.01	0.41 ± 0	0.37 ± 0.01	0.38 ± 0.01
contusion	0.39 ± 0.01	0.40 ± 0.01	0.38 ± 0.01	0.37 ± 0	0.36 ± 0.01
p-value	0.84	0.26	0.0006 *	0.78	0.25

Permutation entropy for unaveraged limb trajectories (5-12 cycles per animal, n=6 per group; Mean±SD) and averaged trajectories (n=5 per group; Mean±SEM). Higher values indicate higher complexity. (*) indicates p<0.05.

Table 2-3 - PCA analysis of hindlimb joint angles

	Sham	iSCI	%change	p-value
%1st	63.9	66.1	-2.3	< 0.1083
%2nd	28.7	27.6	1.1	
%3rd	7.4	6.3	1.2	

Percent of variance accounted for by all three principal components. n=5 per group

Table 2-4 - Phase delays for inter- and intralimb coordination

	HKnee	HAnkle	SElbow
Sham	0.22 ± 0.01	0.13 ± 0.01	-0.18 ± 0.01
iSCI	0.14 ± 0.01 *	0.03 ± 0.01 *	-0.16 ± 0.01

	RHL_LHL	RFL_RHL	LFL_RFL
Sham	0.51 ± 0.01	0.75 ± 0.07	0.48 ± 0.02
iSCI	0.54 ± 0.02	0.55 ± 0.03 *	0.51 ± 0.05

Phase delays are represented by proportion (0-1) of gait cycle out of phase. Phase values are calculated as lead (positive value) or lag (negative value) of the maximum flexion or touchdown for the second item with respect to the first item. HKnee, hip to knee; HAnkle, hip to ankle; SElbow, shoulder to elbow; RHL_LHL, right hindlimb to left hindlimb; RHL_RFL, right hindlimb to right forelimb; and LFL_RFL, left forelimb to right forelimb. Mean±SEM for 5 rats per group. (*) indicates p<0.05 when compared with sham.

Chapter 3

EFFECTS OF SPINAL CORD INJURY INDUCED CHANGES IN MUSCLE ACTIVATION ON FOOT DRAG IN A COMPUTATIONAL RAT ANKLE MODEL

Introduction

During locomotion, ankle muscle activation helps forward propulsion, body support, and accelerating the leg forward during early swing [178]. Changes in ankle load are associated with modulation of hip torque [157, 171] and contribution to the initiation of the stance-to-swing transition [179-181]. Studies in cats have shown that ankle extensor afferents may excite other extensors in the limb [182]. Hence, understanding the mechanisms for control of the ankle joint could also provide insight about hindlimb coordination [183].

Following spinal cord injury (SCI), depending on the severity of the injury supraspinal control of neural cells and circuits distal to the injury is eliminated or altered. The loss/alteration of supraspinal drive changes lumbar motoneuron output and the consequent aberrations in muscle activation patterns result in a decrease in locomotor capabilities [184]. Associated with the severity of the injury, a number of different locomotor impairments can be observed, including those at the ankle [84, 138, 185]. The ankle is particularly important as its kinematics are more affected following injury than any other hindlimb joint in the rat (See Chapter 2 of this dissertation). Among the possible impairments

following injury is foot drag (foot drop), where the foot does not clear the ground during the swing phase of walking [138, 185-187].

In humans, a number of devices have been used to decrease foot drop following incomplete SCI (iSCI). Function electrical stimulation (FES) of the common peroneal nerve (ankle dorsiflexion) has been used to increase walking speed and decrease drop foot [188]. FES of the plantar flexor muscles has been used to increase gait speed following iSCI as well as assist in foot clearance of obstacles such as pavement curbs and stairs [189]. Mechanical devices such as ankle-foot orthoses have also been used for assistance in ambulation for those with drop foot [190]. This has led to the ankle being used as a target for research looking at motor control following SCI [121].

Changes in ankle muscle coordination following iSCI could be responsible for foot drag. iSCI can cause changes in the relative timing of flexor and extensor activations as well as changes in the overall shape of the activations [185, 191]. In a study in rats [185], electromyography (EMG) of the ankle of normal animals showed a roughly rectangular activation profile and an activation delay of about 40 ms between termination of the gastrocnemius medialis muscle burst and the initiation of its antagonist (tibialis anterior) muscle burst. Following iSCI however, the activation profile of the gastrocnemius (primary ankle plantarflexor) began with an initial high burst followed by a gradual decrease and a smaller or nonexistent gap before the initiation of the tibialis anterior (primary ankle dorsiflexor) burst. These changes in coordination have opposing effects. The

decrease in the gap of activation (activation delay) between the two muscles may decrease net ankle torque at the stance-to-swing transition by allowing the residual force in the stronger muscle (the gastrocnemius) to overpower the smaller tibialis anterior. This would increase the likelihood of foot drag following injury. The change in activation shape of the gastrocnemius may decrease this effect, however, by slowly decreasing muscle activation thereby decreasing the residual force in the gastrocnemius when the tibialis anterior activates. This may result in increased ankle torque at the stance-to-swing transition, allowing the animal to regain foot swing (and prevent foot drag) following injury. Therefore, we wished to test the hypothesis that iSCI-induced alterations in muscle coordination consists of positive (adaptive) and negative (maladaptive) changes which may characterize the recovery of foot swing following injury. In order to do this, we constructed a computational model of the rat ankle based on experimentally collected data from normal and iSCI rats to assess the causes of foot drag.

A thoracic level incomplete spinal cord injury was used in this study. In such an injury (any injury to the spinal cord at the thoracic level), function of the arms (or forelimbs), neck, and breathing typically have no deficits. Control of trunk muscles is impaired as well as legs (or hindlimbs). Following the initial injury, secondary processes further damage the cord proximate to the injury site [192]. While the neurons distal to the injury are affected due to the change in their input signals, in many cases, they are not damaged directly by the injury [193]. The rat model of spinal cord contusion injury reproduces the local secondary injury effects of iSCI as seen in many human cases [76, 77] and the general course of rat

hindlimb locomotor recovery following has been well characterized using the Basso, Beattie, Bresnahan locomotor recovery score [84]. Recovery can come from a return to a pre-injury state or from compensatory changes in central control of locomotion resulting in a new gait pattern [194].

Along with these neural changes already discussed, the muscles in the distal limb can undergo changes similar to those seen in many disuse paradigms. The muscles tend to atrophy and muscle fibers shift towards faster twitch, more fatigueable ones [51]. If such changes are detected, they may alter the forces in the ankle joint.

A computational model could help us understand the mechanisms underlying the changes following injury. Using a standard rigid-body mechanics approach to model the bones, along with the applied muscle forces, we can simulate the biomechanics of the hindlimb. Muscles are typically modeled using Hill-type muscle models [101, 110, 195]. The force generating elements of Hill-type muscle models usually include the important Force-Length and Force-Velocity properties of muscles scaled to muscle activation level and maximal force output [102]. This data can be obtained experimentally and applied to existing models for mammalian muscles to create rat muscle models. Measurements of macro- and microscopic properties of muscles are related to their contractile properties [103]. Measurements of musculoskeletal geometry are necessary to determine moment arms for the muscles acting about the joints [196]. Musculoskeletal

models of the rat have been used before to elucidate control mechanisms following SCI [135].

Toward testing the hypothesis that iSCI induced changes in muscle coordination may affect the incidence of foot drag and contribute to foot swing recovery following injury, the goals of this study were: to obtain a set of rat musculoskeletal parameters, obtain rat locomotor kinematic data, and develop a physiologically relevant musculoskeletal model for use in examining the role of altered neural control in production of foot drag. A two dimensional (2D), one degree-of-freedom (DOF) ankle model with gastrocnemius (GAS, primary plantarflexor) and tibialis anterior (TA, primary dorsiflexor) muscles was developed. Since GAS can produce more ankle torque than TA (as GAS is a larger muscle with a similar moment arm), it is hypothesized that GAS activation delay and activation shape significantly affect the ability of the foot to transition from stance-to-swing. Our results suggest that even small changes in the ability to precisely de-activate muscles could lead to the foot drag commonly observed following SCI.

Methods

Study groups

Musculoskeletal and locomotor data were collected from 12 female, adult, Long-Evans rats (270-300g), 6 sham injured and 6 with a mild-moderate T8 vertebral (T9 spinal) spinal cord contusion injury. All rats were kept on a 12 hour light/dark cycle with ad libitum food and water. The study was approved by the

Institutional Animal Care and Use committee (IACUC) of Arizona State University and complied with the Guide for the Care and Use of Laboratory animals.

Surgical procedures

Rats were randomly selected to undergo either sham or mild-moderate contusion injury at the T8 vertebral (T9 spinal) level. Surgeries and contusions were performed similarly to Scheff et. al. 2003[136]. All animals were anesthetized under 1-2% isoflourane and given an injection of analgesic (buprenorphine, 0.02-0.05 mg/kg) for post-surgery pain. Using aseptic techniques, the vertebral process of T8 was removed and a U-shaped laminectomy was preformed. For animals in the contusion (iSCI) group only, T7 and T9 were clamped in place and a mild-moderate contusion (154 ± 3 kdynes) was preformed with a force controlled impactor (IH instruments). Following the contusion for the iSCI animals and the laminectomy for the sham injured animals, the muscles were closed in layers using resorbable sutures and the skin closed with wound clips (which were removed 1-2 weeks following surgery). Animals were then given 5 cc of sterile saline and 33.3 mg/kg of Cefazolin antibiotic and allowed to wake slowly on a heated pad.

Animal care post surgery consisted of twice-daily bladder expression until the animal was able to void on its own along with twice-daily injections of saline, buprenorphine and Cefazolin as above for the first 7 days following injury. Saline administration was continued if the animal remained dehydrated and antibiotic

administration continued an additional week if the animals showed signs of urinary tract infection from a urinalysis test strip. No animals showed signs of continued infection longer than 2 weeks. Following surgery, animals were allowed to move freely in their cages for 4 weeks. During this period, the Basso, Beattie, and Bresnahan (BBB) 21 point locomotor score [84] was collected on the animals every day for the first week and each week thereafter in order to verify injury severity. Rats were observed for four minutes by two experimenters, scoring hindlimb function according to the scale. Notable milestones of interest include motion in the leg, paw position, coordination, and weight support.

Ankle treadmill kinematics

Before surgery, all animals were allowed to acclimatize to their new environment for one week and trained to walk on a treadmill (Columbus Instruments) 2 days for 10 min each at a progression of speeds from 0-21 meters/min. 3D kinematic data was collected 4 weeks post injury on both sets of animals as in Thota et. al. 2004 [88]. Animals were anesthetized under 1-2% isoflourane, shaved, and cone-shaped reflective markers were attached to the bony prominences of the ankle (lateral malleolus) and knee (femoral condoyle) joints. In addition, a strip of reflective tape was placed around the fifth metatarsal of the hindlimb, close to its attachment. The markers were not spherical, as is desirable for centroid calculations, but their small size (approximately 5 mm) minimized any error. Video was recorded from 4 infrared sensitive cameras with co-localized infrared light sources, 2 on each side of the animal. Prior to data collection, a 36 point static calibration object was recorded and the animal was placed on the treadmill.

Treadmill locomotion was recorded at speeds starting at 11 m/min, increasing to 21 m/min in 2 m/min increments. The speed was increased each time the animal completed at least 5 continuous stable step cycles (in the middle of the treadmill at a constant speed). The entire process took approximately 5-10 minutes per animal. Data collection was completed on the following day if the animal was unable to achieve consistent locomotion at all treadmill speeds on the first day.

The video was imported into Vicon Peak-Motus® software for analysis. The calibration object was digitized for odd and even (a total of 2) fields. A segment containing at least 5 stable step cycles at 21 m/min was identified and imported. The video segments from the four cameras were manually synchronized using timestamps. All reflective markers were digitized and the data was processed into ankle angle data versus time. Gait cycles were identified by marking lift-off (the first frame where the toe was not contacting the treadmill) and touchdown (the first frame showing the toe contacting the treadmill). 5-12 cycles per animal were averaged together to create the average profile for that animal. The animals were then further averaged across groups (sham and iSCI). All averaged cycles were computed as % gait cycle.

Musculoskeletal properties

Rats were euthanized under heavy anesthesia and the hindlimb was separated from the remaining tissue. Superficial muscles were removed and the hindlimb was mounted on a rigid frame (Figure 3-1A). Clamps were attached to the foot and pelvis. Tie wrap was used to hold the tail and spinal column. Suture was

used for additional support along the body. Tension was maintained along the axis of the leg to maintain stability in the absence of a clamp on the femur or tibia. Muscle attachment points for ankle muscles and visible bony prominences were measured using a custom designed probe consisting of a flat surface with 6 reflective markers and a coplanar sharp tip (Figure 3-1B). The location of the tip can be calculated from the locations of the 6 markers. The device was manufactured of aluminum according to precise specifications and the distances were verified with a calibrated digital caliber. Reflective surfaces apart from the markers were either covered with matte tape or sandblasted. For each measured point, the tip of the probe was held at the point of interest, with the smallest amount of pressure as not to deform the hindlimb setup, and two video cameras recorded 2 seconds (120 fields) of data. The same calibration object used in the kinematics testing was used for the 3D digitization. Video was collected directly into Vicon Peak-Motus® then digitized and pre-processed into 3D marker locations before exporting to MATLAB™ for tip calculations. For each visible combination of 3 reflective markers, the location of the tip was calculated using vector algebra. 3D tip location was calculated by averaging all three-marker calculations over all 120 fields. No more than 2 markers were obscured in any particular measurement. All points were then transformed into local coordinates systems as shown in Figure 3-1C. The foot coordinate system was defined by the following sets of axes: X: malleolus midpoint (0,0,0) to 2nd and 5th metatarsal midpoint, Y: X crossed with medial to lateral malleolus, and Z: X crossed with Y. The lower leg coordinate system was defined by the following axes: X: condyle

midpoint (0,0,0) to malleolus midpoint, Y: X crossed with lateral to medial condyle, and Z: X crossed with Y.

Following attachment point measurement, ankle muscles were carefully dissected to lactated ringer's solution. Measured muscles included tibialis anterior (TA), gastrocnemius medialis (GM), and gastrocnemius lateralis (GL). Dissected muscles were weighed after light dabbing to remove surface liquid and some muscles had their volume measured by displacement in a graduated cylinder. Volume measurements were used only to calculate muscle density. For 2 animals, the external tendon for both the GAS and TA was measured *ex vivo* with a digital caliper.

Following weighing, muscles were split along the belly and fiber pennation angle was measured using a goniometer and fiber length measured using a digital caliper. Individual fibers or fiber bundles were then dissected off and placed on a glass slide with a small hole in the center. A laser was then beamed through the fiber and the diffraction measured. Diffraction was converted to sarcomere length using the following equation. $d \sin \theta = n\lambda$ [147] where d is the sarcomere length, θ is the angle of diffraction, n is the diffraction order, and λ is the laser wavelength.

Differences in musculoskeletal parameters between sham and iSCI groups were analyzed using standard t-tests with $p < 0.05$. All statistical analyses were run in SAS (SAS institute Inc, Cary, NC).

Musculoskeletal model

An open-loop muscle dynamics model was developed to study the kinematics of the ankle during gait. An approach that combines procedures for developing Forward Dynamics models and Inverse Dynamics models was used. Forward dynamics models work in the order of natural events. Neural signals activate muscle models which generate forces and movements. In an inverse dynamics model, motion is assumed and muscle force and neural control are then inferred or predicted from the motion. Here, ankle kinematics from treadmill walking were used to generate muscle lengths, velocities, and moment arms about the ankle joint. Model muscles were activated to produce force based on EMG profiles for activation based upon the calculated lengths and velocities. Forces were converted into moments using the moment arms. Net ankle moments were then used as an outcome measure. As shown in Figure 3-2, this represents a method in between standard inverse and forward kinematics approaches. Both kinematics (as in inverse dynamics, open loop) and muscle activations (as in forward dynamics, closed loop) are used to drive the model. This way, using a smaller set of experimental data, we can make hypotheses about behavior.

A 2D, 1 DOF model of the rat ankle with one rotational degree of freedom was constructed in the SimMechanics add-on for Matlab™/Simulink R2009b. Figure 3-3A describes the geometry defined: ankle joint, and insertion and origin points for the gastrocnemius and tibialis anterior muscles. Ankle joint geometry was averaged from data collected from 7 animals. The geometry for both muscles included one origin and one insertion point with no via points. The via point for

the TA was used as its insertion for moment arm calculations with the fixed length between the via point and true insertion added in for muscle length calculations. Via points for the gastrocnemius origin were omitted as the knee and upper leg segment were lumped with the lower leg so the moment around the knee was excluded. The lower leg and the foot were each modeled as a single rigid segment connected by a single rotational degree of freedom for the ankle. Ankle motion was imposed to follow rat treadmill kinematics for one stance phase. Representative ankle kinematics from sham and iSCI rodents walking on a treadmill at 21 m/min were used (Figure 3-3C). During this simulated stance phase, muscle lengths and muscle moment arms with time were obtained. This completed the inverse dynamics portion. As motion is determined from kinematics, not muscle forces, gravity has no effect on this model.

The muscle models were constructed using Virtual Muscle 4.0.1 [103, 104] for Matlab™/Simulink R2009b. Virtual Muscle is a Matlab program that creates Simulink blocks which can be integrated with other Matlab and Simulink code (such as SimMechanics) to create a full musculoskeletal model. The Simulink muscle blocks have inputs for muscle length and muscle activation level (0-1) and output muscle force. The models are based upon cat data [197, 198], but each parameter may be modified based on data supplied by the user. The model is an expanded Hill-type model whose contractile element incorporates muscle force-length and force-velocity properties, scaled by muscle physiological cross sectional area (PCSA) and muscle specific tension. A standard Hill-type

contractile element is determined from the basic properties of muscle contraction as detailed in the basic equation:

$$F_m(t) = f(v) \cdot f(l) \cdot a(t) \cdot F_m^{max}$$

Where $F_m(t)$ is the force of the muscle at time t , $f(v)$ is the normalized velocity dependent force, $f(l)$ is the normalized length dependent force, $a(t)$ is the time varying muscle activation level (0-1), and F_m^{max} is the maximum isometric muscle force. The force-length relationship is roughly U-shaped with maximal force at the middle of the range of the muscle. The force-velocity relationship is a roughly negative sigmoid curve, with highest forces during eccentric contractions and lowest forces at highest concentric speeds [102]. Virtual Muscle uses the following simplified PCSA equation assuming a muscle density of 1.06 g/cm:

$$PCSA = \frac{\text{muscle mass}}{\text{muscle density} \times \text{fascicle length}}$$

F_m^{max} is then determined by multiplying PCSA by specific tension [199]. Parallel and series elastic components representing the passive properties of the muscle tissue are also included (Figure 3-4). The software utilizes default parameters for cat muscles published previously by the authors [197, 198]. The default specific tension value of 31.8 N/cm² was used [200]. Sample cat muscle model code for fast muscles was altered to include experimental data from the rat for muscle mass, fiber length, fiber pennation angle, and free tendon length (Table 3-3). Average rat sarcomere length (2.4 μm) was used from Burkholder and Leiber,

2001 [201]. Measured fiber lengths were converted by multiplying the ratio of relaxed sarcomere length (as measured with laser diffraction above) to average sarcomere length from Burkholder and Leiber, 2001 for each muscle before input to Virtual Muscle. Only one type of fast fibers was used because, while ignoring fatigue, both kinds of type II fibers have similar dynamics [202, 203]. The Natural Continuous recruitment model was used to increase computational efficiency. This model lumps multiple motor units of the same muscle fiber type together into a single unit in a way that approximates the discrete recruitment of motor units [104]. Elastic elements were modeled using a log/linear relationship as in [204]. Muscle in-series aponeurosis in the gastrocnemius was modeled by adding 2x (both ends) the cosine of the pennation angle multiplied by measured fascicle length L_0 (measured as fiber length above) to the external tendon measurement (geometric determination of the aponeurosis length). The TA was altered by doing the same, but only 1x as the TA contains little to no origin aponeurosis [205]. GAS was summed or averaged, where appropriate, from GM and GL. Muscle models were run using SIMULINK's ode4 Runge-Kutta fixed step solver with a 0.00001 s time step. The muscle models represent the forward dynamics portion. Muscles were activated using a variety of simplified neural drive profiles described below.

Simulation protocol

Ankle motion was first simulated using the skeletal model with imposed averaged treadmill ankle kinematics for sham and iSCI rats from this study (at 21 m/min). This converted ankle angles into muscle lengths and moment arms versus time.

These muscle lengths, combined with simulated neural drive patterns, were used to drive the muscle model to generate forces. The forces were converted into net ankle torque using the muscle moment arms from the skeletal model. One stance phase was simulated. Maximum net ankle torque was assessed for a 40 ms window at the stance to swing transition. The assessment window was limited to a small period around the stance-to-swing transition for the purposes determining foot swing as forces developed too late after the kinematic stance-to-swing transition would not help a foot that was already dragging. If this value was positive, the trial was defined to have foot swing, if this value was negative; the trial was defined to have foot drag.

Table 3-1 lists the parameters varied between trials: ankle kinematics, muscle activation latency, muscle activation shape, and muscle strength. In order to assess the effect of altered locomotion following injury, ankle treadmill kinematics that were input into the model were the averaged traces obtained from sham, and iSCI rats, and a hypothetical animal dragging its foot (Figure 3-3C) (ankle angle maintained at 155 degrees). Neural drive was simulated to be similar to EMG burst durations determined from literature values of intact Long Evans rats walking on a treadmill [88]. The TA burst was set at 88.5 ms in duration, starting 50 ms prior to initiation of foot swing in the kinematic profile. TA activation magnitude was set to decrease from 1 to 0.4 during the burst. The GAS burst duration was set at 253 ms with its start and end times defined by the muscle activation latency parameter. The latency between the end of the gastrocnemius activation and the beginning of the tibialis anterior activation was varied between

-10 ms (slight co-activation of the GAS and TA muscles) and 50 ms (a gap between TA and GAS muscle activations) in increments of 10 ms to show responses from co-activation through normal activation profiles. Muscle activation shape was varied by changing the gastrocnemius activation profile between rectangular (GAS activation at 1 for the entire burst) and trapezoidal (GAS activation magnitude decreasing from 1 to 0.5 during the burst) as seen in Figure 3-3B to assess the effect of activation shape. These two shapes are simplified forms of the activation profiles seen in Thota, 2004 [185]. Muscle strength was simulated by varying muscle mass between normal (100% each) and moderate iSCI (100%TA, 80% GAS.) [115] in order to study the effect of muscle atrophy due to iSCI.

Results

Locomotion measures indicate mild-moderate injury

As shown in Figure 3-5, sham injured animals all showed normal locomotion on the BBB scale following injury. Initial deficits seen in the iSCI injured animals recovered to and plateaued at appropriately 15 (indicating hindlimb weight support and consistent forelimb-hindlimb coordination) by 2 weeks. Note the early recovery of hindlimb weight support (BBB 8-13).

Averaged rat ankle treadmill kinematics normalized to gait cycle are presented in Figure 3-6. Mean \pm SEM (dotted lines) angle values are reported. The dashed vertical line indicates the stance-to-swing transition. In the sham animals, two local maxima are present. The first one is extension of the ankle through stance

phase; this one is present in the iSCI animals as well. The second local maximum is extension of the ankle in preparation of ground contact. Following iSCI, the ankle loses or minimizes the second local maximum in the curve. This is coupled with a greater range of motion of the ankle joint, particularly overextension near the end of the stance phase. More severe injuries can further alter the gait pattern, leading to irregular gait [81]. Additionally, nearly all forms of injured gait include hyperextension and hyperflexion of the ankle [78].

Musculoskeletal parameters show no difference between sham injured and iSCI rodents

Measured skeletal parameters for the ankle are included in Table 3-2. There were no significant differences between sham and iSCI groups in the musculoskeletal attachment points or joint centers. Table 3-3 summarizes all measured muscle parameters. There was no significant difference in muscle mass between the sham and iSCI groups. There was no significant difference between groups or muscles for sarcomere length, pennation angle, or fiber length. Both the GAS and TA had no measurable origin tendon. The insertion tendon for GAS was 10.4 ± 0.2 mm and for the TA was 14.6 ± 2.1 mm as measured in two sham and two iSCI animals. When adding in-series aponeurosis to the muscle model using the conversion presented in the Methods section, both muscles' fascicle maximum length was 1.60x the optimal length.

Computational model

Figures 3-7 and 3-8 show the results of all model simulations. In both figures, ankle moment is displayed against activation delay. The separate curves represent

the different combinations of factors tested in the model. Each point on each figure is the maximum net ankle moment during a 40 ms window centered around the stance-to-swing transition for a particular set of parameters. Figure 3-7A shows the net moment at the ankle joint obtained at different activation delays for a rectangular muscle activation profile. It examines the changes in these moments in the computational models that include kinematics for sham injury and iSCI injury under conditions mimicking no atrophy of muscles or moderate atrophy of muscle. The four lines representing these comparisons are: variations in muscle atrophy (none: solid versus moderate: dashed) and kinematic profile (sham: square marker versus iSCI: diamond marker). As activation delay decreases, the likelihood of foot swing decreases until foot drag is predicted. iSCI kinematics and, to some degree muscle atrophy, can counteract the effect of decreased activation delay to allow foot swing. Figure 3-7B shows the ankle moment obtained with a trapezoidal muscle activation profile. The same trend in activation delay is noted with the trapezoidal activation however, the values are all higher, with no drag cases. Finally, Figure 3-8 shows the net ankle moments obtained when simulating a drag kinematics profile with every combination of other factors (muscle activation profile and muscle atrophy). In the drag kinematic profile, for one step-cycle previous to the one being assessed, the foot was dragging. A summary of the specific net ankle moment at 0.04s (sham) and 0.01s (iSCI) activation delays is presented in the bar chart in Figure 3-9. For each change in parameter, there is a corresponding change in ankle moment at the stance-to-swing transition. All values increase as you move to the right, with the

combination of rectangular activation, sham kinematics, no atrophy and -0.01 s activation delay being the lowest; and trapezoidal activation, iSCI or drag kinematics, moderate atrophy and 0.04s activation delay being the highest. In all parameters except activation delay, increases in ankle moment are associated with iSCI-type values.

Decreased activation delay decreases likelihood of foot swing

In figures 3-7A, 3-7B and 3-8 for each set of parameters, decreasing activation delay reduces the net force at the stance-to-swing transition, and accordingly, the chance for successful foot swing (as you go from left to right on each line, the net ankle moment decreases). This effect is very minimal in the drag kinematics traces. As the gastrocnemius turns off later and later, there is an increase in overlap of torques produced by activation of the GAS and TA, decreasing the chance for successful foot swing. As the GAS is a stronger muscle with a longer moment arm than the TA, as the activity cycles for the two muscles become closer to one another, the extension caused by GAS activation tends to override the flexion caused by activation of the TA and prevent foot swing.

Trapezoidal activation profile increases chance of foot swing

When comparing figure 3-7A to 3-7B, changing the activation profile from rectangular to trapezoidal decreased the required activation delay for successful foot swing (On comparison of figure 3-7A to 3-7B all moments increase, allowing closer activation of the two muscles while maintaining foot swing). This is due to the gradual decrease in ankle torque provided by activating the GAS lowering its

force sooner and increasing the chance that activation of the TA can overcome the residual muscle force.

Muscle atrophy increases chance of foot swing

In each of figures 3-7A and 3-7B, muscle atrophy did not have an adverse effect on the likelihood of foot swing. All “no atrophy” cases (dashed lines) produce lower net moments than moderate atrophy (solid lines). In the case of moderate atrophy (80% GAS, normal TA), the chance for successful foot swing is increased in all cases as this atrophy profile shifts the torque ratio towards the TA, allowing flexion caused by its activation to more easily overcome the extension caused by activation of the GAS. This effect is not large however (each solid line is only slightly above its paired dashed line).

Injured kinematic profiles increase chance of foot swing

Comparing the net ankle moments obtained in simulations with kinematics from sham injured (square marker) and mildly injured (diamond marker) rats in Figure 3-7A and 3-7B, the kinematics of mildly injured animals did help increase the likelihood of foot swing (all lines with diamond markers are significantly higher than those with square markers). There is a similar effect when comparing the net ankle moment for kinematics from sham injured (Figures 3-7A and 3-7B, square markers) to severely injured (drag) rats (Figure 3-7C). This is due to the weaker position of the GAS on the force-length curve, allowing the TA to more easily generate enough force at the stance-to-swing transition to allow foot swing. Additionally, the drag kinematic profile overpowers all other variations in factors;

all four possible combinations with a drag profile are nearly linear in the figure, with no variation between any factor combinations.

Summary of all factors

The main effect of each factor is summarized in Table 3-4 (Muscle atrophy, muscle activation profile, muscle activation delay, and ankle kinematics). This is the effect of the factor alone, averaged across the levels of other factors, where a level of a factor is a value that factor can take on (such as rectangular and trapezoidal for activation profile). For this table, activation delay is collapsed to two physiological values, -0.01s (iSCI) and 0.04s (normal). The largest main effect is seen in kinematic profile, particularly sham-drag where using the drag profiles results in an average increase in net ankle moment of 0.56 N-cm.

Following that is sham-iSCI at 0.34 N-cm. This effect is due to changes in the length and velocity of the muscle. Activation delay has the next largest effect (0.33 N-cm). This effect is due to the residual force in the gastrocnemius muscle following termination of activation. This is one aspect of the forward dynamics modeling: muscle forces responding to activation level in a time appropriate manner. The closer the activations of the two muscles are, the larger the residual force. Activation profile and muscle atrophy have the next largest main effects, in order.

Discussion

We collected the necessary data to construct and test a 2D model of the rat ankle to assess the causes of foot drag following iSCI. As hypothesized, timing of

gastrocnemius muscle activation delay has a large effect on the likelihood of foot swing. Even slight variations in the shut-off time for GAS resulted in large variations in net ankle torque. Due to the characteristic patterns of muscle atrophy seen following injury, the resultant loss of muscle strength did not interfere with foot swing, it in fact assisted it. Muscle force-length properties dominated the effects of changes in joint kinematics. When ankle kinematics took on a more injured profile, the increased ankle angle near the stance-to-swing transition helped the TA-caused flexion to overcome the GAS-caused extension, thereby ameliorating foot drag. Finally, when assuming the foot had been dragging for the previous step cycle, foot swing was facilitated due to the weaker position of GAS on the force-length curve. Overall, changes in neural control (activation delay and activation profile) and kinematics had a larger effect than muscle atrophy.

In our model, we used a combination of inverse and forward dynamics to arrive at a behavioral prediction. Inverse dynamics was used to provide lengths and velocities to the muscles, while a forward dynamics method was used to drive the muscles to produce forces in response to these kinematic inputs and muscle activation. By using this method, we were able to simulate the model in the absence of information about body segment parameters and force platform data typically needed for a forward dynamics model. We were able to alter interesting parameters and see their resultant effect on the model outcome. Additionally, this method allowed us to ignore the complexities of foot contact and liftoff inherent in forward dynamics models. This technique of combining forward and inverse

dynamics has been used previously to avoid computational difficulties involved in initial contact simulations [206] and for efficiency of computation [207].

Open/closed hybrid models have also been used with success in control of [109] or improving optimization of [208] musculoskeletal models. Finally, simplified neural drive patterns were used in order to exaggerate the differences in muscle activation profiles. The model also does not include the passive properties of the rat ankle that have been recently reported [209]. These may affect the outcomes of the models quantitatively, but the trends seen will be sustained. As this model only simulated one step-cycle and only looked at the outcome at the stance-to-swing transition, the results cannot be extrapolated beyond that event.

In the absence of supraspinal input, forces at the ankle tend to synchronize muscle activity in the limb. As flexion and extension are synchronized [182], the delay between flexors and extensors of various limbs may be altered, including the decrease in activation delay at the ankle. The adaptation to trapezoidal activation profiles may take place on the scale of weeks as the rats return to coordinated walking. Initially, the forelimb-hindlimb gait pattern is uncoordinated (as seen in BBB scores) with the hindlimb adopting an alternating drag-swing pattern. As the shape of GAS activation adapts, the rats develop coordinated gait. This effect could be further studied by assessing muscle activation (EMG) in injured animals as they recover from iSCI.

Net ankle joint moment was used as an outcome measure for two reasons. First, at the stance to swing transition, the ankle is free hanging and any positive net

torque would contribute to foot swing. Secondly, joint torques reflect muscle strength [210], which is often an indicator of recovery. For example, Wirth et. al. 2009, in a voluntary contraction study with humans, indicated that muscle strength is more impaired than muscle control following injury [120]. However, the outcome measure used to identify control was time to maximal contraction which does not represent the same control scheme used during locomotion. They addressed this in another study where they mentioned that these results do not necessarily correlate with recovery of gait following injury [121]. As mentioned earlier, force in the ankle extensors has been implicated in control of the stance-to-swing transition [180]. In this case, muscle strength and control would be intertwined. Decreasing ankle extensor force due to decreased weight bearing or inability to generate maximal contraction following injury could lead to a decrease in afferent feedback. This may lead to a delay of the stance-to-swing transition. As the signal to initiate swing is delayed, the gastrocnemius burst is lengthened, and the GAS-TA activation delay is decreased. This may increase chance of foot drag.

Following iSCI, human subjects lose the ability to complete voluntary single joint movements and lose reciprocity between flexor-extensor pairs [122]. This may be due to alteration in circuits controlling coordination in the limbs, specifically those involved in flexor-extensor coordination [4], possibly allowing overlap in activation of agonist-antagonist pairs [194]. Our results suggest that this is not a compensatory mechanism for rats as such co-activation would result in the gastrocnemius activation overpowering the tibialis anterior activation and rats

would almost never see foot swing following a severe injury. This may be due to the biomechanical difference between digitigrade walking seen in the rat hindlimb and plantigrade walking used by humans.

While increased co-activation of agonist/antagonist pairs can be seen as a power loss for the joint, it can also be seen as an adaptive behavior to increase stability in that joint. In unimpaired human subjects, or in the unimpaired side of a stroke subject, co-activation at the ankle is normal and lends itself to stability [211]. However in a variety of sensory (proprioception) impaired individuals, stroke [174], SCI [212], aging [213], etc., co-contraction leads to a reduction in motor performance. As such, co-activation following SCI should not be seen as a positive adaptive behavior.

This model uses very simplified activation profiles to control the muscles in question. One extension of the model could be to include a more realistic control strategy involving a model of the spinal cord control mechanism for locomotion such as a central pattern generator (CPG) model or one involving multiple modeled neurons. The results of change in control strategy shown from this expanded model could be used to enhance control of an ankle prosthesis. Either supplementing ankle dorsiflexion while the gastrocnemius is active or attempting to limit gastrocnemius activation during late stance phase could be a useful strategy to employ. The model used in this study could be applied to either different populations (other types of rats, humans, etc.) or specific individuals within those populations to tailor their rehabilitation protocol. Using the Virtual

Muscle model and supplementing it with subject-specific or population-specific muscle parameters and geometry and presenting a simple torque balance, data-specific predictions about foot swing could be obtained. However, the muscle activation timing and profile have the greatest effect on likelihood of foot swing and accurate measurement of those values will have the greatest impact on the outcome measure.

Conclusions

From the combined results of the model it is hypothesized that rats may adjust the shape of their gastrocnemius activation (extensor) to compensate for the problems resulting from decrease in activation delay between the gastrocnemius and the tibialis anterior (flexor). In other words, they change their GAS activation profile from a rectangular one to a trapezoidal one in order to allow foot swing following injury. This suggests a time course of recovery of foot swing. Initially after injury, flexor-extensor coordination is impaired causing an irregular gait, with alternating foot swing and foot drag across the whole animal step cycle. As the animal recovers, it alters the activation profile of its gastrocnemius muscle as to slowly turn it off during its activation phase (adopting the trapezoidal activation profile) allowing it to regain foot swing despite continued intralimb coordination impairments.

Confirming our hypothesis, the musculoskeletal model revealed that movement dynamics are not equally sensitive to different aspects of neural output. Failure to precisely deactivate the gastrocnemius muscle could result in foot drag following

SCI. Although muscle activation is an important contributor to movement dynamics, intrinsic muscle properties also substantially affected motor output. Future models could examine the role of the stretch reflex, as it is known to change after SCI [214], possibly affecting foot drag as co-contraction is often an attempt to compensate for decreased stretch reflex signals [215]. One other possible explanation for foot drag may lie in the joints not modeled here. Work in cats has suggested that foot drag during treadmill walking may be due to impaired intralimb coupling between the hip and knee at the stance to swing transition [184]. Adding additional joints to future versions of the model may further determine the exact mechanism of foot drag. While not unexpected, the implication for human recovery of foot swing is that timing and control are more important than muscle strength following injury for foot drop. Purposefully weakening the ankle extensors to allow foot swing would not be a feasible rehabilitation plan and would likely have undesired consequences in other aspects of gait. Strengthening of the tibialis anterior muscles would also have limited success, as muscle strength was the weakest factor of those tested in this study. It would be impractical to make the tibialis anterior stronger than the gastrocnemius.

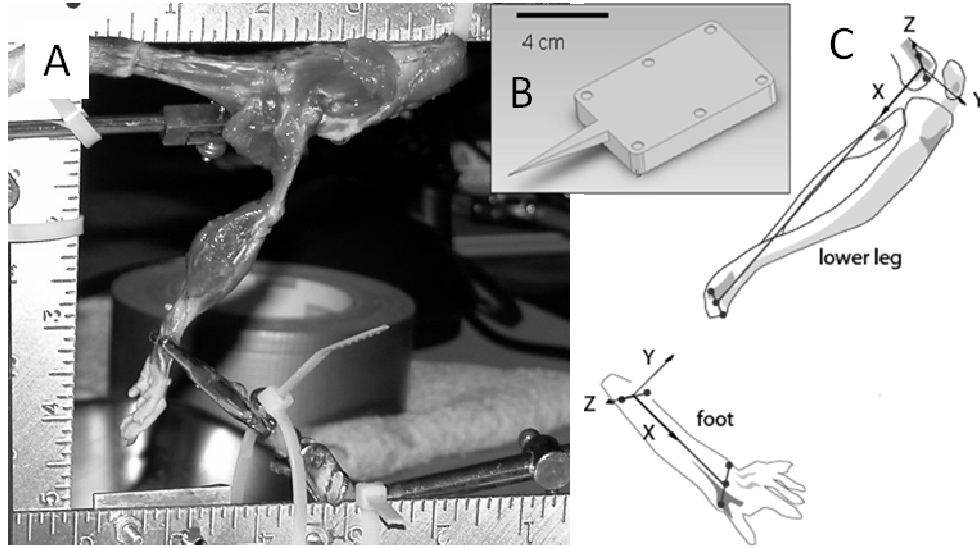


Figure 3-1 - Procedures for determining musculoskeletal geometry.

Musculoskeletal geometry was obtained from sham and iSCI rats four weeks following injury. *A*: Dissected hindlimb mounted for digitization. Clamps hold the pelvis and foot. A tie wrap hold the tail and the spinal column along with suture. Tension is maintained along the axis of the leg. *B*: Aluminum probe used to digitize points of interest. Numbered reflective markers are at each circle in the same plane as the sharp tip. Relative locations of the tip and markers were defined in manufacture and verified with a calibrated digital caliper. For each point of interest, the tip was held touching the point while marker positions were recorded via 2 video cameras for 120 frames. *C*: Coordinate system definition for skeletal geometry. Red dots show digitized locations of bony prominences used to establish axes for local coordinate systems. One coordinate system was used for each of the ankle and lower leg. The primary axis in each case was the proximal to distal one.

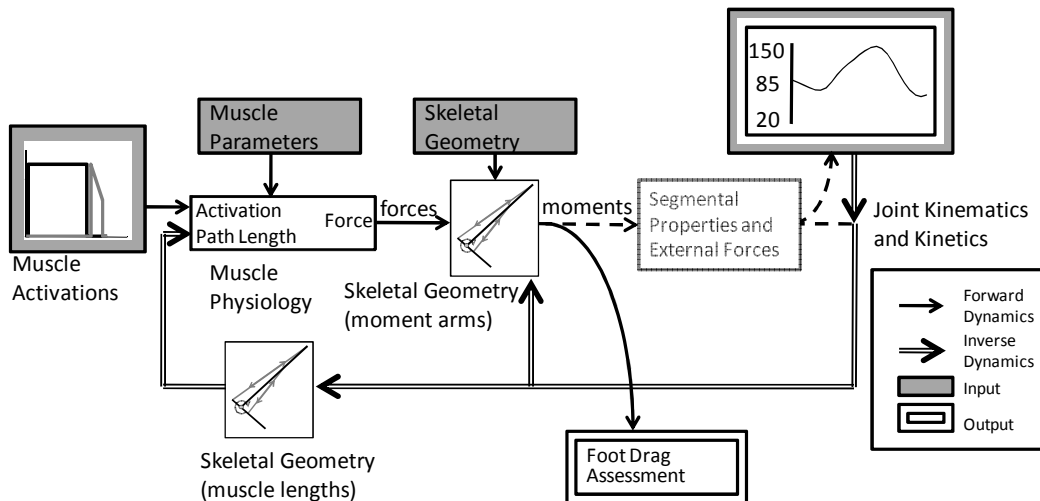


Figure 3-2 - Musculoskeletal model organization.

A combined forward dynamics and inverse dynamics approach was utilized for development of the musculoskeletal model. Muscle model Simulink blocks were formulated from base Virtual Muscle cat data, supplemented with collected rat musculoskeletal parameters. Muscles were driven by simplified neural drive profiles and ankle joint kinematics which were converted into muscle lengths using the experimental skeletal geometry. Muscle force output was converted into joint torque using dynamic muscle moment arms from the skeletal model. If net ankle torque was positive during a small window at the stance-to-swing transition of the selected kinematic profile, then the trial was determined to have successful foot swing. If the net torque was negative, then trial was said to indicate foot drag. Dotted lines indicate the unused portion of a closed loop system. By breaking the loop before converting moments into kinematics, we are able to make behavioral predictions in the absence of segment properties, ground reaction forces and numerical instabilities inherent to traditional forward dynamics simulations.

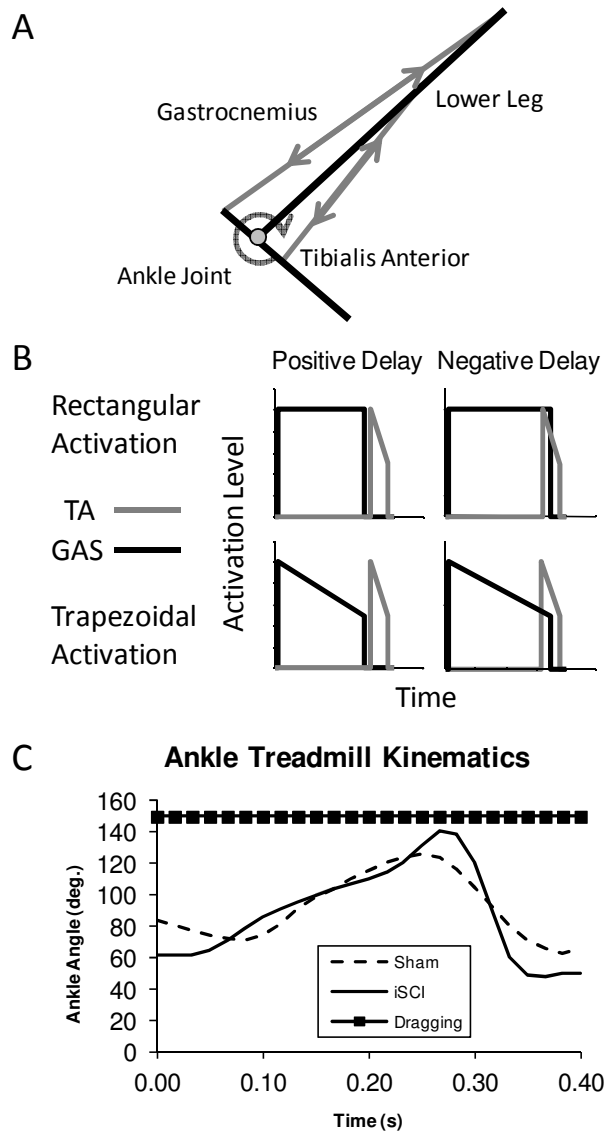


Figure 3-3 - Musculoskeletal model components

Musculoskeletal model structure and time varying inputs. *A*: Model includes lower leg fixed to ground attached to a foot with a single degree rotational joint. Gastrocnemius and tibialis anterior muscles are attached between the two segments. *B*: Muscle activation was varied between rectangular and trapezoidal profiles and the activation delay was varied from positive (a gap) to negative (overlap/co-activation) values. *C*: Ankle joint kinematic profiles for stance used to determine muscle lengths. Notice the overextension and lack for a second local minima in the iSCI trajectory. Dragging was a theoretical profile assuming that the foot had been dragging for at least one entire step cycle before the current foot swing attempt.

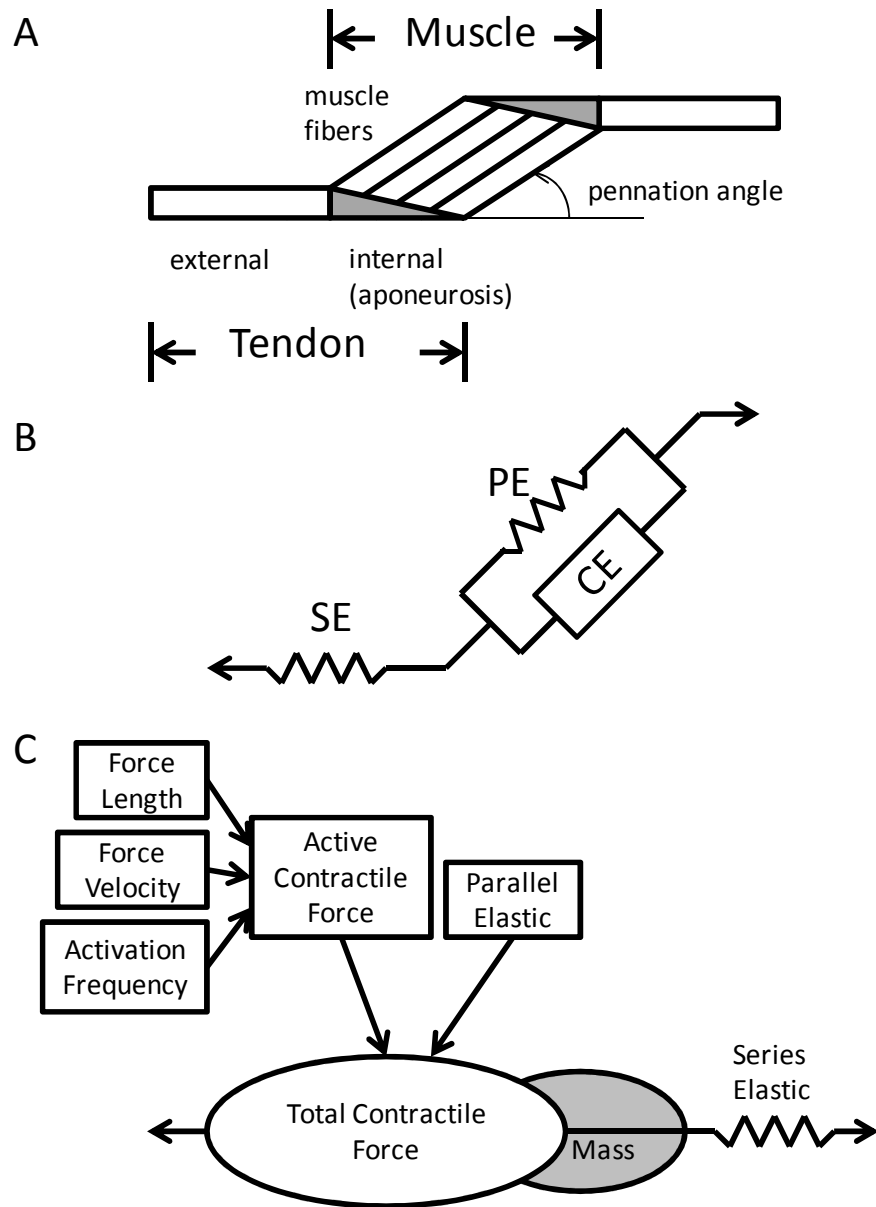


Figure 3-4 - Modified Hill-type muscle model

The muscle model is an expanded Hill-type model whose contractile element incorporates muscle force-length and force-velocity properties, scaled by muscle physiological cross sectional area and muscle specific tension. *A*: Physiological representation of the muscle. *B*: Schematic representation of the muscle. Parallel and series elastic (PE and SE) components representing the passive properties of the muscle tissue as well as a contractile element (CE) are included. SE is constructed from aponeurosis and external (free) tendon. *C*: Components that contribute to the contractile element model include contributions of length, velocity, and activation level.

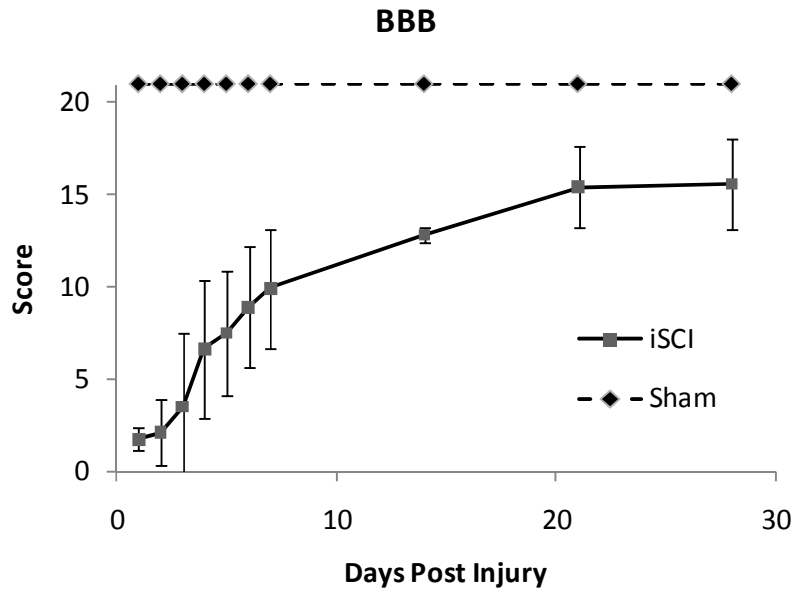


Figure 3-5 - Basso-Beattie-Bresnahan (BBB) locomotor scores for 4 weeks post injury.

Sham injured rodents had a score of 21 indicating no injury. The BBB score for the iSCI group increased from approximately 2 at 1 day post injury and plateaued at approximately 15 by day 21 indicating recovery of hindlimb weight support and forelimb-hindlimb coordination. Data are mean \pm SD.

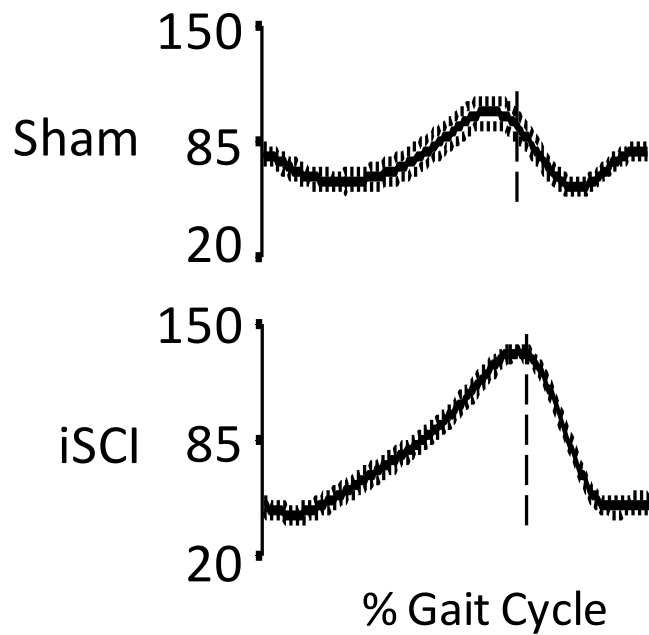


Figure 3-6 - Treadmill ankle joint kinematics

Averaged joint kinematics (in degrees) \pm SEM across the step cycle for n=5 animals in each group. Range of motion was increased in the iSCI animals, particularly in overextension in the ankle. Additionally, the trajectory is simplified, losing a second local minimum seen in the normal animals.

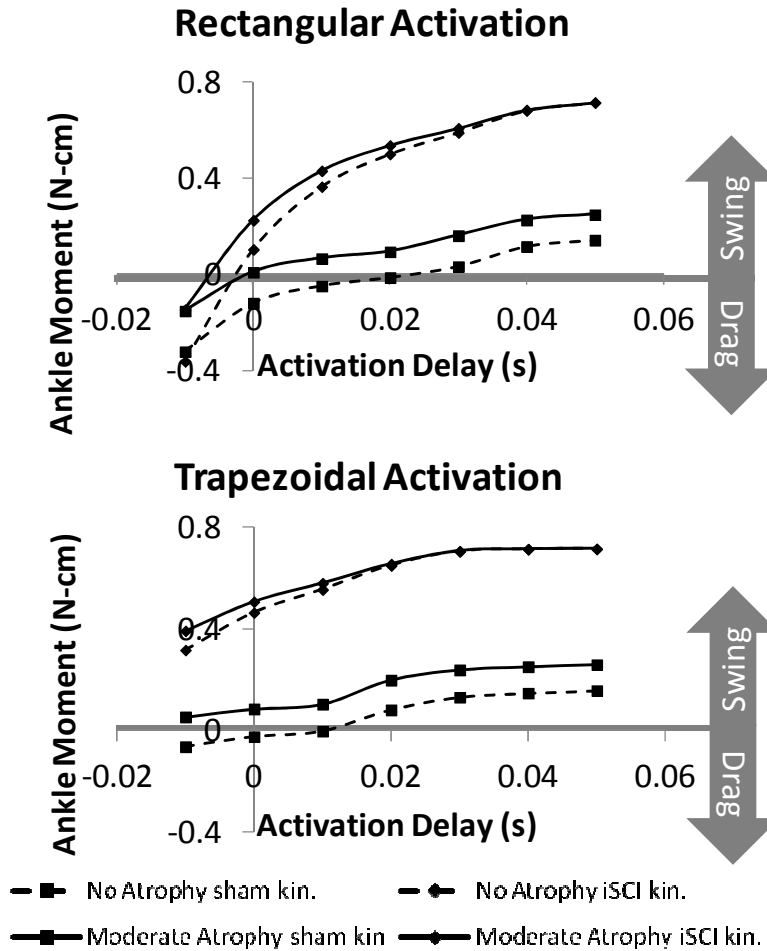


Figure 3-7 - Ankle moment at stance-to-swing transition: sham and iSCI kinematics.

Ankle moment is displayed versus activation delay. The separate curves represent the different combinations of factors tested in the model. Each point on each figure is the maximum net ankle moment during a 40 ms window centered around the stance-to-swing transition for a particular set of parameters. The four lines representing the parameters are: variations in muscle atrophy (none: solid versus moderate: dashed) and kinematic profile (sham: square marker versus iSCI: diamond marker). *A*: net moment at the ankle joint obtained at different activation delays for a rectangular muscle activation profile. *B*: ankle moment obtained with a trapezoidal muscle activation profile. As the activation delay is reduced following injury, the chance of foot swing is decreased. The change in activation pattern from rectangular to trapezoidal following injury counteracts the decrease in ankle moment to allow foot swing. Similar positive adaptations are seen for changes in kinematic profile and muscle atrophy representative of injured animals.

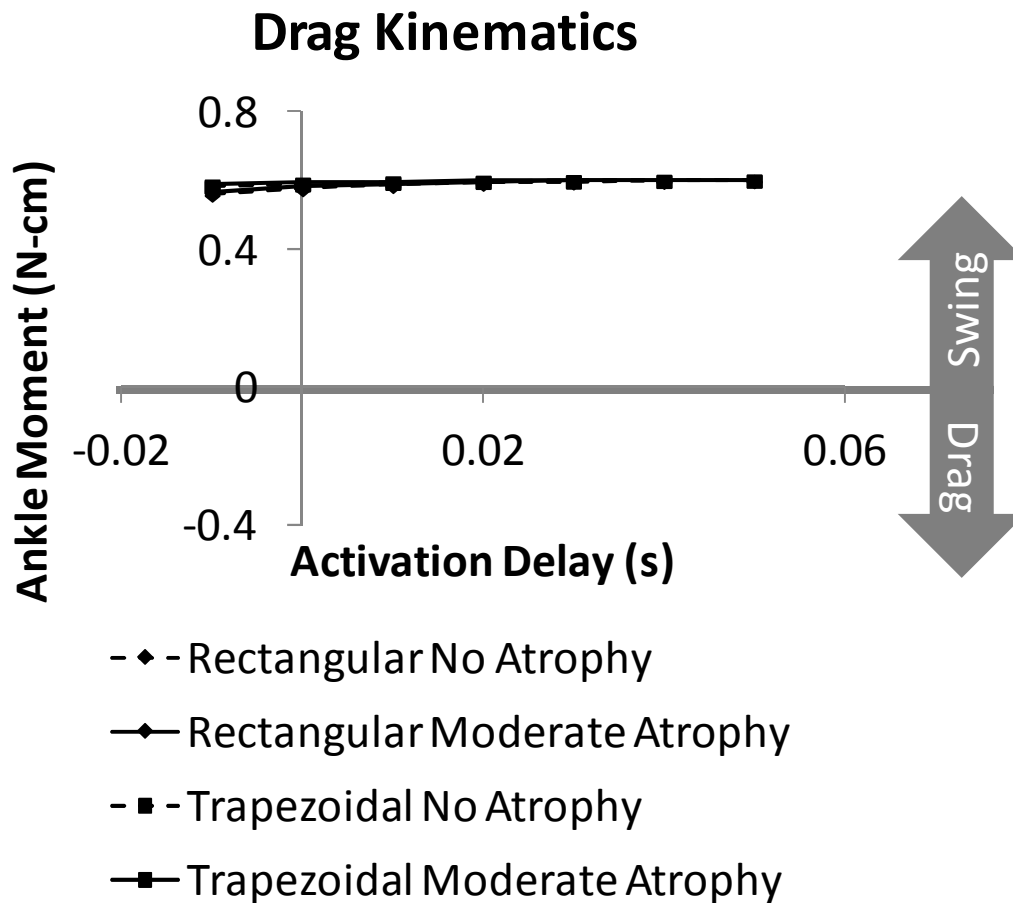


Figure 3-8 - Ankle moment at stance-to-swing transition: drag kinematics.

Ankle moment is displayed versus activation delay. The separate curves represent the different combinations of factors tested in the model. Each point on each figure is the maximum net ankle moment during a 40 ms window centered around the stance-to-swing transition for a particular set of parameters. The four lines representing the parameters are: variations in muscle atrophy (none: solid versus moderate: dashed) and activation profile (rectangular: diamond marker versus trapezoidal: square marker). Note the near similarity of each curve. As long as the animal was dragging its foot in the previous step, the following step should result in swing. This can lead to an alternating pattern where the foot drags in some steps and swings in others.

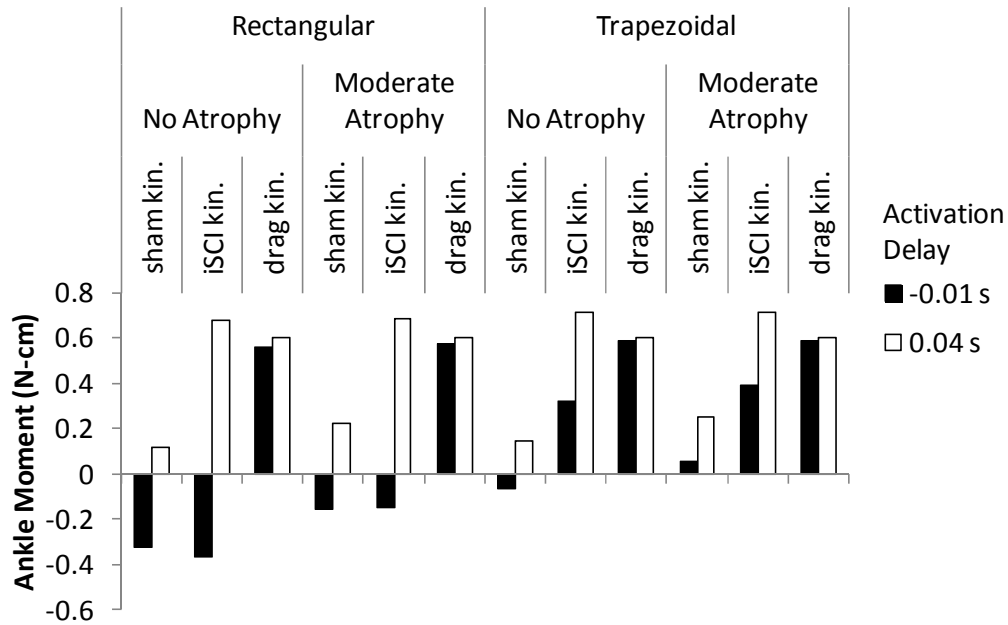


Figure 3-9 - Ankle moment for all combinations of model factors

Model results when activation delay is collapsed to two values, 0.04 s and -0.01 s. Values above 0 indicate foot swing while values below zero indicate foot drag. For each change in parameter there is a corresponding change in ankle torque at the stance-to-swing transition. All values increase as you move to the right, with rectangular activation, sham kinematics, no atrophy and 0.04 s activation delay being the lowest and trapezoidal activation, iSCI or drag kinematics, moderate atrophy and -0.01s activation delay being the highest. In all parameters except activation delay, increases in ankle moment are associated with iSCI-type values.

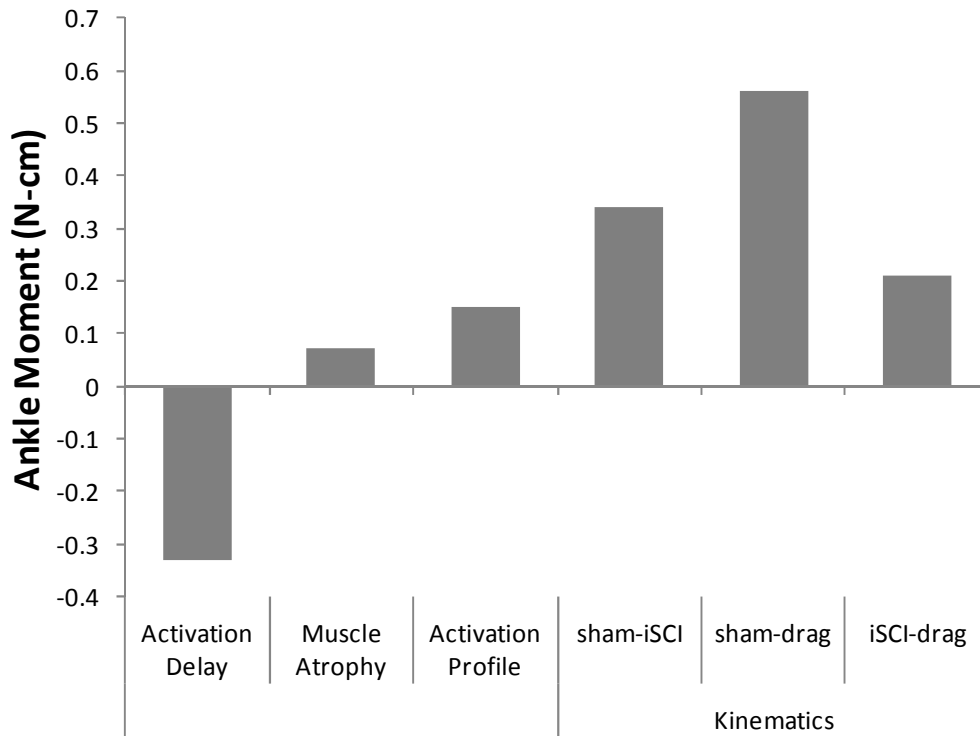


Figure 3-10 - Main effect of each model factor

The main effect is the effect of the factor alone, averaged across the levels of other factors, where a level of a factor is a value that factor can take on (such as rectangular and trapezoidal for activation profile). The difference in ankle moment cause by the change in level of that factor is summarized in this figure. Ankle kinematics tended to have the largest effect on foot swing, particularly the drag profile. Activation delay was the next strongest factor followed by activation profile and finally, muscle atrophy.

Table 3-1 - Simulation parameters

Parameter	Kinematic Profile	GAS Profile	GAS Activation Delay (ms)	Muscle Atrophy
	Normal	Rectuangular	-10 to 50	Normal
Value	Mild iSCI Dragged	Trapezoidal		Moderate iSCI

All variable simulation parameters. Kinematic profile describes the ankle kinematics used as an input in the model to determine muscle lengths, velocities, and moment arms. Normal and iSCI are data collected in this experiment while dragged is a hypothetical profile where the ankle was dragging in the step previous to the one being analyzed. GAS profile is the shape of the gastrocnemius muscle activation burst. GAS activation delay is the gap (or overlap if negative) between the end of the GAS burst and the beginning of the tibialis anterior burst (varied in 10 ms increments). Muscle atrophy determines the mass of the muscle being simulated.

Table 3-2 - Musculoskeletal geometry

	Point	Average X(cm)
Foot	Ankle	0.00 ± 0.00
	TA insertion	0.19 ± 0.16
	GAS insertion	-0.33 ± 0.08
Lower Leg	Ankle	-4.10 ± 0.10
	TA Origin	-0.50 ± 0.10
	GAS Origin	0.00 ± 0.00

Ankle joint is defined as (0,0), positive values are more distal. 3D position values were projected on to the single line segments. No significant differences were seen between groups. Values are mean ± SD.

Table 3-3 - Ankle musculoskeletal properties

	Muscle Weight (g)		Pennation Angle (deg)		Fiber Length (mm)		Sarcomere Length (mm)	
	Sham	Contusion	Sham	Contusion	Sham	Contusion	Sham	Contusion
GM	0.80 ± 0.10	0.82 ± 0.10	29.7 ± 9.0	23.3 ± 5.6	10.63 ± 4.53	7.77 ± 0.62	1.99 ± 0.15	2.12 ± 0.23
GL	1.24 ± 0.20	1.18 ± 0.11	31.0 ± 7.4	27.3 ± 7.6	10.92 ± 6.57	9.93 ± 2.36	2.03 ± 0.07	2.10 ± 0.19
TA	0.69 ± 0.06	0.66 ± 0.03	32.3 ± 11.6	26.3 ± 9.0	13.32 ± 3.16	11.72 ± 3.98	2.24 ± 0.32	2.07 ± 0.25

GM: Gastrocnemius Medialis, GL: Gastrocnemius Lateralis, TA: Tibialis Anterior. No statistically significant differences were seen between groups for any measure indicating a lack of muscle atrophy. GAS was summed or averaged, where appropriate, from GM and GL. Values are mean ± SD

Chapter 4

CONCLUSIONS

Summary

Incomplete spinal cord injury (iSCI) caused large changes in locomotion in rats in this study. These changes were evident in kinematics of treadmill walking following iSCI, the largest of which were at the ankle. There was not a whole-limb decrease in complexity of movement as predicted by stroke experiments, but a joint-specific decrease at the ankle. These joint-specific changes in complexity of movement may be due to differences in motor control between the various joints of the hindlimb. Some of these changes in motor control at the ankle may be responsible for foot drag, a common locomotor deficiency observed in the early stages following injury in the rat; others may be compensatory and allow foot swing as recovery of gait ensues with time post injury.

A computational model of the rat ankle based on experimentally collected data gave evidence of which factors may be most responsible for foot drag and which may compensate to allow foot swing. A decrease in the delay between the cessation of activity in the gastrocnemius muscles and initiation of activity in the tibialis anterior muscle was the only identified maladaptive change in our model. Changes in muscle atrophy, gastrocnemius activation profile, and ankle kinematics were all helpful following injury, counteracting the decreased activation delay to allow foot swing. Of these, changes in the joint angle

kinematic profile and gastrocnemius muscle activation profile had the largest positive effects.

In both studies, small changes in neural control had large changes on behavior (foot swing or foot drag). Small changes in ankle complexity had large changes on ankle kinematics. Small changes in muscle activations had large changes on foot drag.

Locomotor Control

Changes in locomotion seen in this study were likely due to the unique control scheme for the ankle joint as compared to other joints in the hindlimb. Unlike the other joints in the hindlimb, ankle movement is primarily governed by inputs from local proprioceptors [163]. Cutaneous receptors also provide strong inputs to the control of the ankle, but they also affect the whole limb. Activation of plantar cutaneous receptors (as during stance) facilitates whole leg extension while lack of activation (as seen during normal swing) facilitates whole leg flexion and the continuation of swing phase [216, 217]. Stimulation of dorsal cutaneous receptors on the other hand facilitates whole limb flexion as well. In normal quadrupeds, this helps the hindlimb clear any obstacle hit by the leg during swing [32]. However, following injury, dorsal activation is used to assist in clearance of smooth surfaces as well if the ankle does not properly rotate at the stance-to-swing transition. Finally, ankle load is used as a trigger for the stance-to-swing transition and ankle activation facilitates activation of other muscles in the leg [180].

These points suggest that the ankle is a significant controller of locomotion patterns, instead of being significantly controlled by the locomotor control circuitry of the central nervous system (CNS). Why then, does the ankle joint have the largest changes in kinematics following incomplete SCI, a change in input from the CNS? This may indicate that the ankle does not receive significant modulation from the spinal cord, relying more on brain-derived signals for alterations of pattern shape. The basic locomotor pattern (left-right and flexor-extensor alternation) is maintained following injury; however, the shape of the pattern is changed, which could be due to disruptions of the connections to the brain. This hypothesis is supported by the fact that the ankle has no short term, feed-forward control following iSCI in humans [157]. This hypothesis is further supported by the type of injury sustained. As described in the surgical methods for the experiments, the contusion injury applied to the animals strikes the dorsal surface of the cord. This leads to significant damage to the dorsal tracts [136]. In the rat, the primary dorsal tracts are the dorsal corticospinal tract, the fasciculus gracilis (trunk and hindlimbs) and the fasciculus cuneatus (forelimbs) [167, 168]. In rats, the corticospinal tract serves a very limited purpose, only directly controlling individual digit movements [169, 170]. However, it also serves to modulate lumbar stretch reflexes [169]. As the ankle is primarily controlled by local reflexes, damage to the dorsal corticospinal tract would lead to significant changes in ankle control. More work is necessary to determine the actual control mechanism at play.

Significance

This dissertation focused on assessing changes following iSCI. The first study assessed locomotion in experimental animals while the second assessed changes in an experimental model. First, this research has given new insight into the role of the ankle in locomotion, leading to further study of its control. While this work did not directly test a rehabilitation technique, the knowledge gained here can be used in applied settings. The most direct application is using the effect of changing muscle activation timing and delays in the development of functional electrical stimulation devices. Understanding the significant role of the ankle in locomotion may lead to better robotic trainers and manual locomotor training. For example, the Locomat® robotic trainer uses passive control at the ankle while the knee and hip are actively controlled. Adding active control of the ankle may improve locomotor recovery results from use of the device.

Future Work

Changes in muscle activations following iSCI

A possible time course of recovery of foot swing following injury was proposed in Chapter 3. Immediately following injury, the delay between gastrocnemius deactivation and tibialis anterior activation may decrease, increasing incidence of foot drag. During recovery, changes in kinematics and muscle activation profile compensate for the decreased delay, allowing foot swing to return. One way to test this hypothesis would be to measure EMG and kinematics for rats during the recovery stage, 0-4 weeks following injury. Following incomplete spinal cord injury, locomotor coordination distal to the level of injury is impaired. This is due

partly to the disruption of supraspinal drive controlling locomotor circuits, but also to the secondary changes that occur as a result of the injury. Frequently, disruptions to normal gait arise as a result of impaired coordination. This includes impairments in intralimb coordination, flexor-extensor as well as multi-joint; and interlimb coordination, left-right and forelimb-hindlimb. Following incomplete injury, intralimb coordination is markedly changed while left-right coordination can be maintained or regained [138, 218]. This is most noticeable in the retention or recovery of symmetry in the left-right angle-angle kinematic plots. Thus, while SCI primarily disrupts the supraspinal drive to the hindlimbs, the behavioral effect is greater on the network involved in intralimb coordination than that controlling interlimb coordination. Additionally, Chapter 3 suggested that impaired intralimb coordination following iSCI is implicated in foot drag. It also suggested that the rat may undergo adaptations in motor control, specifically activation shape, in order to regain foot swing in the later stages of recovery. Bilateral, flexor-extensor electromyograms (EMG) of the rat ankle muscles would allow us to determine changes in left-right and flexor-extensor coordination as well as the shape of the muscle activation burst. This method has been used previously to assess control of locomotion in normal rats [88, 219, 220], and normal and spinal cord injured mice [221]. Locomotor coordination is important for assessment of recovery following SCI and often not captured by simple behavioral measures [222]. The ankle is of particular interest when looking at gait coordination as ankle load may modulate intralimb coordination as shown in previous EMG studies in humans [171]. Differential loss of intralimb over interlimb

coordination may be due to the nature of the procedures used to create the standard rat SCI experimental model. Long descending propriospinal tract (LDPT) axons are spared more than short thoracic propriospinal tract axons during weight drop contusion injuries in rats, with LDPT neurons being particularly important in interlimb coordination [223].

Below, brief descriptions of a future study to address the proposed hypothesis (that changes in muscle activation delay lead to foot drag which is then compensated for by changes in muscle activation shape) are presented. Long Evans rats would be selected and trained using the same method described for the studies presented in Chapter 2 and 3. Spinal cord injury surgery and post-surgical care would be the same as well. Combined kinematic and EMG analysis would take place on data collected pre and 1, 2, 3, and 4 weeks post injury. EMG electrodes would be implanted bi-laterally in the tibialis anterior and gastrocnemius medialis for the duration of each EMG/kinematics session and removed immediately following testing. EMG electrodes would be constructed from Teflon coated stainless steel wire, deinsulated 3 mm at the tip. The wire would be inserted in a 27 gauge needle and bent around the tip to create a barb. A larger, multistranded wire would be used to create a ground electrode. Animals would be anesthetized before electrode implantation and the electrode sites shaved and cleaned with alcohol and betadine. The ground electrode would be inserted in the middle of the back. EMG electrodes would be inserted subcutaneously, pointing distally and sutured to the skin near their exit. One pair of electrodes would be inserted near each of the four muscles to be measured,

approximately 2 mm apart. All 9 electrodes would be routed to the back using tape and attached to a differential amplifier. The signals would then be amplified and filtered and sampled at an appropriate rate using a data acquisition device in a personal computer. EMG data would be full wave rectified and passed through a 50 ms moving average before being normalized to maximum amplitude. Cross correlation between flexor-extensor and left-right pairs could be conducted to determine coordination, phase lag and overlap between the two signals. Muscle activation shape could be determined by segmenting the EMG signal into individual muscle bursts and normalized to a magnitude and pulse width of 1. These bursts would then be compared to three possible activation profiles. Profile one, a rectangular waveform with an amplitude and pulse width of 1 (Rectangular). Profile two, a trapezoidal profile starting with an amplitude of 1 and decreasing to an amplitude of 0.5 with a pulse width of 1 (Decreasing). Profile three, a trapezoidal profile starting with an amplitude of 0.5, increasing to an amplitude of 1 with a pulse width of 1 (Increasing).

By analyzing the shape and sequence of muscle activations alongside kinematics it would be possible to see the effects of muscle coordination on locomotion directly. For instance, if a decreased delay (phase lag) between the gastrocnemius and tibialis anterior is seen during most instances of foot drag, then the foot drag hypothesis would be supported.

Higher degree-of-freedom model

While our computational model addressed the largest muscles and forces involved in foot swing, additional insight may be gained by adding more joints and 3D to the model. Ankle inversion/eversion may play an as of yet undetermined role in foot swing as the forces at the rat ankle are significant outside of the sagittal plane [85]. Adding the knee and upper leg with via points for the gastrocnemius may increase the accuracy of the moment arm and muscle length calculations. The first steps of such a model would include testing the passive properties of the leg. Passive torques for the joints could be added [107] based on experimental data collected from anesthetized animals using manual perturbations. Passive torques for rat hindlimbs have recently been reported [209] and could be used in such models. Result from such a model may indicate the importance of other muscles in foot swing.

Experimentally measured muscle forces

The structurally determined muscle models used in Chapter 3 may not perfectly represent the muscle forces produced in the rat. Changes following spinal cord injury may include ones not measured in the experiments. Data from isometric and isotonic isolated muscle force experiments may be used to verify the muscles forces produced in the computational model. As spinal cord injury may have effects such as atrophy or change in muscle length-tension properties [149, 224], verifying the structural based model is important. Following iSCI, there is a decrease in mobility, which leads to disuse-type effects in the muscles following injury. These changes stem from the lack of loading of the limbs which can cause

decreases in bone density, muscle atrophy, or hypertrophy if spasticity is significant [225]. Apart from atrophy, the contractile properties of the muscles may be affected [226, 227]. Additionally, location of the muscle along its force-length curve may change following injury [224]. This may lead to improper estimates of force using a structurally derived model. While the results should be similar to those produced using the structurally determined muscle model, they may provide slightly different contractile properties that may affect the results of Chapter 3.

REFERENCES

1. Kandel ER, Schwartz JH, Jessell TM: *Principles of neural science*. 4th edn. New York: McGraw-Hill, Health Professions Division; 2000.
2. Drew T, Jiang W, Widajewicz W: **Contributions of the motor cortex to the control of the hindlimbs during locomotion in the cat.** *Brain Res Brain Res Rev* 2002, **40**:178-191.
3. Frigon A, Rossignol S: **Experiments and models of sensorimotor interactions during locomotion.** *Biol Cybern* 2006, **95**:607-627.
4. Kiehn O: **Locomotor circuits in the mammalian spinal cord.** *Annu Rev Neurosci* 2006, **29**:279-306.
5. Kiehn O, Kjaerulff O: **Distribution of central pattern generators for rhythmic motor outputs in the spinal cord of limbed vertebrates.** *Ann N Y Acad Sci* 1998, **860**:110-129.
6. Frigon A: **Central pattern generators of the mammalian spinal cord.** *Neuroscientist* 2012, **18**:56-69.
7. McCrea DA, Rybak IA: **Organization of mammalian locomotor rhythm and pattern generation.** *Brain Res Rev* 2008, **57**:134-146.
8. Yakovenko S: **Chapter 10--a hierarchical perspective on rhythm generation for locomotor control.** *Prog Brain Res* 2011, **188**:151-166.
9. Brown TG: **On the nature of the fundamental activity of the nervous centres; together with an analysis of the conditioning of rhythmic activity in progression, and a theory of the evolution of function in the nervous system.** *J Physiol* 1914, **48**:18-46.
10. Friesen WO: **Reciprocal inhibition: a mechanism underlying oscillatory animal movements.** *Neurosci Biobehav Rev* 1994, **18**:547-553.
11. Barbeau H, Rossignol S: **Recovery of locomotion after chronic spinalization in the adult cat.** *Brain Res* 1987, **412**:84-95.
12. Grillner S, Zangger P: **The effect of dorsal root transection on the efferent motor pattern in the cat's hindlimb during locomotion.** *Acta Physiol Scand* 1984, **120**:393-405.
13. Juvin L, Simmers J, Morin D: **Locomotor rhythmogenesis in the isolated rat spinal cord: a phase-coupled set of symmetrical flexion extension oscillators.** *J Physiol* 2007, **583**:115-128.

14. Nathan PW: **Effects on movement of surgical incisions into the human spinal cord.** *Brain* 1994, **117** (Pt 2):337-346.
15. Brustein E, Rossignol S: **Recovery of locomotion after ventral and ventrolateral spinal lesions in the cat. I. Deficits and adaptive mechanisms.** *J Neurophysiol* 1998, **80**:1245-1267.
16. Gorska T, Bem T, Majczynski H, Zmyslowski W: **Unrestrained walking in cats with partial spinal lesions.** *Brain Res Bull* 1993, **32**:241-249.
17. Orlovsky GN: **The effect of different descending systems on flexor and extensor activity during locomotion.** *Brain Res* 1972, **40**:359-371.
18. Armstrong DM, Drew T: **Forelimb electromyographic responses to motor cortex stimulation during locomotion in the cat.** *J Physiol* 1985, **367**:327-351.
19. Schubert M, Curt A, Jensen L, Dietz V: **Corticospinal input in human gait: modulation of magnetically evoked motor responses.** *Exp Brain Res* 1997, **115**:234-246.
20. Petersen NT, Butler JE, Marchand-Pauvert V, Fisher R, Ledebt A, Pyndt HS, Hansen NL, Nielsen JB: **Suppression of EMG activity by transcranial magnetic stimulation in human subjects during walking.** *J Physiol* 2001, **537**:651-656.
21. Nathan PW, Smith M, Deacon P: **Vestibulospinal, reticulospinal and descending propriospinal nerve fibres in man.** *Brain* 1996, **119** (Pt 6):1809-1833.
22. Lawrence DG, Kuypers HG: **The functional organization of the motor system in the monkey. I. The effects of bilateral pyramidal lesions.** *Brain* 1968, **91**:1-14.
23. Jordan LM, Liu J, Hedlund PB, Akay T, Pearson KG: **Descending command systems for the initiation of locomotion in mammals.** *Brain Res Rev* 2008, **57**:183-191.
24. Sherrington CS: **Remarks on the reflex mechanism of the step.** *Brain* 1910, **33**:1-25.
25. Duysens J, Pearson KG: **Inhibition of flexor burst generation by loading ankle extensor muscles in walking cats.** *Brain Res* 1980, **187**:321-332.
26. Andersson O, Grillner S: **Peripheral control of the cat's step cycle. II. Entrainment of the central pattern generators for locomotion by**

- sinusoidal hip movements during "fictive locomotion."** *Acta Physiol Scand* 1983, **118**:229-239.
27. Prochazka A, Gillard D, Bennett DJ: **Positive force feedback control of muscles.** *J Neurophysiol* 1997, **77**:3226-3236.
 28. Dietz V, Duysens J: **Significance of load receptor input during locomotion: a review.** *Gait Posture* 2000, **11**:102-110.
 29. Sinkjaer T, Andersen JB, Larsen B: **Soleus stretch reflex modulation during gait in humans.** *J Neurophysiol* 1996, **76**:1112-1120.
 30. Bouyer LJ, Rossignol S: **Contribution of cutaneous inputs from the hindpaw to the control of locomotion. I. Intact cats.** *J Neurophysiol* 2003, **90**:3625-3639.
 31. Forssberg H: **Stumbling corrective reaction: a phase-dependent compensatory reaction during locomotion.** *J Neurophysiol* 1979, **42**:936-953.
 32. Zehr EP, Komiyama T, Stein RB: **Cutaneous reflexes during human gait: electromyographic and kinematic responses to electrical stimulation.** *J Neurophysiol* 1997, **77**:3311-3325.
 33. Abbas JJ, Chizeck HJ: **Neural network control of functional neuromuscular stimulation systems: computer simulation studies.** *IEEE Trans Biomed Eng* 1995, **42**:1117-1127.
 34. Grillner S, Zangger P: **On the central generation of locomotion in the low spinal cat.** *Exp Brain Res* 1979, **34**:241-261.
 35. Stein PS: **Neuronal control of turtle hindlimb motor rhythms.** *J Comp Physiol A Neuroethol Sens Neural Behav Physiol* 2005, **191**:213-229.
 36. Grillner S, Halbertsma J, Nilsson J, Thorstensson A: **The adaptation to speed in human locomotion.** *Brain Res* 1979, **165**:177-182.
 37. Frigon A, Gossard JP: **Asymmetric control of cycle period by the spinal locomotor rhythm generator in the adult cat.** *J Physiol* 2009, **587**:4617-4628.
 38. Kjaerulff O, Kiehn O: **Distribution of networks generating and coordinating locomotor activity in the neonatal rat spinal cord in vitro: a lesion study.** *J Neurosci* 1996, **16**:5777-5794.

39. Cowley KC, Schmidt BJ: **Regional distribution of the locomotor pattern-generating network in the neonatal rat spinal cord.** *J Neurophysiol* 1997, **77**:247-259.
40. Jankowska E, Krutki P, Matsuyama K: **Relative contribution of Ia inhibitory interneurons to inhibition of feline contralateral motoneurons evoked via commissural interneurons.** *J Physiol* 2005, **568**:617-628.
41. Quinlan KA, Kiehn O: **Segmental, synaptic actions of commissural interneurons in the mouse spinal cord.** *J Neurosci* 2007, **27**:6521-6530.
42. Bannatyne BA, Edgley SA, Hammar I, Jankowska E, Maxwell DJ: **Networks of inhibitory and excitatory commissural interneurons mediating crossed reticulospinal actions.** *Eur J Neurosci* 2003, **18**:2273-2284.
43. Eide AL, Glover J, Kjaerulff O, Kiehn O: **Characterization of commissural interneurons in the lumbar region of the neonatal rat spinal cord.** *J Comp Neurol* 1999, **403**:332-345.
44. Kiehn O, Butt SJ: **Physiological, anatomical and genetic identification of CPG neurons in the developing mammalian spinal cord.** *Prog Neurobiol* 2003, **70**:347-361.
45. Butt SJ, Kiehn O: **Functional identification of interneurons responsible for left-right coordination of hindlimbs in mammals.** *Neuron* 2003, **38**:953-963.
46. Stein PSG: *Neurons, networks, and motor behavior.* Cambridge, Mass.: MIT Press; 1997.
47. Bonnot A, Whelan PJ, Mentis GZ, O'Donovan MJ: **Locomotor-like activity generated by the neonatal mouse spinal cord.** *Brain Res Brain Res Rev* 2002, **40**:141-151.
48. McCrea DA, Pratt CA, Jordan LM: **Renshaw cell activity and recurrent effects on motoneurons during fictive locomotion.** *J Neurophysiol* 1980, **44**:475-488.
49. Pratt CA, Jordan LM: **Ia inhibitory interneurons and Renshaw cells as contributors to the spinal mechanisms of fictive locomotion.** *J Neurophysiol* 1987, **57**:56-71.
50. Bajotto G, Shimomura Y: **Determinants of disuse-induced skeletal muscle atrophy: exercise and nutrition countermeasures to prevent protein loss.** *J Nutr Sci Vitaminol (Tokyo)* 2006, **52**:233-247.

51. Shields RK: **Muscular, skeletal, and neural adaptations following spinal cord injury.** *J Orthop Sports Phys Ther* 2002, **32**:65-74.
52. Schwab ME, Bartholdi D: **Degeneration and regeneration of axons in the lesioned spinal cord.** *Physiol Rev* 1996, **76**:319-370.
53. Hulsebosch CE: **Recent advances in pathophysiology and treatment of spinal cord injury.** *Adv Physiol Educ* 2002, **26**:238-255.
54. **Facts and Figures at a Glance 2009**
[https://www.nscisc.uab.edu/public_content/facts_figures_2009.aspx]
55. Strauss DJ, Devivo MJ, Paculdo DR, Shavelle RM: **Trends in life expectancy after spinal cord injury.** *Arch Phys Med Rehabil* 2006, **87**:1079-1085.
56. Dietz V, Harkema SJ: **Locomotor activity in spinal cord-injured persons.** *J Appl Physiol* 2004, **96**:1954-1960.
57. Kay ED, Deutsch A, Wuermser LA: **Predicting walking at discharge from inpatient rehabilitation after a traumatic spinal cord injury.** *Arch Phys Med Rehabil* 2007, **88**:745-750.
58. Marino RJ, Graves DE: **Metric properties of the ASIA motor score: subscales improve correlation with functional activities.** *Arch Phys Med Rehabil* 2004, **85**:1804-1810.
59. Anderson KD: **Targeting recovery: priorities of the spinal cord-injured population.** *J Neurotrauma* 2004, **21**:1371-1383.
60. Widerstrom-Noga EG, Turk DC: **Exacerbation of chronic pain following spinal cord injury.** *J Neurotrauma* 2004, **21**:1384-1395.
61. Patki P, Hamid R, Shah J, Craggs M: **Fertility following spinal cord injury: a systematic review.** *Spinal Cord* 2007, **45**:187.
62. Weaver LC, Marsh DR, Gris D, Brown A, Dekaban GA: **Autonomic dysreflexia after spinal cord injury: central mechanisms and strategies for prevention.** *Prog Brain Res* 2006, **152**:245-263.
63. McKinley WO, Jackson AB, Cardenas DD, DeVivo MJ: **Long-term medical complications after traumatic spinal cord injury: a regional model systems analysis.** *Arch Phys Med Rehabil* 1999, **80**:1402-1410.
64. Botel U, Glaser E, Niedeggen A: **The surgical treatment of acute spinal paralysed patients.** *Spinal Cord* 1997, **35**:420-428.

65. Fehlings MG, Perrin RG: **The timing of surgical intervention in the treatment of spinal cord injury: a systematic review of recent clinical evidence.** *Spine (Phila Pa 1976)* 2006, **31**:S28-35; discussion S36.
66. Bracken MB, Shepard MJ, Collins WF, Holford TR, Young W, Baskin DS, Eisenberg HM, Flamm E, Leo-Summers L, Maroon J, et al.: **A randomized, controlled trial of methylprednisolone or naloxone in the treatment of acute spinal-cord injury. Results of the Second National Acute Spinal Cord Injury Study.** *N Engl J Med* 1990, **322**:1405-1411.
67. Bracken MB, Shepard MJ, Holford TR, Leo-Summers L, Aldrich EF, Fazl M, Fehlings M, Herr DL, Hitchon PW, Marshall LF, et al: **Administration of methylprednisolone for 24 or 48 hours or tirilazad mesylate for 48 hours in the treatment of acute spinal cord injury. Results of the Third National Acute Spinal Cord Injury Randomized Controlled Trial. National Acute Spinal Cord Injury Study.** *JAMA* 1997, **277**:1597-1604.
68. Lee HC, Cho DY, Lee WY, Chuang HC: **Pitfalls in treatment of acute cervical spinal cord injury using high-dose methylprednisolone: a retrospect audit of 111 patients.** *Surg Neurol* 2007, **68 Suppl 1**:S37-41; discussion S41-32.
69. Nesathurai S: **The role of methylprednisolone in acute spinal cord injuries.** *J Trauma* 2001, **51**:421-423.
70. Chantraine A, Nusgens B, Lapiere CM: **Bone remodeling during the development of osteoporosis in paraplegia.** *Calcif Tissue Int* 1986, **38**:323-327.
71. Jiang SD, Dai LY, Jiang LS: **Osteoporosis after spinal cord injury.** *Osteoporos Int* 2006, **17**:180-192.
72. Baldi JC, Jackson RD, Moraille R, Mysiw WJ: **Muscle atrophy is prevented in patients with acute spinal cord injury using functional electrical stimulation.** *Spinal Cord* 1998, **36**:463-469.
73. Lotta S, Scelsi R, Alfonsi E, Saitta A, Nicolotti D, Epifani P, Carraro U: **Morphometric and neurophysiological analysis of skeletal muscle in paraplegic patients with traumatic cord lesion.** *Paraplegia* 1991, **29**:247-252.
74. Dietz V: **Quadrupedal coordination of bipedal gait: implications for movement disorders.** *J Neurol* 2011, **258**:1406-1412.
75. Zehr EP, Hundza SR, Vasudevan EV: **The quadrupedal nature of human bipedal locomotion.** *Exerc Sport Sci Rev* 2009, **37**:102-108.

76. Onifer SM, Rabchevsky AG, Scheff SW: **Rat models of traumatic spinal cord injury to assess motor recovery.** *Ilar J* 2007, **48**:385-395.
77. Kwon BK, Oxland TR, Tetzlaff W: **Animal models used in spinal cord regeneration research.** *Spine (Phila Pa 1976)* 2002, **27**:1504-1510.
78. Barbeau H, Ladouceur M, Norman KE, Pepin A, Leroux A: **Walking after spinal cord injury: evaluation, treatment, and functional recovery.** *Arch Phys Med Rehabil* 1999, **80**:225-235.
79. Hosoido T, Goto M, Sano Y, Mori F, Nakajima K, Morita F, Wada N: **Hoffmann reflex in a rat bipedal walking model.** *Neurosci Lett* 2011, **505**:263-267.
80. Ichiyama RM, Courtine G, Gerasimenko YP, Yang GJ, van den Brand R, Lavrov IA, Zhong H, Roy RR, Edgerton VR: **Step training reinforces specific spinal locomotor circuitry in adult spinal rats.** *J Neurosci* 2008, **28**:7370-7375.
81. Cao Q, Zhang YP, Iannotti C, DeVries WH, Xu XM, Shields CB, Whittemore SR: **Functional and electrophysiological changes after graded traumatic spinal cord injury in adult rat.** *Exp Neurol* 2005, **191 Suppl 1**:S3-S16.
82. Bareyre FM, Schwab ME: **Inflammation, degeneration and regeneration in the injured spinal cord: insights from DNA microarrays.** *Trends Neurosci* 2003, **26**:555-563.
83. Sedy J, Urdzikova L, Jendelova P, Sykova E: **Methods for behavioral testing of spinal cord injured rats.** *Neurosci Biobehav Rev* 2008, **32**:550-580.
84. Basso DM, Beattie MS, Bresnahan JC: **A sensitive and reliable locomotor rating scale for open field testing in rats.** *J Neurotrauma* 1995, **12**:1-21.
85. Johnson WL, Jindrich DL, Roy RR, Edgerton VR: **Quantitative metrics of spinal cord injury recovery in the rat using motion capture, electromyography and ground reaction force measurement.** *J Neurosci Methods* 2012, **206**:65-72.
86. Muir GD, Webb AA: **Mini-review: assessment of behavioural recovery following spinal cord injury in rats.** *Eur J Neurosci* 2000, **12**:3079-3086.

87. Thota A, Carlson S, Jung R: **Recovery of locomotor function after treadmill training of incomplete spinal cord injured rats.** *Biomed Sci Instrum* 2001, **37**:63-67.
88. Thota AK, Watson SC, Knapp E, Thompson B, Jung R: **Neuromechanical control of locomotion in the rat.** *J Neurotrauma* 2005, **22**:442-465.
89. Buchanan TS, Lloyd DG, Manal K, Besier TF: **Neuromusculoskeletal modeling: estimation of muscle forces and joint moments and movements from measurements of neural command.** *J Appl Biomech* 2004, **20**:367-395.
90. Peckham PH, Knutson JS: **Functional electrical stimulation for neuromuscular applications.** *Annu Rev Biomed Eng* 2005, **7**:327-360.
91. Langhorne P, Coupar F, Pollock A: **Motor recovery after stroke: a systematic review.** *Lancet Neurol* 2009, **8**:741-754.
92. Hull ML, Jorge M: **A method for biomechanical analysis of bicycle pedalling.** *J Biomech* 1985, **18**:631-644.
93. Davoodi R, Brown IE, Loeb GE: **Advanced modeling environment for developing and testing FES control systems.** *Med Eng Phys* 2003, **25**:3-9.
94. Valero-Cuevas FJ, Hoffmann H, Kurse MU, Kutch JJ, Theodorou EA: **Computational Models for Neuromuscular Function.** *IEEE Rev Biomed Eng* 2009, **2**:110-135.
95. Olney SJ, Griffin MP, Monga TN, McBride ID: **Work and power in gait of stroke patients.** *Arch Phys Med Rehabil* 1991, **72**:309-314.
96. An KN, Chao EY, Cooney WP, Linscheid RL: **Forces in the normal and abnormal hand.** *J Orthop Res* 1985, **3**:202-211.
97. van Langelaan EJ: **A kinematical analysis of the tarsal joints. An X-ray photogrammetric study.** *Acta Orthop Scand Suppl* 1983, **204**:1-269.
98. Zajac FE: **How musculotendon architecture and joint geometry affect the capacity of muscles to move and exert force on objects: a review with application to arm and forearm tendon transfer design.** *J Hand Surg Am* 1992, **17**:799-804.
99. Garner BA, Pandy MG: **The Obstacle-Set Method for Representing Muscle Paths in Musculoskeletal Models.** *Comput Methods Biomech Biomed Engin* 2000, **3**:1-30.

100. Huxley AF: **Muscle structure and theories of contraction.** *Prog Biophys Biophys Chem* 1957, **7**:255-318.
101. Hill AV: **The heat of shortening and the dynamic constants of muscle.** *Proc R Soc Lond B* 1938, **126**:136-195.
102. Nigg BM, Herzog W: *Biomechanics of the musculo-skeletal system.* 2nd edn. Chichester ; New York: Wiley; 1999.
103. Cheng EJ, Brown IE, Loeb GE: **Virtual muscle: a computational approach to understanding the effects of muscle properties on motor control.** *J Neurosci Methods* 2000, **101**:117-130.
104. Song D, Raphael G, Lan N, Loeb GE: **Computationally efficient models of neuromuscular recruitment and mechanics.** *J Neural Eng* 2008, **5**:175-184.
105. Piazza SJ: **Muscle-driven forward dynamic simulations for the study of normal and pathological gait.** *J Neuroeng Rehabil* 2006, **3**:5.
106. Winter DA: *Biomechanics and motor control of human movement.* 3rd edn. Hoboken, New Jersey: John Wiley & Sons; 2005.
107. Yamaguchi GT: *Dynamic modeling of musculoskeletal motion : a vectorized approach for biomechanical analysis in three dimensions.* Boston: Kluwer Academic Publishers; 2001.
108. Colacino FM, Rustighi E, Mace BR: **An EMG-driven musculoskeletal model for the estimation of biomechanical parameters of wrist flexors.** *Conf Proc IEEE Eng Med Biol Soc* 2010, **2010**:4870-4873.
109. Mazurek KA, Holinski BJ, Everaert DG, Stein RB, Etienne-Cummings R, Mushahwar VK: **Feed forward and feedback control for over-ground locomotion in anaesthetized cats.** *J Neural Eng* 2012, **9**:026003.
110. Winters MJ, Woo SLY: *Multiple muscle systems : biomechanics and movement organization.* New York: Springer-Verlag; 1990.
111. Montazemi PT, Davoodi, R., and Loeb, G. E.: **Comparison of dynamic engines for musculoskeletal modeling software MSMS.** In *Proceedings of the American Society of Biomechanics Conference.* 2004
112. Ackery A, Tator C, Krassioukov A: **A global perspective on spinal cord injury epidemiology.** *J Neurotrauma* 2004, **21**:1355-1370.
113. Bradbury EJ, McMahon SB: **Spinal cord repair strategies: why do they work?** *Nat Rev Neurosci* 2006, **7**:644-653.

114. Thuret S, Moon LD, Gage FH: **Therapeutic interventions after spinal cord injury.** *Nat Rev Neurosci* 2006, **7**:628-643.
115. Hutchinson KJ, Linderman JK, Basso DM: **Skeletal muscle adaptations following spinal cord contusion injury in rat and the relationship to locomotor function: a time course study.** *J Neurotrauma* 2001, **18**:1075-1089.
116. Talmadge RJ, Castro MJ, Apple DF, Jr., Dudley GA: **Phenotypic adaptations in human muscle fibers 6 and 24 wk after spinal cord injury.** *J Appl Physiol* 2002, **92**:147-154.
117. Stein RB, Chong SL, James KB, Kido A, Bell GJ, Tubman LA, Belanger M: **Electrical stimulation for therapy and mobility after spinal cord injury.** *Prog Brain Res* 2002, **137**:27-34.
118. Bloomfield SA: **Changes in musculoskeletal structure and function with prolonged bed rest.** *Med Sci Sports Exerc* 1997, **29**:197-206.
119. Cornachione A, Cacao-Benedini LO, Shimano MM, Volpon JB, Martinez EZ, Mattiello-Sverzut AC: **Morphological comparison of different protocols of skeletal muscle remobilization in rats after hindlimb suspension.** *Scand J Med Sci Sports* 2008, **18**:453-461.
120. Wirth B, van Hedel HJ, Curt A: **Ankle dexterity is less impaired than muscle strength in incomplete spinal cord lesion.** *J Neurol* 2008, **255**:273-279.
121. Wirth B, Van Hedel HJ, Curt A: **Changes in corticospinal function and ankle motor control during recovery from incomplete spinal cord injury.** *J Neurotrauma* 2008, **25**:467-478.
122. Maegele M, Muller S, Wernig A, Edgerton VR, Harkema SJ: **Recruitment of spinal motor pools during voluntary movements versus stepping after human spinal cord injury.** *J Neurotrauma* 2002, **19**:1217-1229.
123. Ollivier-Lanvin K, Lemay MA, Tessler A, Burns AS: **Neuromuscular transmission failure and muscle fatigue in ankle muscles of the adult rat after spinal cord injury.** *J Appl Physiol* 2009, **107**:1190-1194.
124. Ranganathan R, Krishnan C: **Extracting synergies in gait: Using EMG variability to evaluate control strategies.** *J Neurophysiol* 2012.
125. Perry J: *Gait analysis : normal and pathological function.* Thorofare, NJ: SLACK; 1992.

126. Clark DJ, Ting LH, Zajac FE, Neptune RR, Kautz SA: **Merging of healthy motor modules predicts reduced locomotor performance and muscle coordination complexity post-stroke.** *J Neurophysiol* 2010, **103**:844-857.
127. Yang JF, Gorassini M: **Spinal and brain control of human walking: implications for retraining of walking.** *Neuroscientist* 2006, **12**:379-389.
128. Tresch MC, Jarc A: **The case for and against muscle synergies.** *Curr Opin Neurobiol* 2009, **19**:601-607.
129. Shemmell J, Johansson J, Portra V, Gottlieb GL, Thomas JS, Corcos DM: **Control of interjoint coordination during the swing phase of normal gait at different speeds.** *J Neuroeng Rehabil* 2007, **4**:10.
130. Den Otter AR, Geurts AC, Mulder T, Duysens J: **Gait recovery is not associated with changes in the temporal patterning of muscle activity during treadmill walking in patients with post-stroke hemiparesis.** *Clin Neurophysiol* 2006, **117**:4-15.
131. Ivanenko YP, Poppele RE, Lacquaniti F: **Distributed neural networks for controlling human locomotion: lessons from normal and SCI subjects.** *Brain Res Bull* 2009, **78**:13-21.
132. Couto PA, Filipe VM, Magalhaes LG, Pereira JE, Costa LM, Melo-Pinto P, Bulas-Cruz J, Mauricio AC, Geuna S, Varejao AS: **A comparison of two-dimensional and three-dimensional techniques for the determination of hindlimb kinematics during treadmill locomotion in rats following spinal cord injury.** *J Neurosci Methods* 2008, **173**:193-200.
133. Courtine G, Gerasimenko Y, van den Brand R, Yew A, Musienko P, Zhong H, Song B, Ao Y, Ichiyama RM, Lavrov I, et al: **Transformation of nonfunctional spinal circuits into functional states after the loss of brain input.** *Nat Neurosci* 2009, **12**:1333-1342.
134. Negrodo P, Rivero JL, Gonzalez B, Ramon-Cueto A, Manso R: **Slow- and fast-twitch rat hind limb skeletal muscle phenotypes 8 months after spinal cord transection and olfactory ensheathing glia transplantation.** *J Physiol* 2008, **586**:2593-2610.
135. Johnson WL, Jindrich DL, Zhong H, Roy RR, Edgerton VR: **Application of a rat hindlimb model: a prediction of force spaces reachable through stimulation of nerve fascicles.** *IEEE Trans Biomed Eng* 2011, **58**:3328-3338.

136. Scheff SW, Rabchevsky AG, Fugaccia I, Main JA, Lumpp JE, Jr.: **Experimental modeling of spinal cord injury: characterization of a force-defined injury device.** *J Neurotrauma* 2003, **20**:179-193.
137. Winstein CJ, Garfinkel A: **Qualitative dynamics of disordered human locomotion: a preliminary investigation.** *J Mot Behav* 1989, **21**:373-391.
138. Jung R, Belanger A, Kanchiku T, Fairchild M, Abbas JJ: **Neuromuscular stimulation therapy after incomplete spinal cord injury promotes recovery of interlimb coordination during locomotion.** *J Neural Eng* 2009, **6**:55010.
139. Jung R, Brauer EJ, Abbas JJ: **Real-time interaction between a neuromorphic electronic circuit and the spinal cord.** *IEEE Trans Neural Syst Rehabil Eng* 2001, **9**:319-326.
140. Bandt C, Pompe B: **Permutation entropy: a natural complexity measure for time series.** *Phys Rev Lett* 2002, **88**:174102.
141. Rathleff MS, Samani A, Olesen CG, Kersting UG, Madeleine P: **Inverse relationship between the complexity of midfoot kinematics and muscle activation in patients with medial tibial stress syndrome.** *J Electromyogr Kinesiol* 2011, **21**:638-644.
142. Olofsen E, Sleight JW, Dahan A: **Permutation entropy of the electroencephalogram: a measure of anaesthetic drug effect.** *Br J Anaesth* 2008, **101**:810-821.
143. Cao Y, Tung WW, Gao JB, Protopopescu VA, Hively LM: **Detecting dynamical changes in time series using the permutation entropy.** *Phys Rev E Stat Nonlin Soft Matter Phys* 2004, **70**:046217.
144. Lee M, Roan M, Smith B: **An application of principal component analysis for lower body kinematics between loaded and unloaded walking.** *J Biomech* 2009, **42**:2226-2230.
145. Deluzio KJ, Astephen JL: **Biomechanical features of gait waveform data associated with knee osteoarthritis: an application of principal component analysis.** *Gait Posture* 2007, **25**:86-93.
146. Sadeghi H, Prince F, Sadeghi S, Labelle H: **Principal component analysis of the power developed in the flexion/extension muscles of the hip in able-bodied gait.** *Med Eng Phys* 2000, **22**:703-710.

147. Lieber RL, Yeh Y, Baskin RJ: **Sarcomere length determination using laser diffraction. Effect of beam and fiber diameter.** *Biophys J* 1984, **45**:1007-1016.
148. Pribe C, Grossberg S, Cohen MA: **Neural control of interlimb oscillations. II. Biped and quadruped gaits and bifurcations.** *Biol Cybern* 1997, **77**:141-152.
149. Gregory CM, Vandenborne K, Castro MJ, Dudley GA: **Human and rat skeletal muscle adaptations to spinal cord injury.** *Can J Appl Physiol* 2003, **28**:491-500.
150. Liu M, Bose P, Walter GA, Thompson FJ, Vandenborne K: **A longitudinal study of skeletal muscle following spinal cord injury and locomotor training.** *Spinal Cord* 2008, **46**:488-493.
151. Thomason DB, Biggs RB, Booth FW: **Protein metabolism and beta-myosin heavy-chain mRNA in unweighted soleus muscle.** *Am J Physiol* 1989, **257**:R300-305.
152. Armstrong RB, Phelps RO: **Muscle fiber type composition of the rat hindlimb.** *Am J Anat* 1984, **171**:259-272.
153. Boonyarom O, Kozuka N, Matsuyama K, Murakami S: **Effect of electrical stimulation to prevent muscle atrophy on morphologic and histologic properties of hindlimb suspended rat hindlimb muscles.** *Am J Phys Med Rehabil* 2009, **88**:719-726.
154. Ivanenko YP, Grasso R, Zago M, Molinari M, Scivoletto G, Castellano V, Macellari V, Lacquaniti F: **Temporal components of the motor patterns expressed by the human spinal cord reflect foot kinematics.** *J Neurophysiol* 2003, **90**:3555-3565.
155. Ballermann M, Tse AD, Misiaszek JE, Fouad K: **Adaptations in the walking pattern of spinal cord injured rats.** *J Neurotrauma* 2006, **23**:897-907.
156. Yakovenko S, Gritsenko V, Prochazka A: **Contribution of stretch reflexes to locomotor control: a modeling study.** *Biol Cybern* 2004, **90**:146-155.
157. Gordon KE, Wu M, Kahn JH, Schmit BD: **Feedback and feedforward locomotor adaptations to ankle-foot load in people with incomplete spinal cord injury.** *J Neurophysiol* 2010, **104**:1325-1338.

158. Daley MA, Felix G, Biewener AA: **Running stability is enhanced by a proximo-distal gradient in joint neuromechanical control.** *J Exp Biol* 2007, **210**:383-394.
159. Pearson KG: **Role of sensory feedback in the control of stance duration in walking cats.** *Brain Res Rev* 2008, **57**:222-227.
160. Drew T, Kalaska J, Krouchev N: **Muscle synergies during locomotion in the cat: a model for motor cortex control.** *J Physiol* 2008, **586**:1239-1245.
161. Lam T, Pearson KG: **The role of proprioceptive feedback in the regulation and adaptation of locomotor activity.** *Adv Exp Med Biol* 2002, **508**:343-355.
162. Grillner S, Rossignol S: **On the initiation of the swing phase of locomotion in chronic spinal cats.** *Brain Res* 1978, **146**:269-277.
163. Hiebert GW, Pearson KG: **Contribution of sensory feedback to the generation of extensor activity during walking in the decerebrate Cat.** *J Neurophysiol* 1999, **81**:758-770.
164. Prochazka A, Gritsenko V, Yakovenko S: **Sensory control of locomotion: reflexes versus higher-level control.** *Adv Exp Med Biol* 2002, **508**:357-367.
165. Pearson KG, Misiaszek JE: **Use-dependent gain change in the reflex contribution to extensor activity in walking cats.** *Brain Res* 2000, **883**:131-134.
166. Donelan JM, Pearson KG: **Contribution of force feedback to ankle extensor activity in decerebrate walking cats.** *J Neurophysiol* 2004, **92**:2093-2104.
167. Schwartz ED, Cooper ET, Chin CL, Wehrli S, Tessler A, Hackney DB: **Ex vivo evaluation of ADC values within spinal cord white matter tracts.** *AJNR Am J Neuroradiol* 2005, **26**:390-397.
168. Gullapalli J, Krejza J, Schwartz ED: **In vivo DTI evaluation of white matter tracts in rat spinal cord.** *J Magn Reson Imaging* 2006, **24**:231-234.
169. Chen XY, Wolpaw JR: **Probable corticospinal tract control of spinal cord plasticity in the rat.** *J Neurophysiol* 2002, **87**:645-652.

170. Cheney PD, Fetz EE, Mewes K: **Neural mechanisms underlying corticospinal and rubrospinal control of limb movements.** *Prog Brain Res* 1991, **87**:213-252.
171. Gordon KE, Wu M, Kahn JH, Dhaher YY, Schmit BD: **Ankle load modulates hip kinetics and EMG during human locomotion.** *J Neurophysiol* 2009, **101**:2062-2076.
172. Daley MA, Usherwood JR, Felix G, Biewener AA: **Running over rough terrain: guinea fowl maintain dynamic stability despite a large unexpected change in substrate height.** *J Exp Biol* 2006, **209**:171-187.
173. Lamy JC, Iglesias C, Lackmy A, Nielsen JB, Katz R, Marchand-Pauvert V: **Modulation of recurrent inhibition from knee extensors to ankle motoneurons during human walking.** *J Physiol* 2008, **586**:5931-5946.
174. Dyer JO, Maupas E, Melo Sde A, Bourbonnais D, Forget R: **Abnormal coactivation of knee and ankle extensors is related to changes in heteronymous spinal pathways after stroke.** *J Neuroeng Rehabil* 2011, **8**:41.
175. Finley JM, Perreault EJ, Dhaher YY: **Stretch reflex coupling between the hip and knee: implications for impaired gait following stroke.** *Exp Brain Res* 2008, **188**:529-540.
176. Daley MA, Biewener AA: **Running over rough terrain reveals limb control for intrinsic stability.** *Proc Natl Acad Sci U S A* 2006, **103**:15681-15686.
177. Wang H, Jung R: **Variability analyses suggest that supraspino-spinal interactions provide dynamic stability in motor control.** *Brain Res* 2002, **930**:83-100.
178. Allen JL, Neptune RR: **Three-dimensional modular control of human walking.** *J Biomech* 2012.
179. Hiebert GW, Whelan PJ, Prochazka A, Pearson KG: **Contribution of hind limb flexor muscle afferents to the timing of phase transitions in the cat step cycle.** *J Neurophysiol* 1996, **75**:1126-1137.
180. Ekeberg O, Pearson K: **Computer simulation of stepping in the hind legs of the cat: an examination of mechanisms regulating the stance-to-swing transition.** *J Neurophysiol* 2005, **94**:4256-4268.
181. Wu M, Schmit BD: **Spastic reflexes triggered by ankle load release in human spinal cord injury.** *J Neurophysiol* 2006, **96**:2941-2950.

182. Guertin P, Angel MJ, Perreault MC, McCrea DA: **Ankle extensor group I afferents excite extensors throughout the hindlimb during fictive locomotion in the cat.** *J Physiol* 1995, **487 (Pt 1):**197-209.
183. Rossignol S, Frigon A: **Recovery of locomotion after spinal cord injury: some facts and mechanisms.** *Annu Rev Neurosci* 2011, **34:**413-440.
184. Rossignol S, Barriere G, Alluin O, Frigon A: **Re-expression of locomotor function after partial spinal cord injury.** *Physiology (Bethesda)* 2009, **24:**127-139.
185. Thota AK: **NEUROMECHANICAL CONTROL OF LOCOMOTION IN INTACT AND INCOMPLETE SPINAL CORD INJURED RATS.** *Master's Thesis.* University of Kentucky, 2004.
186. Miwa T, Iwasaki M, Miyauchi A, Okuda S, Oda T: **Foot drop caused by a lesion in the thoracolumbar spine.** *J Spinal Disord Tech* 2011, **24:**E21-25.
187. Barthelemy D, Willerslev-Olsen M, Lundell H, Conway BA, Knudsen H, Biering-Sorensen F, Nielsen JB: **Impaired transmission in the corticospinal tract and gait disability in spinal cord injured persons.** *J Neurophysiol* 2010, **104:**1167-1176.
188. Thompson AK, Lapallo B, Duffield M, Abel BM, Pomerantz F: **Repetitive common peroneal nerve stimulation increases ankle dorsiflexor motor evoked potentials in incomplete spinal cord lesions.** *Exp Brain Res* 2011, **210:**143-152.
189. Bajd T, Kralj A, Stefancic M, Lavrac N: **Use of functional electrical stimulation in the lower extremities of incomplete spinal cord injured patients.** *Artif Organs* 1999, **23:**403-409.
190. Chin R, Hsiao-Wecksler ET, Loth E, Kogler G, Manwaring SD, Tyson SN, Shorter KA, Gilmer JN: **A pneumatic power harvesting ankle-foot orthosis to prevent foot-drop.** *J Neuroeng Rehabil* 2009, **6:**19.
191. Domingo A, Sawicki GS, Ferris DP: **Kinematics and muscle activity of individuals with incomplete spinal cord injury during treadmill stepping with and without manual assistance.** *J Neuroeng Rehabil* 2007, **4:**32.
192. Barbeau H, McCrea DA, O'Donovan MJ, Rossignol S, Grill WM, Lemay MA: **Tapping into spinal circuits to restore motor function.** *Brain Res Brain Res Rev* 1999, **30:**27-51.

193. Dietz V: **Behavior of spinal neurons deprived of supraspinal input.** *Nat Rev Neurol* 2010, **6**:167-174.
194. Kaegi S, Schwab ME, Dietz V, Fouad K: **Electromyographic activity associated with spontaneous functional recovery after spinal cord injury in rats.** *Eur J Neurosci* 2002, **16**:249-258.
195. Fung YC: *Biomechanics : mechanical properties of living tissues.* 2nd edn. New York: Springer-Verlag; 1993.
196. Johnson WL, Jindrich DL, Roy RR, Reggie Edgerton V: **A three-dimensional model of the rat hindlimb: musculoskeletal geometry and muscle moment arms.** *J Biomech* 2008, **41**:610-619.
197. Brown IE, Cheng EJ, Loeb GE: **Measured and modeled properties of mammalian skeletal muscle. II. The effects of stimulus frequency on force-length and force-velocity relationships.** *J Muscle Res Cell Motil* 1999, **20**:627-643.
198. Brown IE, Loeb GE: **Measured and modeled properties of mammalian skeletal muscle: IV. dynamics of activation and deactivation.** *J Muscle Res Cell Motil* 2000, **21**:33-47.
199. Sacks RD, Roy RR: **Architecture of the hind limb muscles of cats: functional significance.** *J Morphol* 1982, **173**:185-195.
200. Brown IE, Satoda T, Richmond FJ, Loeb GE: **Feline caudofemoralis muscle. Muscle fibre properties, architecture, and motor innervation.** *Exp Brain Res* 1998, **121**:76-91.
201. Burkholder TJ, Lieber RL: **Sarcomere length operating range of vertebrate muscles during movement.** *J Exp Biol* 2001, **204**:1529-1536.
202. Botterman BR, Iwamoto GA, Gonyea WJ: **Gradation of isometric tension by different activation rates in motor units of cat flexor carpi radialis muscle.** *J Neurophysiol* 1986, **56**:494-506.
203. Kernell D, Eerbeek O, Verhey BA: **Relation between isometric force and stimulus rate in cat's hindlimb motor units of different twitch contraction time.** *Exp Brain Res* 1983, **50**:220-227.
204. Brown IE, Scott SH, Loeb GE: **Mechanics of feline soleus: II. Design and validation of a mathematical model.** *J Muscle Res Cell Motil* 1996, **17**:221-233.
205. Maganaris CN, Paul JP: **In vivo human tendinous tissue stretch upon maximum muscle force generation.** *J Biomech* 2000, **33**:1453-1459.

206. Meyer AR, Wang M, Smith PA, Harris GF: **Modeling initial contact dynamics during ambulation with dynamic simulation.** *Med Biol Eng Comput* 2007, **45**:387-394.
207. Kistemaker DA, Van Soest AJ, Bobbert MF: **Is equilibrium point control feasible for fast goal-directed single-joint movements?** *J Neurophysiol* 2006, **95**:2898-2912.
208. Higginson JS, Ramsay JW, Buchanan TS: **Hybrid models of the neuromusculoskeletal system improve subject-specificity.** *Proc Inst Mech Eng H* 2012, **226**:113-119.
209. Wu MM, Pai DK, Tresch MC, Sandercock TG: **Passive elastic properties of the rat ankle.** *J Biomech* 2012, **45**:1728-1732.
210. Fukunaga T, Miyatani M, Tachi M, Kouzaki M, Kawakami Y, Kanehisa H: **Muscle volume is a major determinant of joint torque in humans.** *Acta Physiol Scand* 2001, **172**:249-255.
211. Lamontagne A, Richards CL, Malouin F: **Coactivation during gait as an adaptive behavior after stroke.** *J Electromyogr Kinesiol* 2000, **10**:407-415.
212. Leroux A, Fung J, Barbeau H: **Adaptation of the walking pattern to uphill walking in normal and spinal-cord injured subjects.** *Exp Brain Res* 1999, **126**:359-368.
213. Nelson-Wong E, Appell R, McKay M, Nawaz H, Roth J, Sigler R, Third J, Walker M: **Increased fall risk is associated with elevated co-contraction about the ankle during static balance challenges in older adults.** *Eur J Appl Physiol* 2012, **112**:1379-1389.
214. Thompson FJ, Reier PJ, Lucas CC, Parmer R: **Altered patterns of reflex excitability subsequent to contusion injury of the rat spinal cord.** *J Neurophysiol* 1992, **68**:1473-1486.
215. Mazzaro N, Nielsen JF, Grey MJ, Sinkjaer T: **Decreased contribution from afferent feedback to the soleus muscle during walking in patients with spastic stroke.** *J Stroke Cerebrovasc Dis* 2007, **16**:135-144.
216. Varejao AS, Filipe VM: **Contribution of cutaneous inputs from the hindpaw to the control of locomotion in rats.** *Behav Brain Res* 2007, **176**:193-201.
217. van Wezel BM, van Engelen BG, Gabreels FJ, Gabreels-Festen AA, Duysens J: **Abeta fibers mediate cutaneous reflexes during human walking.** *J Neurophysiol* 2000, **83**:2980-2986.

218. Field-Fote EC, Tepavac D: **Improved intralimb coordination in people with incomplete spinal cord injury following training with body weight support and electrical stimulation.** *Phys Ther* 2002, **82**:707-715.
219. Gramsbergen A: **Posture and locomotion in the rat: independent or interdependent development?** *Neurosci Biobehav Rev* 1998, **22**:547-553.
220. Roy RR, Hutchison DL, Pierotti DJ, Hodgson JA, Edgerton VR: **EMG patterns of rat ankle extensors and flexors during treadmill locomotion and swimming.** *J Appl Physiol* 1991, **70**:2522-2529.
221. Leblond H, L'Esperance M, Orsal D, Rossignol S: **Treadmill locomotion in the intact and spinal mouse.** *J Neurosci* 2003, **23**:11411-11419.
222. Koopmans GC, Deumens R, Honig WM, Hamers FP, Steinbusch HW, Joosten EA: **The assessment of locomotor function in spinal cord injured rats: the importance of objective analysis of coordination.** *J Neurotrauma* 2005, **22**:214-225.
223. Conta AC, Stelzner DJ: **Differential vulnerability of propriospinal tract neurons to spinal cord contusion injury.** *J Comp Neurol* 2004, **479**:347-359.
224. Lieber RL, Friden J: **Spasticity causes a fundamental rearrangement of muscle-joint interaction.** *Muscle Nerve* 2002, **25**:265-270.
225. Biewener AA: **Biomechanics of mammalian terrestrial locomotion.** *Science* 1990, **250**:1097-1103.
226. Yamaguchi GT, Zajac FE: **Restoring unassisted natural gait to paraplegics via functional neuromuscular stimulation: a computer simulation study.** *IEEE Trans Biomed Eng* 1990, **37**:886-902.
227. Gregory CM, Vandenborne K, Huang HF, Ottenweller JE, Dudley GA: **Effects of testosterone replacement therapy on skeletal muscle after spinal cord injury.** *Spinal Cord* 2003, **41**:23-28.